

# Development and physico-chemical characterization of nanocapsules



Dissertation  
zur Erlangung des akademischen Grades  
doctor rerum naturalium (Dr. rer. nat.)

vorgelegt der  
Mathematisch-Naturwissenschaftlich-Technischen Fakultät  
(mathematisch-naturwissenschaftlicher Bereich)  
der Martin-Luther-Universität Halle-Wittenberg

von  
Andrea Rübe  
geboren am 15. Mai 1978 in Lich

Gutachter:

1. Prof. Dr. Karsten Mäder
2. Prof. Dr. Reinhard Neubert
3. Prof. Dr. Jürgen Siepmann

Halle (Saale), den 10.04.2006

**urn:nbn:de:gbv:3-000010359**

[<http://nbn-resolving.de/urn/resolver.pl?urn=nbn%3Ade%3Agbv%3A3-000010359>]

„Fantasie haben heißt nicht, sich etwas auszudenken, es heißt,  
sich aus den Dingen etwas zu machen.“

*Thomas Mann*

Dedicated to the ones I love.

# Contents

<b>1</b>	<b>Introduction</b>	<b>1</b>
1.1	Why nanocapsules?	1
1.2	Use of electron spin resonance spectroscopy (ESR) in pharmaceutical applications	7
1.2.1	Basics of ESR	7
1.2.2	Information provided by ESR spectra	11
1.2.3	Instrumentation	13
1.3	Research objectives	15
<b>2</b>	<b>Preparation and physico-chemical characterization of poly(D,L-lactide) and poly(ethylene glycol)-poly(D,L-lactide) nanocapsules</b>	<b>17</b>
2.1	Introduction	17
2.2	Materials	19
2.3	Methods	19
2.3.1	Nanocapsule preparation	19
2.3.2	Dynamic light scattering (PCS/3D-DLS)	22
2.3.3	Zeta potential measurements	24
2.3.4	Transmission electron microscopy (TEM)	24
2.3.5	Electron spin resonance (ESR) spectroscopy	25
2.3.5.1	In vitro determination of spin probe distribution	25
2.3.5.2	Dilution assay	25
2.3.5.3	External incorporation of spin probe to nanocapsules	25
2.3.5.4	Ascorbic acid reduction assay	26
2.3.6	Nuclear magnetic resonance (NMR) spectroscopy of protons	26
2.3.7	Small angle neutron scattering (SANS)	26
2.4	Results and discussion	28
2.4.1	Characterization of nanocapsules by TEM, PCS and $\zeta$ potential	28
2.4.2	Spin probe distribution in nanocapsules studied by ESR and NMR	30
2.4.3	ESR study on the dynamics of polymeric nanocapsules	36

2.4.4	Core-shell structure of poly(D,L-lactide) nanocapsules studied by SANS and DLS	44
2.5	Conclusion	53
3	<b>A novel coazervation-based process for the preparation of oil-loaded nanocapsules</b>	54
3.1	Introduction	54
3.2	Materials	57
3.3	Methods	59
3.3.1	Nanocapsule preparation	59
3.3.2	Experimental techniques	60
3.4	Results and discussion	61
3.4.1	Optimization of the production process	61
3.4.2	Layer formation followed by $\zeta$ potential measurements	64
3.4.3	Morphology of polyelectrolyte nanocapsules	65
3.5	Conclusion	67
4	<b>Development of an ESR online-method for the monitoring of in vitro fat digestion</b>	68
4.1	Introduction	68
4.2	Materials	70
4.3	Methods	70
4.3.1	In vitro digestion model	70
4.3.2	ESR-based digestion monitoring	70
4.4	Results and discussion	71
4.4.1	Monitoring of in vitro fat digestion by ESR	71
4.5	Conclusion	78
5	<b>Application of the ESR online-method for the monitoring of nanocapsule digestion</b>	79
5.1	Introduction	79
5.2	Materials and methods	81
5.3	Results and discussion	81
5.4	Conclusion	87

<b>6</b>	<b>Behaviour of nanocapsules in mice after oral application - an ex vivo ESR study</b>	<b>88</b>
6.1	Introduction	88
6.2	Materials and methods	90
6.2.1	Cell toxicity studies	90
6.2.2	Ex vivo ESR measurements	90
6.3	Results and discussion	92
6.3.1	Cell toxicity	93
6.3.2	Ex vivo ESR	93
6.4	Conclusion	98
<b>7</b>	<b>Summary and perspectives</b>	<b>99</b>
7.1	English version	99
7.2	German version	105
	<b>Literature</b>	<b>111</b>

## Abbreviations

BCS	Biopharmaceutical classification system
BS	Bile salts
CMC	Critical micelle concentration
CW	Continuous wave
DLS	Dynamic light scattering
EPR	Electron paramagnetic resonance
ESR	Electron spin resonance
GI	Gastrointestinal
HD-PMI I	2-Heptadecyl-2,3,4,5,5-pentamethylimidazolidine-1-oxyl
HD-PMI II	2-Heptadecyl-2,4,5,5-tetramethyl-3-imidazoline-1-oxyl
HLB	Hydrophilic lipophilic balance
HPLC	High performance layer chromatography
HPTLC	High performance thin-layer chromatography
i.m.	Intramuscular
i.v.	Intravenous
LBL	Layer-by-layer
Log P	Log octanol/water partition coefficient
LCT	Long chain triglycerides
MCT	Middle chain triglycerides
MF	Melamine formaldehyde
MPS	Mononuclear phagocytes system
NC	Nanocapsules
NE	Nanoemulsion
NIBS	Non-invasive backscattering
NLC	Nanostructured lipid carriers
NMR	Nuclear magnetic resonance
PCL	Poly( $\epsilon$ -caprolactone)
PDI	Polydispersity index
PE	Polyelectrolyte
PEG	Poly(ethylene glycol)
PEG-PLA	Poly(ethylene glycol)-Poly(D,L-lactide)
PIBCA	Poly(isobutylcyanoacrylate)

PLA	Poly(D,L-lactide)
PLGA	Poly(lactide-co-glycolide)
PSS	Poly(styrene sulfonate)
s.c.	Subcutaneous
SLN	Solid lipid nanoparticles
SEDDS	Self emulsifying drug delivery system
TEM	Transmission electron microscopy
SEM	Scanning electron microscopy
PCS	Photon correlation spectroscopy
SANS	Small angle neutron scattering

# 1 Introduction

## 1.1 Why nanocapsules?

Before asking ourselves about the need for nanocapsules we should start with the keynote of drug delivery and drug targeting. The fundamental idea traces back to Paul Ehrlich's vision of a "magic bullet" which transports the drug directly to the targeted organism bypassing healthy tissue. Although this exceptionally gifted scientist died ninety years ago, his idea is up-to-date.

When we combine Ehrlich's vision with the ideals of our age, the age of nanotechnology, we end up with nano-scaled carriers. Nano-scaled drug delivery systems, or as a synonym, colloidal drug carriers, are only defined by their submicron size. They are made from different materials and include a variety of structures [1].

A lot of research has been going on during the last two decades to develop adequate drug delivery systems for challenging drug candidates which belong to the classes II and IV of the biopharmaceutical classification system (BCS) [2-4]. There is a need for nano-sized carriers because often the therapeutic goal can not be achieved with micro-sized or even larger drug delivery systems. Regarding i.v. application, poor water solubility of injection candidates and active drug targeting are some of the tasks which can only be solved by colloidal carriers. Especially for the parenteral way of application, nanoparticles are superior to microparticles because they can be administered without any risk of embolia. Furthermore high food dependency or insufficient bioavailability after peroral application can only be circumvented by carriers in the nano-scale.

While intensive research lead to marketed products for microemulsions [5-13] (Sandimmun Optoral™, Neoral™), nanoemulsions [14-21] (Diazepam Lipuro™), mixed micelles [22-24] (Konakion MM™), nanosuspensions [25-30] (Rapamune™), liposomes [31-39] (AmBisome™) and liquid crystalline structures [40-42] (Elyzol™), solid lipid nanoparticles (SLN) [43-46], nanostructured lipid carriers (NLC) [46,47], nanospheres [48,49] and nanocapsules are still in the research state.

Nanocapsules are submicroscopic colloidal drug carriers which can morphologically be ranged between nanoemulsions and nanospheres (Figure 1.1). Compared to nanoemulsions, nanocapsules hold a solid shell around the oily core. The core can



also be aqueous as it is in the so-called polymersomes which are generated by vesicular self-assembly of polymers [50,51]. Nanospheres can be distinguished from nanocapsules by their completely solid character.

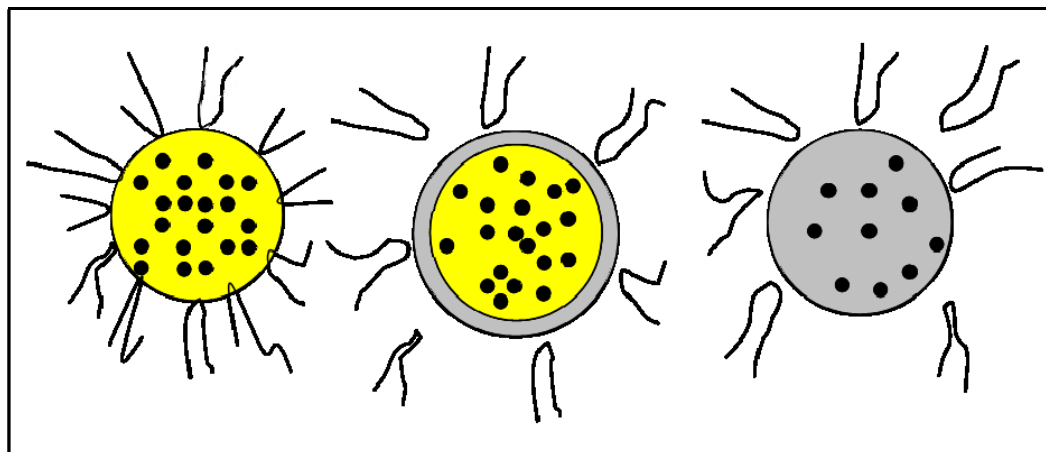


Figure 1.1 Schematic representation of a nanoemulsion droplet (left), nanocapsule (middle) and nanosphere (right).

In nanospheres the drug is dispersed within the polymer throughout the particle, in nanoemulsions and nanocapsules the drug is located in the oily moiety which is in the case of nanocapsules surrounded by a polymeric shell.

Preparative separation of nanocapsules from nanoemulsions and nanospheres can be carried out by centrifugation in a density gradient, whereas the density of nanocapsules was found to be intermediate between that of nanospheres and nanoemulsions [52].

In theory nanocapsules are superior to nanoemulsions because the shell prevents direct contact of the encapsulated drug with the environment. Therefore fast interactions between drug and physiological contents should be minimized and the drug may be better protected from degradation. Also irritation at the site of administration might be reduced. Furthermore the polymeric shell is responsible for the long term stability of the particles (storage). The advantage over nanospheres is a much higher degree of drug load. In physically loaded nanocapsules, the drug to polymer ratio can be as high as 5:1, when the core consists of pure drug, while this ratio is usually around 1:10 for nanospheres [53]. Another advantage is their low polymer content compared to nanospheres. It is also beneficial that a burst effect may be avoided by incorporating the drug in a cavity. Besides nanoemulsions, nanocapsules compete with lipid-based nanocarriers like SLN and NLC (oil-loaded SLN). Though for both systems nearly 100% incorporation

rate, controlled release and protection from the outer environment had been claimed [43,54-57], former [58-60] and recent studies [46] showed fundamental problems within these formulations. For both systems missing protection from the outer environment and low incorporation capacities as well as poor long-term stability (gelation, particle growth) were found. These refuting findings are in accordance with physical laws, e.g. crystalline solid lipids do not tend to incorporate large amounts of foreign molecules or controlled release cannot be achieved when diffusion paths are in the nanometer range. Therefore SLN and NLC are not really competitors to nanocapsules. Concerning peroral application, the incorporation rates are too low and particle growth and platelet shape are a risk for the intravenous route.

When regarding the oral administration of nanocapsules, they can be classified after Pouton [61] as lipid delivery systems, which generally consist of a drug dissolved in a blend of two or more excipients, which may be triglyceride oils, partial glycerides, lipophilic or hydrophilic surfactants or co-surfactants [61]. Lipid formulations are pharmaceutically attractive due to their ability to keep hydrophobic drugs in a dissolved state throughout their transit through the gastrointestinal (GI) tract. Thereby a slow dissolution step is avoided. By presenting the drug as a solubilisate within a colloidal dispersion the availability of the drug for absorption can be enhanced further leading to improved bioavailability. The group of Pouton [62] developed a simple classification system for lipid formulations for oral administration of drugs based on the polarity of the excipients used (Table 1.1).

Table 1.1 Classification system of liquid formulations according to Pouton [61].

	<i>Increasing hydrophilic content →</i>			
	Type I	Type II	Type IIIA	Type IIIB
Typical composition (%)				
<i>Triglycerides or mixed glycerides</i>	100	40-80	40-80	<20
<i>Surfactants</i>	-	20-60 (HLB<12)	20-40 (HLB>11)	20-50 (HLB>11)
<i>Hydrophilic cosolvents</i>	-	-	0-40	20-50
Particle size of dispersion (nm)	Coarse	100-250	100-250	50-100
Significance of aqueous dilution	Limited importance	Solvent capacity unaffected	Some loss of solvent capacity	Significant phase changes and potential loss of solvent capacity
Significance of digestibility	Crucial requirement	Not crucial but likely to occur	Not crucial but may be inhibited	Not required and not likely to occur

Formulations which comprise drug dissolved in triglycerides and/or mixed glycerides are classified as type I, the so-called non-emulsifying drug delivery systems. Type II systems contain an additional lipophilic surfactant (HLB<12) which promotes emulsification and improves solvent capacity of formulations. These systems are known as self-emulsifying drug delivery systems (SEDDS). In addition to the already mentioned excipients, type III systems include water-soluble components (hydrophilic surfactants with a HLB>11 and/or water-soluble co-solvents as propylene glycol, poly(ethylene glycol) or ethanol. Type IIIB can be distinguished from type IIIA by its very hydrophilic properties. Due to very small particle sizes of the resulting dispersions type III systems are named "self-microemulsifying drug delivery systems", with Neoral™ being a prominent representative. Depending on the different types of lipid formulations, aqueous dilution and digestion have significant influence on the bioavailability of incorporated drugs. In general the highly lipophilic formulations are dependent on digestibility whereas the highly hydrophilic "lipid" formulations are sensitive to dilution.

From the viewpoint of composition, nanocapsules, which comprise an oily core composed of triglycerides, can be classified as a type I lipid system. Taking fat digestion into consideration, the polymer shell of nanocapsules might partly protect the oily core before digestion. This might lead to an uptake of entire nanocapsules from the GI tract. Although this happens to a certain extent, the

availability of the majority of encapsulated drug will depend on digestion, which again follows type I in the lipid classification system. On the other hand nanocapsule dispersions have mean particle sizes of approximately 200 nm which are typical for type II or III. Therefore nanocapsules can not clearly be classified by Pouton's system.

Parenteral application of nanocapsules aims at the active targeting to specific cells within the vasculature. In the future this goal might be achieved by tailored modification of the polymer shell.

Most of the literature concerning nanocapsules deals with oil-containing nanocapsules but nanocapsules with aqueous cores are published as well [63]. The first oil-containing nanocapsules, prepared in 1986, were proposed as a new type of vesicular colloidal polymeric drug carrier [64]. They were prepared by interfacial polymerisation of alkylcyanoacrylate [65]. The disadvantage of this method is the probable presence of residual, potentially toxic monomers or oligomers.

Two years later, in 1988, Fessi et al. [66,67] presented a novel procedure for the preparation of biodegradable and excretable nanocapsules by interfacial deposition of a preformed polymer following solvent displacement.

Due to its simplicity and robustness this method has been applied by several groups for the encapsulation of lipophilic substances [68-70] making use of biodegradable polymers such as poly(D,L-lactide) [67,70], poly(D,L-lactide-co-glycolide) [71,72], poly( $\epsilon$ -caprolactone) [73,74] and poly(ethylene glycol) surface-modified poly(D,L-lactide) [75]. In 1998 Quintanar-Guerrero et al. [52] presented a new process for the preparation of nanocapsules based on an emulsification-diffusion technique.

Another approach is the inversion-based process for the preparation of lipid nanocarriers [76-79] though it is the question if lecithin stabilized oil droplets should be termed nanocapsule or nanoemulsion. A new type of designer capsule prepared via layer-by-layer self-assembly of oppositely charged polyelectrolytes [80-82] was introduced by Möhwald's group and will be discussed in detail in chapter 3.

Approaches to tune the permeability of polymer shells to achieve controlled release have not been successful for nanocapsules produced by polymer deposition so far. Moreover it is claimed that the rate of diffusion of the drug through the thin polymeric barrier does not seem to be a limiting factor, nor does the nature of the

polymeric wall [83]. Benoit and his group [77] have shown sustained release properties for amiodarone from lipid nanocapsules produced by the inversion-based process. Antipov [84] summarized how permeability of polyelectrolyte multilayer capsules can be tuned leading to controlled release. Though it is out of the question that release from 18-layered capsules within 10 minutes can be called delayed release. Xing et al. [85] recently published sustained release of capsaicin from polyelectrolyte nanocapsules prepared by complex coazervation of gelatine, acacia and tannin.

Research also focused on stimuli-responsive capsules. Thermosensitive nanocapsules based on poly(N-isopropyl acrylamide) have been described recently [86]. Möhwald's group [80] and Sauer et al. [87] published pH-sensitive nanocapsules based on polyelectrolytes.

After systemic administration, conventional nanoparticles are rapidly opsonized and cleared by macrophages of the mononuclear phagocytes system (MPS) leading to higher concentrations of the encapsulated drug in liver, spleen and lung [88,89]. To overcome the recognition of nanocapsules by the mononuclear phagocyte system (MPS) Barratt's group [75] developed "Stealth" nanocapsules which are "invisible" to macrophages. This was achieved with surface-modified nanocapsules from poly(D,L-lactide-)-poly(ethylene glycol) diblock copolymers which provide a "cloud" of hydrophilic chains at the particle surface and thereby prevent opsonization and recognition by macrophages.

Mosqueira et al. [75] showed that covalently attached PEG chains can substantially reduce nanocapsule clearance from the blood compartment after i.v. administration and alter their biodistribution in mice.

Active targeting [90], where ligand decoration of nanocarriers allows targeting to specific cells within the vasculature, has not yet been successfully established for nanocapsules. Though for nanospheres it was shown that folate-conjugation of the carriers led to selective targeting towards cancer cells which overexpress folate receptors on their surface [91,92]. The idea of functionalized nanocapsule surfaces is patented by Weber et al. [93]. Integrins as ligands for gastrointestinal, renal, biliary and pulmonary targeting are suggested.

## 1.2 Use of electron spin resonance spectroscopy (ESR) in pharmaceutical applications

Electron spin resonance spectroscopy (ESR), also known as electron paramagnetic resonance spectroscopy (EPR), is based on the interaction of electron spins with an applied magnetic field.

Therefore ESR measurements require materials with unpaired electrons. Natively paramagnetic molecules can be found as free radicals or metal centres. Since in the normal case pharmaceutical formulations contain neither of them, paramagnetic molecules, the so-called spin probes, must be incorporated into the system of interest when ESR measurements are performed. This can be done by physical incorporation. The most widely used spin probes are stable nitroxide radicals. Another possibility is the covalent coupling of paramagnetic species to the molecules of interest which is called spin labelling. Gamma irradiation of crystalline drugs or polymers can also lead to the formation of stable radicals, which can be used as endogenous paramagnetic species [94,95].

ESR offers the unique opportunity to perform non-invasive studies in non-transparent samples both in vitro and in vivo and has entered the fields of medicine and pharmacy during the last decade [94,96-102]. In detail ESR was used to seize the microviscosity and micropolarity of systems [103], to characterize colloidal drug carriers [104], to monitor the microacidity in biodegradable polymers [103] and to follow drug release mechanisms [105].

### 1.2.1. Basics of ESR

As the name suggests *electron spin resonance spectroscopy* is a form of absorption *spectroscopy* where the transition of *electron spins* from the ground to the excited level is induced by a quantized energy of electromagnetic radiation which satisfies the *resonance* condition.

Unpaired electrons spin around their own axis and thereby act like compass needles. In a magnetic field both electron spins and compass needles can take different orientations which are presented by different energy levels (Figure 1.2).

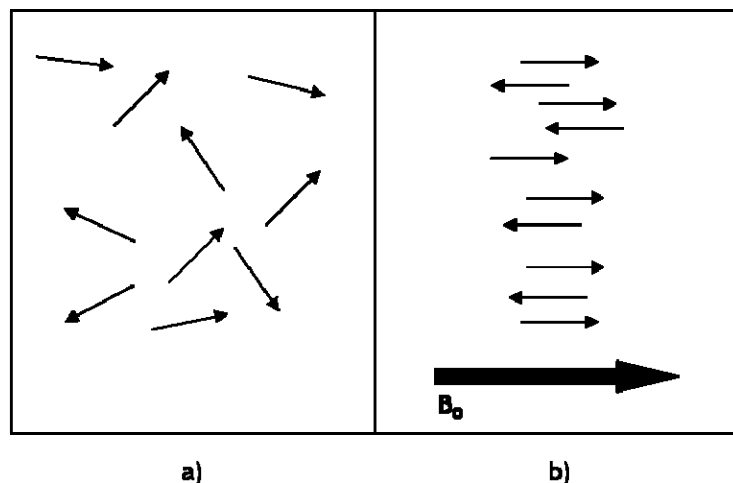


Figure 1.2 Severely simplified depiction of spin orientation  
(a) Random spin orientation in absence of magnetic field  
(b) Parallel and antiparallel spin alignment in an external magnetic field  $B_0$ .

But unlike compass needles the electron spin can not take optional orientations in the magnetic field because it is quantized with the values  $+1/2$  and  $-1/2$ , the so-called electron spin quantum numbers.

When an external magnetic field is applied to unpaired electrons, they can either align with this field which is the ground state ( $-1/2$ ) or they may be forced into the opposite direction, the excited state ( $+1/2$ ) (Figure 1.3). This phenomenon is known as Zeeman splitting.

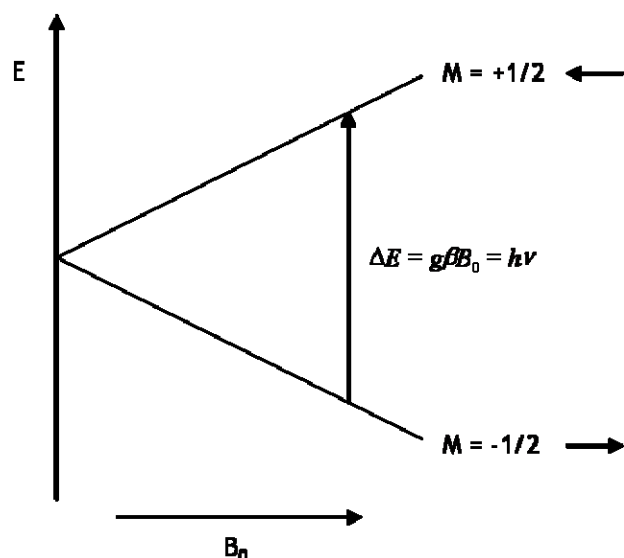


Figure 1.3 Energy levels for an electron ( $S = 1/2$ ) in an applied magnetic field (Zeeman effect). Transitions between both spin states can be induced by electromagnetic radiation when the irradiated energy equals the energy difference  $\Delta E$ .

The transition from the ground to the excited state can be induced by electromagnetic radiation when the resonance condition according to Planck is satisfied. This is the case when the radiated energy ( $h\nu$ ), where  $h$  is the Planck's constant, is equal to the energy which is necessary for the transition from the lower to the higher energy level ( $\Delta E$ )

$$\Delta E = h\nu.$$

The energy difference  $\Delta E$ , which is dependent on the strength of the magnetic field  $B_0$  is given by:

$$\Delta E = g\beta B_0$$

where  $g$  is the spectroscopic splitting factor, the so-called "g-factor", which is close to 2 for free radicals, and  $\beta$  is the Bohr magneton, a fundamental physical constant.

By equating the two given energies

$$\Delta E = g\beta B_0 = h\nu,$$

the frequency of the radiation needed for the transition from the ground to the excited state can be calculated as follows:

$$\nu = \frac{\Delta E}{h} = g\beta B_0 \text{ or}$$

$$B_0 = \frac{\nu h}{g\beta}.$$



As the magnetic field typically used in X-band spectrometers is 3400 G (0.34 T), the corresponding resonance frequency is 9.5 GHz. Radiation in the microwave range, precisely of 32 mm, has to be applied to the sample to induce spin transition.

In nitroxide radicals, electrons are often located in the vicinity of nitrogen and the unpaired protons of isotope  $^{14}\text{N}$ , with 99.64% most abundant in nature, also spin. This alters the strength of the magnetic field experienced by the electron. Like the electron spin, the nuclear spin is quantized.  $^{14}\text{N}$  has the nuclear spin quantum numbers -1, 0 and +1. As a consequence the magnetic field seen by both orientations for the unpaired electron ( $+1/2$  and  $-1/2$ ) in the vicinity of nitrogen is shifted. The local magnetic field will be increased when the nucleus spin (+1) is in the direction of the external magnetic field and vice versa (-1). It can also be left unchanged (0) when no coupling occurs. As a consequence microwave energy can be absorbed at three different levels instead of only one leading to an ESR spectrum with a hyperfine structure of three lines (Figure 1.4).

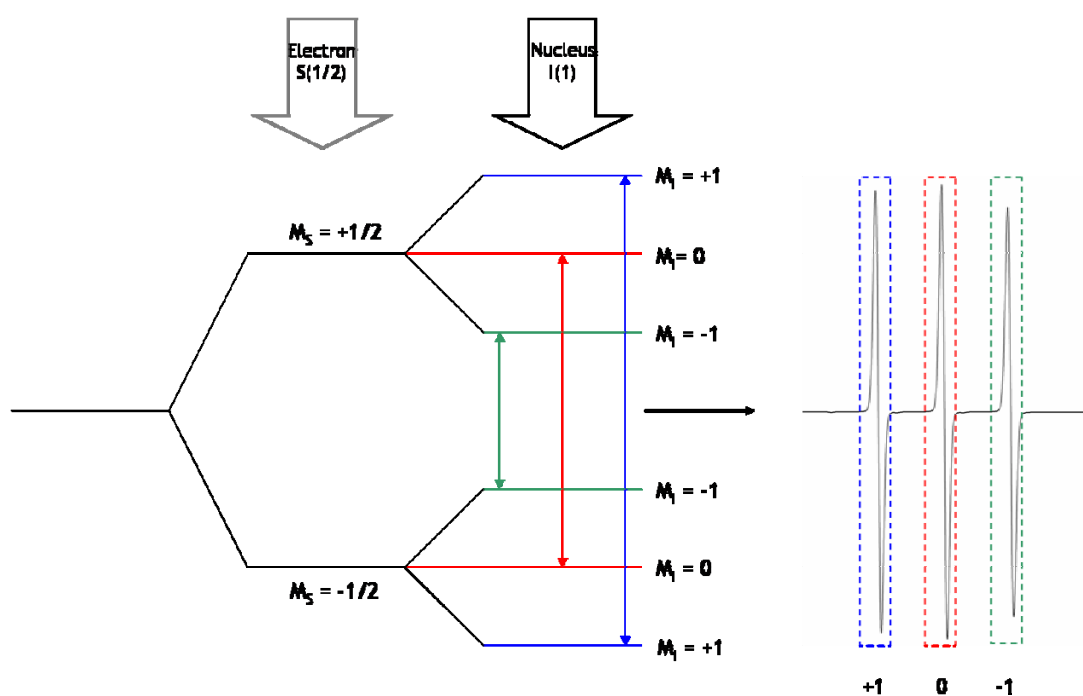


Figure 1.4 The energy levels and transitions for a nitroxide radical ( $S=1/2$  and  $I=1$ ).

The splitting of the single electron resonance line into three lines due to the interaction with the nucleus is called *hyperfine splitting* or *hyperfine coupling*.

Electrons in the excited state will return to the ground state with time. During this relaxation process released energy can be either delivered to the environment or

to other paramagnetic molecules. The first case is known as spin-lattice relaxation  $T_1$ , the second case as spin-spin relaxation  $T_2$ .

### 1.2.2 Information provided by ESR spectra

Stable nitroxide spin probes are the most widely used molecules for ESR measurements in systems that do not naturally contain paramagnetic species. Incorporation of the spin probes into systems allows the measurement of their molecular mobility (*microviscosity*) and the *micropolarity* of their molecular environment. How this can be done is described in detail in the next paragraph.

The electron density of nitroxide radicals can be described by two mesomeric forms (Figure 1.5).

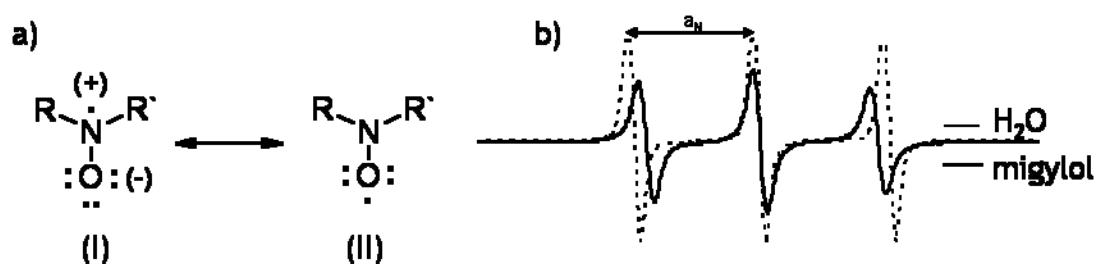


Figure 1.5 Principles of polarity measurements by ESR

(a) Mesomeric forms (I+II) of nitroxyl radical

(b) Hyperfine splitting constant ( $a_N$ ) of nitroxyl radicals in polar/apolar liquids.

Only the nuclear spin of the nitrogen of mesomeric form I can contribute to the hyperfine splitting of the ESR signal because of the missing nuclear spin of oxygen. The *hyperfine coupling constant*  $a_N$  is the first important information that can be retrieved from the ESR spectrum. It is expressed by the distance between the single lines, which is given in milliTesla (mT) or Gauss (G) whereas 1 mT equals 10 G. Since polar liquids favor the existence of mesomeric form I,  $H_2O$  generates higher hyperfine coupling constants than apolar environments like Miglyol (Figure 1.5). Therefore  $a_N$  is a dimension for the *polarity* of the environment around the spin probes.

The second important information that is given by the ESR spectrum is the line width, which is a sensitive parameter to the *microviscosity*. Precondition is the anisotropy of the hyperfine splitting. The reason for this anisotropy lies in the location of the electron that spins.

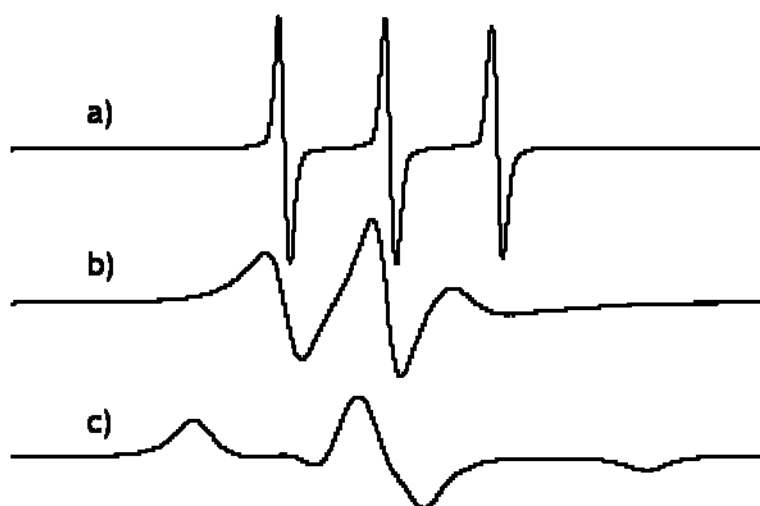


Figure 1.6 X-Band ESR spectra of Tempol in

a)  $\text{H}_2\text{O}$ , 22°C

b) glycerol, 22°C

c) glycerol, -50°C

reflecting the sensitivity of the line shape to the viscosity of the microenvironment.

When this free electron is located in the N atom it occupies the p orbital which is laying in the z direction. Therefore the highest splitting of the peak will occur when the Z orbital is parallel to the external magnetic field leading to a direction-depending anisotropy of the hyperfine coupling constant. This effect is not always visible. It can only be seen in immobilized spectra, where the spectrum is a supercomposition of all three possible orientations (z, y and x) resulting in a spectrum with broad lines (Figure 1.6 b+c). In media of low viscosity like water the spin probe rotates so fast that the rotations around the x, y and z axes can not be distinguished and the spectrum is an averaging of the three contributions. In opposite to immobile environments this results in a spectrum with three lines of almost the same peak-to-peak distances and amplitudes (Figure 1.6 a).

Line broadening can also occur when the spin probe concentration in a sample is very high leading to spin-spin exchange. But this effect can be distinguished from line broadening due to viscous media by the number of affected peaks. Spin-spin exchange has an influence on all lines. Upon viscosity-induced line broadening the high field line of nitroxide spectra is most affected, followed by the low field and central line [106].

The third information which can be obtained by the ESR spectrum is the line *amplitude* which gives information on the *concentration* of the spin probe in diluted systems.

### 1.2.3 Instrumentation

Most commonly continuous wave (CW) ESR equipments are used. Continuous wave means that the magnetic field is swept at a constant microwave frequency. A second scenario is thinkable where the microwave is swept at a constant magnetic field but this is technically much more complicated.

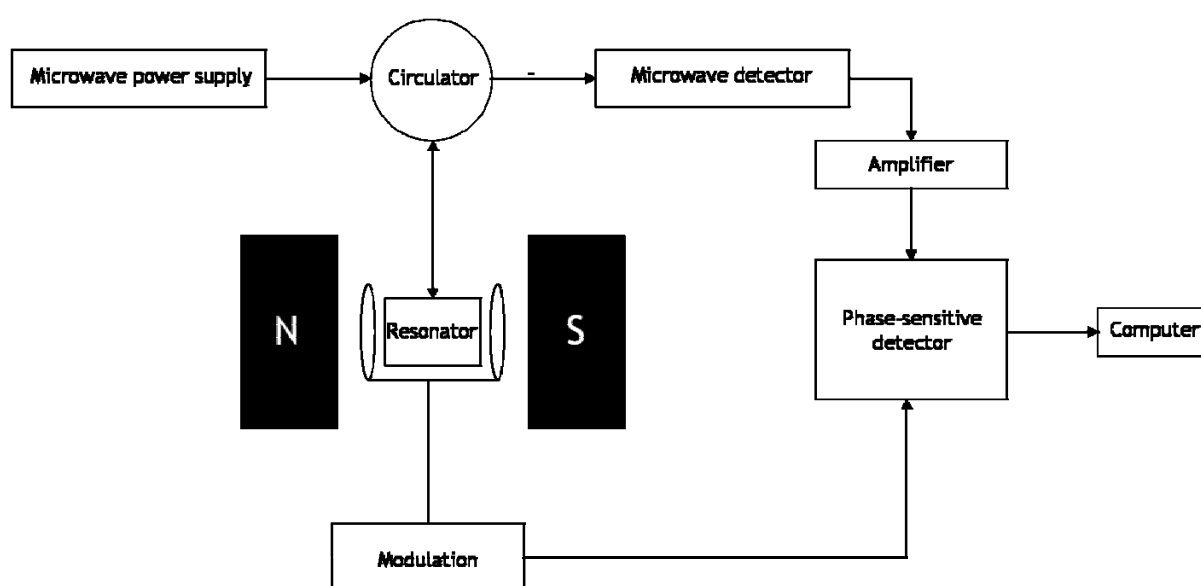


Figure 1.7 Simplified depiction of the construction of an ESR spectrometer.

The sample containing the unpaired electrons is placed in the cavity of the resonator. Microwave power is radiated from the microwave bridge into the resonator. Meanwhile the magnetic field is swept continuously and the amplitude of the external field is modulated at 100 KHz for improved sensitivity. When the resonance condition is fulfilled the sample absorbs a quantity of energy which is detected as a loss of energy by the receiver diode of the microwave bridge. This change in the amplitude of the absorption signal is detected phase-sensitive.

Therefore ESR signals are not detected as absorption signals but as the first derivative of it.

For pharmaceutical and medical research two different ESR standard equipments are of interest. The so called X and L bands, which originally come from the radar technology, can be classified by their resonance frequency which is 9-10 GHz for X band and 1-2 GHz for L band. Due to the higher frequency X band shows a higher sensitivity. On the other hand the penetration depth of the microwave radiation, which is inversely dependent on the frequency, is higher for L band equipments. Also in water-containing samples like biological samples X band frequencies are absorbed to a greater degree than the lower L band frequencies. Therefore only L band spectrometers are suitable for in vivo measurements on small animals.

### 1.3 Research objectives

The present thesis deals with one particular class of submicrometer colloidal carriers: nanocapsules. Though the number of publications dealing with nanoemulsions and nanospheres is much higher up to now, nanocapsules have attracted increased interest during the last years due to their unique combination of high solubilisation (liquid core) and high stability (solid shell). The shell offers the theoretical potential to control release, to protect encapsulated drugs from the environment and vice versa and to target the capsule *in vivo*. However, it has been observed that the diffusion coefficient of encapsulated drugs was not reduced through the shell [71,83]. Therefore this work focuses on the physico-chemical characterization of nanocapsules to gain a better understanding on these colloidal drug carrier systems. Advantages and disadvantages of nanocapsules as carrier systems for challenging drug candidates will be examined. Studies focus on the oral way of application. Detailed knowledge will be gained concerning the

- Drug localization in nanocapsule dispersions
- Influence of the shell on the partition coefficient of encapsulated drugs
- Behaviour of nanocapsules upon dilution
- Accessibility of encapsulated drug by the surrounding aqueous environment
- Quantitative determination of the shell thickness of nanocapsules
- Quantitative determination of the core-shell structure of nanocapsules
- Development of a new production method for polyelectrolyte nanocapsules
- Behaviour of nanocapsules in intestinal fluids (*in vitro*)
- Behaviour of cells upon nanocapsule contact
- Behaviour of nanocapsules in mice after oral application (*ex vivo*).

A detailed characterization of nanocapsules is difficult because submicron systems can not be studied with conventional analytical methods. Therefore electron spin resonance spectroscopy (ESR), small angle neutron scattering (SANS), transmission electron microscopy (TEM), dynamic light scattering (DLS), nuclear magnetic resonance (NMR) and ▫ potential measurements were combined to receive a detailed picture on nanocapsules. Since little is known about the behaviour of nanocapsules in biological environment, e.g. in the presence of digestion enzymes,

a method was developed to study the fate of nanocapsules in simulated intestinal fluids by coupling the non-invasive ESR technique with an in vitro digestion assay.

## 2 Preparation and physico-chemical characterization of poly(D,L-lactide) and poly(ethylene glycol)-poly(D,L-lactide) nanocapsules

### 2.1 Introduction

Both physical and technical parameters were studied for the different nanocapsule preparation methods to optimize formulations. Characterization of nanocapsules has been performed by various groups. Information on the morphology of nanocapsules can be gained by transmission electron microscopy (TEM) [67,70,72,86,107,108] or scanning electron microscopy (SEM) [52,63,71] TEM after freeze-fracture gives the most useful information about nanocapsule structures [109]. Although electron microscopy gives some information about nanocapsule size, the particle size and size distribution are usually obtained by photon correlation spectroscopy (PCS), which is a dynamic light scattering (DLS) technique. Besides particle size and size distribution,  $\zeta$  potential measurements give useful information about the stability of nanocapsules. High  $\zeta$  potentials lead to repulsion between single nanocapsules and therefore to more stable dispersions. Density measurements can be used to distinguish between nanocapsules, nanospheres and nanoemulsions [52]. Another important property is the encapsulation efficiency of nanocapsules. For this purpose nanocapsules are first separated from the continuous phase by size exclusion chromatography or ultrafiltration and then the drug concentration in the supernatant is measured by HPLC [109,110].

Studies have also been performed regarding the in vitro drug release kinetics of nanocapsules [71,74] and their in vivo fate following parenteral administration [75]. For in vitro release profiles the "bulk-equilibrium reverse dialysis bag technique" [111] is suitable where the nanocapsule dispersion is placed directly into a stirred sink solution and the amount of released drug is measured in a dialysis bag which is only accessible for dissolved drug molecules.

Despite all efforts, this field of research is still far from commercial application.

The difficulty is to control drug release by the design of the shell which plays a predominant role for the protection of incorporated drugs as well as for the release profile.



Although the thickness of the polymer wall is thought to be important, no appropriate values exist. Cauchetier et al. [74] calculated the wall thickness of poly( $\epsilon$ -caprolactone), poly(D,L-lactide) and poly(D,L-lactide-co-glycolide) nanocapsules with 20 nm. Several groups estimated values of 10 nm using transmission electron microscopy (TEM) [67,107,108,112). Though one has to take into account that electron microscopy shows single particles and does not give statistically averaged values.

Besides uncertainties concerning the shell structure, the characterization of nanocapsules is not a trivial task due to their submicron size range and size-dependent changes of their physico-chemical properties. Furthermore the coexistence of several colloidal species might complicate the characterization. Especially the knowledge about the microenvironment and dynamics of these systems is still very limited. Although the permeability of capsule shells and their capability of molecular adsorption to the capsules surface have been investigated by nuclear magnetic resonance spectroscopy for alkylcyanoacrylate nanocapsules [113-115], there is no comparable knowledge present for biodegradable polymeric nanocapsules of pharmaceutical interest.

In this chapter the preparation and physico-chemical characterization of poly(D,L-lactide) and poly(ethylene glycol)-poly(D,L-lactide) nanocapsules will be discussed. The main aim of this study was to receive a better understanding on the inner structure and dynamic phenomena of nanocapsules by using SANS and ESR. SANS studies with additional information from DLS and TEM have been used to obtain a detailed picture on the core shell structure of nanocapsules.

By means of ESR and  $^1\text{H}$ -NMR spectroscopy the molecular environment (mobility, polarity) of paramagnetic model drugs inside the nanocapsules was investigated. Furthermore information on dynamical processes during dilution and the resistance of the incorporated spin probe to reduction with ascorbic acid depending on different shell materials was collected by ESR.

## 2.2 Materials

MePEG2kDaPLA20kDa (PEG-PLA-10%) and MePEG5kDaPLA20kDa (PEG-PLA-25%) were kindly provided by Prof. A. Göpferich, University of Regensburg. Poly(D,L-lactide) PLA50 of MW 9 kDa (PLA) was obtained from Boehringer Ingelheim Pharma GmbH & Co. KG, Germany. Miglyol 812 was purchased from Caelo, Germany. Poloxamer 188 (Lutrol F 68) was purchased from BASF AG, Germany. TEMPOL-benzoate (4-hydroxy-TEMPO-benzoate, 4-benzoyloxy-2,2,6,6-tetramethyl-piperidine-1-oxyl; TB) was obtained from Aldrich Chem. Co, USA.

2-Heptadecyl-2,3,4,5,5-pentamethylimidazolidine-1-oxyl and 2-Heptadecyl-2,4,5,5-tetramethyl-3-imidazoline-1-oxyl (HD-PMI) was obtained by Prof. V.V. Khramtsov, Institute of Chemical Kinetics and Combustion, Novosibirsk, Russia. L(+) ascorbic acid sodium salt was purchased from Sigma-Aldrich, Steinheim, Germany. Deuterium oxide (D<sub>2</sub>O), 99.9% D, was purchased from Merck KGaA, Germany.

## 2.3 Methods

### 2.3.1 Nanocapsule preparation

Nanocapsules were prepared by the method described by Fessi et al. [67] based on interfacial deposition of preformed polymer after solvent displacement. Briefly, in this process, polymer, oil, drug and optionally a lipophilic stabilizer are dissolved in a semi-polar water-miscible solvent (e.g. acetone or ethanol) which is poured or injected into an aqueous solution containing a hydrophilic stabilizer (e.g. Poloxamer 188 or poly(vinyl alcohol)). Nanocapsules are formed instantaneously by rapid diffusion of the solvent into the water phase. In a subsequent step the solvent is eliminated from the suspension under reduced pressure.

PLA, PEG-PLA-10% and PEG-PLA-20% were used as coating polymers and Miglyol as the oily phase. The chemical structures of PLA and PEG-PLA are shown in Figure 2.1.

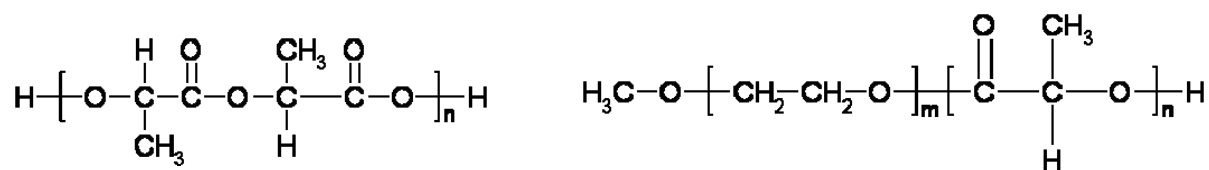


Figure 2.1 Chemical structures of PLA (left) and MePEG-PLA (right).

Polymer and oil, and if required for ESR measurements, the lipophilic spin probes TEMPOL-benzoate (TB), 2-Heptadecyl-2,3,4,5,5-pentamethylimidazolidine-1-oxyl or 2-Heptadecyl-2,4,5,5-tetramethyl-3-imidazoline-1-oxyl (HD-PMI) were dissolved in acetone.

10 ml of the acetone solution (containing the polymer, Miglyol and if required the spin probe) were injected into 20 ml of external aqueous phase, with or without Poloxamer 188 as a hydrophilic surfactant, under moderate agitation. The solvents were evaporated to 10 ml under reduced pressure. An overview of all investigated formulations is given in Table 2.1.

Table 2.1 Sample compositions in the final volume.

sample nr.	sample	% shell polymer (w/w)	% Miglyol (w/w)	% Poloxamer (w/w)	concentration spin probe per liter
1	PLA-NC	0.6	2.5	0.3	0.1 mmol
2	PLA-NC	0.6	2.5	0.6	0.1 mmol
3	PEG-PLA-10%-NC	0.6	2.5	0	0.1 mmol
4	PEG-PLA-10%-NC	0.6	2.5	0.3	0.1 mmol
5	PEG-PLA-10%-NC	0.6	2.5	0.6	0.1 mmol
6	PEG-PLA-25%-NC	0.6	2.5	0	0.1 mmol
7	PEG-PLA-25%-NC	0.6	2.5	0.3	0.1 mmol
8	Poloxamer-NE	0	2.5	2.5	0.1 mmol

The “interfacial deposition of preformed polymer after solvent displacement” technique [66,67] for nanocapsule preparation was used because it is known for its simplicity and robustness at small scale [72,116]. In the literature there are several reviews [117,118] and articles which discuss the spontaneous emulsification process that leads to nanoparticle formation using explanations such as Marangoni effect [67,119]. Only recently the group of Katz [120,121] provided new insights into the physical phenomenon behind this method. They named this spontaneous emulsification phenomenon Ouzo effect, derived from the aperitif, which is an ethanol-water extract of anis seeds containing the water-insoluble substance

anethol. Upon dilution with water Ouzo becomes cloudy and remains so for a long time. This general phenomenon can occur upon mixing large amounts of water with almost any solution consisting of a small concentration of oil in a hydrophilic solvent over a small range of concentrations.

In Figure 2.2 a schematic description of the Ouzo effect is given.

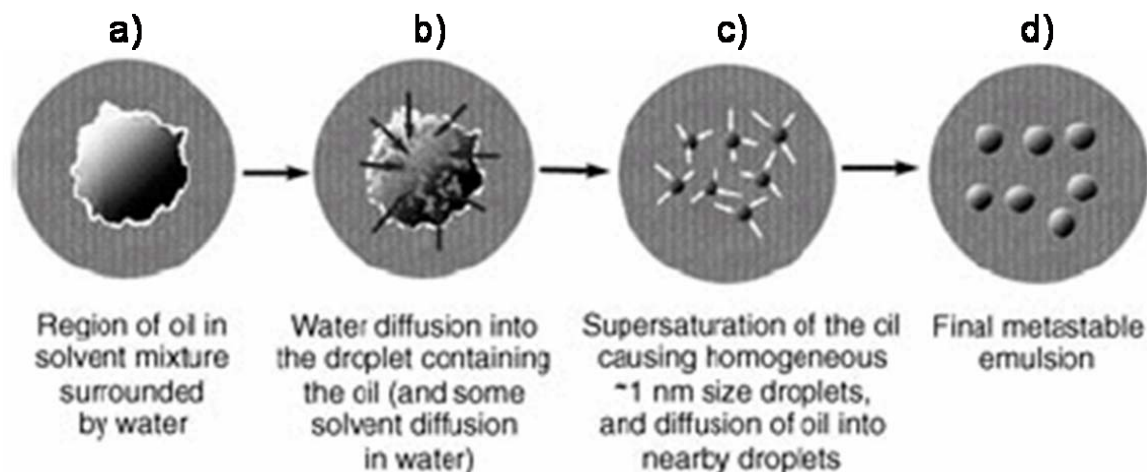


Figure 2.2 Schematic of the liquid-liquid nucleation process or Ouzo effect (from [121]).

The solvent phase, containing the water-immiscible oil, is poured into the aqueous phase, which may contain a surfactant (Figure 2.2 a). Upon diffusion of water into the oil-containing solvent droplet (b) supersaturation of oil is induced and droplet nucleation (c) occurs. Droplet growth ends when the aqueous phase is no longer supersaturated with the oil (d).

These metastable dispersions can be generated when mixing occurs in a special region in the phase diagram of water, the organic solvent and oil. Upon diffusion of the organic solvent into the water phase, the polymer diffuses with the organic solvent and is stranded at the interface between oil and water forming an envelope around the oil droplet.

An oil-to-preformed-polymer ratio of approximately 3:1 was chosen because preliminary tests with this ratio yielded the best results. Poloxamer 188 was used at the same concentration of the polymer or at half the concentration. Whereas the production of PEG-PLA nanocapsules in the absence of Poloxamer was successful, though the polydispersity index was high compared to the presence of Poloxamer, this attempt failed for PLA nanocapsules. The chosen compositions lack lecithin as a stabilizer which is commonly used in nanoemulsion and nanocapsule

preparations [70]. This decision was made on two accounts. One reason was to avoid the coexistence of liposomes. Groves and colleagues [122] reported that liposomal structures are normally present in phospholipid-stabilized emulsions and Mosqueira and colleagues [70] identified liposomes in addition to nanocapsules on TEM micrographs. Since the intention of this study was to get a deep understanding of nanocapsules by ESR and SANS, an easy model system was needed. The coexistence of other colloidal species should be avoided. A second aim was to achieve a higher stability of nanocapsules in physiological media by omitting lecithin, which is known to be sensitive for hydrolysis and thereby forms the haemolytic product lysolecithin [123,124].

Nanoemulsions composed of 2.5% (v/v) Miglyol, 2.5% (w/v) Poloxamer 188 and water served as reference systems to nanocapsules.

Nanoemulsions were prepared by high pressure homogenization. Initially TB (0.1mM referring to the TB concentration in the final sample volume) was dissolved in Miglyol and heated to 80°C. The oily phase, which contained the spin probe, was added to the aqueous phase of the same temperature which contained 2.5% (w/v) of the hydrophilic stabilizer Poloxamer. An emulsion was formed using a rotor-stator mixer (Ultra turrax®, IKA® T18 basic, IKA®-Works, NC) for 120 s at 22.000 rpm. The emulsion was passed through a high pressure homogenizer (nG7400.270 P, Standsted Fluid Power Ltd., UK-Stansted) three times at 80°C and 500 bar.

Nanoemulsions were produced via high pressure homogenization at 80°C to obtain a system very similar to the examined nanocapsules but omitting the polymer wall. The Poloxamer concentration had to be increased from 0.3% for nanocapsules to 2.5% for nanoemulsions to stabilize these systems. Nanoemulsions were not produced by the solvent displacement method which was used for nanocapsule production because with this method lecithin is required for stable nanoemulsions.

### 2.3.2 Dynamic light scattering (PCS/3D-DLS)

For photon correlation spectroscopy (PCS) measurements, the non-invasive backscattering (NIBS, Malvern) technology was used, which suppresses multiple scattering in turbid colloidal suspensions.

Photon correlation spectroscopy is based on dynamic light scattering caused by Brownian movement of particles [125-127]. Diffusion of small isometric particles in

liquids is fast, causing faster fluctuations in the intensity of scattered light compared to big particles which diffuse more slowly. These intensity fluctuations are recorded in the PCS experiment. Autocorrelation analysis of the measured diffusion coefficients, under assumption of a spherical shape of the particles, yields a mean particle diameter which is expressed as z-average. The polydispersity index (PDI) provides information on the heterogeneity of the sample, whereas the PDI value can be connected with the polydispersity (in %) by the following equation:

$$\text{Polydispersity}(\%) = 100 * \sqrt{PDI} \text{ [128]}.$$

PCS measurements were performed at a scattering angle of 173° (Malvern HPPS, Malvern Instruments, UK). The nanocapsule dispersions, containing 2.5% (v/v) Miglyol, were measured without further dilution. Contributions from multiple scattering can be excluded because reference measurements of diluted samples were performed. Only SANS samples (sample 1, Table 2.1) were diluted to a Miglyol concentration of 1% (v/v) before measurements because that was the concentration for SANS measurements. The mean radius of the nanocapsules and size distribution of the colloidal systems were determined at 25°C. Measurements were done in triplicate. Data treatment was performed using the Malvern software. For comparison particle size measurements of the SANS samples (sample 1) were also performed using a 3D-DLS (LS Instruments GmbH, Fribourg, Switzerland). Here a DLS technique using cross-correlation schemes suppresses contributions from multiple scattering [129]. To get a better intercept in the DLS signal the sample was diluted to 0.33% (v/v) Miglyol, 0.08% (w/v) poly(D,L-lactide) and 0.12% (w/v) Poloxamer. Dynamic light scattering measurements with variable scattering angles from 20 -140° were carried out at 20°C. Cumulant analysis was applied to the cross correlation function in the same way as for the NIBS measurement to receive the hydrodynamic radius.

Since the aqueous dispersion medium of the nanocapsules contained Poloxamer, the given viscosity values for water were replaced by the Poloxamer solution values in the data analysis software.

The viscosity alteration of the Poloxamer solutions compared to pure water was considered for both methods. The viscosities for different Poloxamer solutions were determined by Ubbelohdeviscosimeter at 20 and 25 °C. The viscosity data are shown in Table 2.

Table 2.2 Viscosity values for different Poloxamer solutions.

concentration Poloxamer [w/v]	viscosity at 25 °C [cP]	viscosity at 20 °C [cP]
0.12	0.9035	1.015
0.3	0.9346	-
0.6	0.9941	-

### 2.3.3 Zeta potential measurements

The  $\zeta$  potential was measured with a Zetasizer Nano ZS and a ZetaSizer 3000HS (Malvern Instruments, UK). All samples were diluted (1:1) with a solution of KCl (0.002 mol/l). The samples were measured at 25°C and 30 zeta runs were performed per sample at the Zetasizer Nano ZS. When using the ZetaSizer 3000HS four measurements with automatic measurement duration were carried out per sample.

### 2.3.4 Transmission electron microscopy (TEM)

For transmission electron microscopy nanocapsules were freeze-fixed using a propane jet-freeze device JFD 030 (BAL-TEC, Balzers, Liechtenstein). Afterwards the samples were freeze-fractured and freeze-etched (90 s; -110 °C) with a freeze-etching system BAF 060 (BAL-TEC, Balzers, Liechtenstein). The surfaces were shadowed with platinum to produce good topographic contrast (2 nm layer, shadowing angle 45°) and subsequently with carbon to stabilize the ultra-thin metal film (20 nm layer, shadowing angle 90°). The replica were floated in sodium chloride (4 % NaCl; Roth, Karlsruhe, Germany) for 30 minutes, rinsed in distilled water (10 minutes), washed in 30% acetone (Roth, Karlsruhe, Germany) for 30 minutes and rinsed again in distilled water (10 minutes). Thereafter the replica were mounted on grids and observed with a transmission electron microscope (TEM 900, Carl Zeiss SMT, Oberkochen) operating at 80 kV. Pictures were taken with a Variospeed SSCCD camera SM-1k-120 (TRS, Moorenweis, Germany).

### 2.3.5 Electron spin resonance (ESR) spectroscopy

#### 2.3.5.1 In vitro determination of spin probe distribution

For ESR measurements undiluted aqueous nanocapsule dispersions were used which contained 0.1 mM spin probe (referring to the final volume). An ESR spectrometer of 9.5 GHz (X-Band; Miniscope MS 200) from Magnettech (Berlin, Germany) was used, where the probe is examined inside a glass capillary. Measurements were conducted at room temperature with the following typical parameters: B<sub>0</sub> field: 335.4 mT; sweep: 10 mT (precisely 9.800 or 9.893 mT); modulation frequency: 100 kHz; microwave power: 20 mW; scan time: 30 s; modulation amplitude: 0.1 mT.

#### 2.3.5.2 Dilution assay

For dilution assays nanocapsule dispersions containing 0.1 mM spin probe were diluted with water in different ratios (1:1, 1:2, 1:3, 1:4). Immediately after dilution the samples were placed inside the ESR spectrometer and changes in the spectral shape were monitored for one hour.

Centrisat is a ready-made unit for the centrifugal ultrafiltration of volumes up to 2.5 ml. Ultrafiltration is carried out against the centrifugal force. Centrisat tubes are usually used for the separation of proteins from small molecules. 500 µl of PLA-NK (sample 1, Table 2.1) were diluted with 2000 µl of H<sub>2</sub>O. The 2500 µl of nanocapsule dilution were put into a Centrisart (Centrisart I, Sartorius, cut-off 300.000) tube and the diluted nanocapsule sample was concentrated to a volume of 500 µl. ESR measurements were performed from the undiluted nanocapsule dispersion, the diluted nanocapsule dispersion, the concentrated nanocapsule dispersion after centrifugation and from the filtrate.

#### 2.3.5.3 External incorporation of spin probe to nanocapsules

To study whether the spin probe was capable of penetrating from the aqueous environment through the nanocapsule wall into the oily core of the nanocapsule, spin-probe-free nanocapsule dispersions were prepared.

The appropriate volume of a TB stock solution in acetone was added to an empty test tube, acetone was evaporated and the TB-free nanocapsule dispersion was



added to the test tube. The tube was warmed up to 80°C for a few seconds. ESR spectra were recorded immediately.

#### 2.3.5.4 Ascorbic acid reduction assay

A reduction assay of the spin probe (0.1mM) in the samples was conducted by time-dependent ESR measurements after mixing (1:1 v/v) with 1.6 mM aqueous ascorbic acid sodium salt solution [104]. The chosen ascorbic acid concentration guaranteed a reduction speed which lead to quantifiable ESR spectra at the given times. The decrease of ESR signal intensity was calculated down to 10% only, because at lower intensities no proper simulation of the spectrum was possible because of an interfering spectrum of the ascorbic acid radical.

Simulation of the ESR spectra was performed by means of Public ESR Software Tools (P.E.S.T.) from National Institutes of Health (National Institute of Environmental Health Sciences, Research Triangle Park, NC 27709) [130]. The optimization method used was LMB1.

#### 2.3.6 Nuclear magnetic resonance (NMR) spectroscopy of protons

<sup>1</sup>H-NMR experiments were performed on a Bruker DRX 500 spectrometer (Bruker AG, Karlsruhe, Germany) with 500 MHz resonance frequency for protons. The experiments were run on the aqueous nanocapsule dispersions. D<sub>2</sub>O (150mg/sample) was used as an internal spin lock substance. The nanocapsule dispersions contained different concentrations (0, 1, 2 or 3 mM) of the spin probe TB. T<sub>1</sub> (spin-lattice relaxation) was measured using a saturation-recovery pulse sequence. T<sub>2</sub> was measured with a CPMG (Car-Purcell-Gill-Meiboom) pulse.

#### 2.3.7 Small angle neutron scattering (SANS)

Small angle neutron scattering (SANS) is a technique, where cold *neutrons* permeate materials and, when they hit upon nano-sized structures, they are *scattered* to *small angles*. From the scattering image the structures can be reconstructed. SANS allows the characterization of structures or objects in the nanometer scale, typically in the range between 1 nm and 200 nm. The information one can extract from SANS is primarily the average size, size distribution and spatial correlation of nanoscale structures, as well as shape and internal structure

of particles (e.g. core-shell structure). All in all, SANS is a valuable technique, widely used in many fields, to characterize particles (in solution or in bulk), clusters, (macro-) molecules, voids and precipitates in the nanometer size range.

SANS measurements were carried out at the SANS facility of SINQ at Paul Scherrer Institute, Switzerland, using a neutron wavelength of  $\lambda=1.3$  nm and two sample-detector distances of 6 and 18 m. The range of momentum transfer  $0.01 < Q$  ( $\text{nm}^{-1}$ )  $< 0.5$  was covered. The momentum transfer  $Q$  is defined in the usual way as  $Q = 4\pi/\lambda \sin(\theta/2)$ , where  $\theta$  is the scattering angle. All measurements were performed at 20°C. The intensity data were corrected for background and transmission and for non-uniform detector efficiency by referring to the incoherent scattering of a water sample [131].

For SANS measurements two nanocapsule dispersions were produced, one sample with H<sub>2</sub>O and one with D<sub>2</sub>O. The nanocapsule dispersions, which were produced as described above (2.3.1), were diluted with H<sub>2</sub>O or D<sub>2</sub>O to a final concentration of 1% (v/v) Miglyol, 0.24% (w/v) poly(D,L-lactide) and 0.12% (w/v) Poloxamer. The H<sub>2</sub>O and the D<sub>2</sub>O samples were mixed to receive the desired scattering contrast.

## 2.4 Results and discussion

### 2.4.1 Characterization of nanocapsules by TEM, PCS and $\zeta$ potential

The nanocapsule preparation procedure has already been described in the experimental section, where the mechanism of nanocapsule formation is outlined in Figure 2.2.

TEM photomicrographs show the so-produced PEG-PLA-10% (Figure 2.3 a+b) and PLA (Figure 2.3 c-f) nanocapsules. The fractured nanocapsules (Figure 2.3 c-f) exhibit a capsular structure with homogeneous shells. The capsule radius can be estimated with 130 nm for nanocapsules c) and d), 125 nm for nanocapsule e) and with 115 nm for nanocapsule f). The PEG-PLA-10% nanocapsule in Figure 2.3 a) shows an overall radius of 100 nm. PEG-PLA nanocapsules are generally slightly smaller than PLA nanocapsules. All figures of fractured nanocapsules demonstrate a spherical oily core which is surrounded by a thin polymer shell of approximately 10 nm (Figure 2.3 e). In comparison to the partly-fractured PLA-NC (Figure 2.3 c) with a smooth shell surface, the unbroken PEG-PLA-10%-NC (Figure 2.3 a) exhibits a rough surface which can be attributed to the presence of PEG chains.

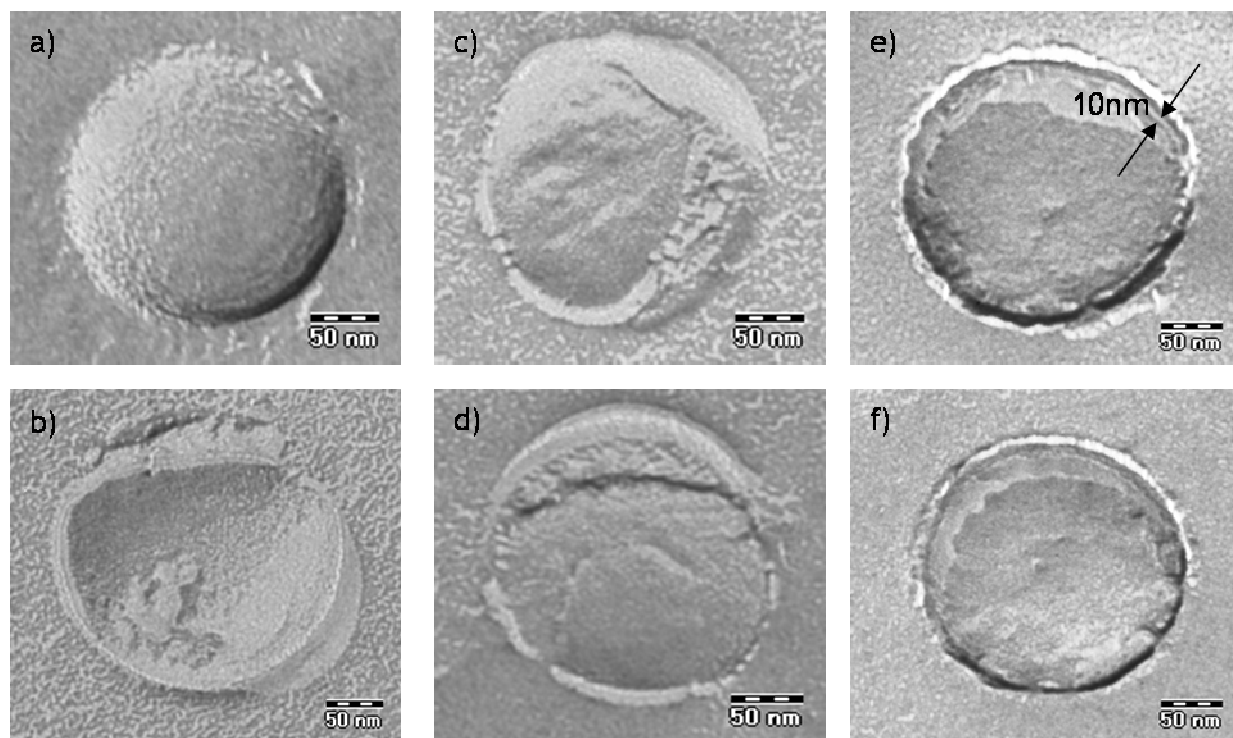


Figure 2.3 TEM photomicrographs of (a+b) PEG-PLA-10% nanocapsules (sample 5, Table 2.1), (c+d and e+f) PLA nanocapsules (sample 2 and 1) treated by freeze fracture and etching. The arrows (e) mark the PLA shell, which can be estimated to be 10 nm.

The mean particle size, measured by PCS, was around 200 nm ( $\pm 50$  nm) with larger values for PLA nanocapsules than for PEG-PLA nanocapsules (Table 2.3). The polydispersity was less than 0.15 which indicates a monodisperse size distribution. The  $\zeta$  potential of nanocapsules can be affected by the oily core, shell polymer and Poloxamer (and lecithin if present) [132-134]. PLA as a poly( $\alpha$ -hydroxy acid) imparts negative charge due to carboxyl groups. Further possible sources for the surface charge of nanocapsules can be impurity traces of free fatty acids in Miglyol or adsorbed ions. Poloxamer as a non-ionic surfactant tends to reduce the absolute value of zeta potential [72]. The  $\zeta$  potential of the examined nanocapsules decreased with increasing Poloxamer or PEG content. Though the Poloxamer-stabilized nanoemulsion showed a very low  $\zeta$  potential due to the high Poloxamer content of 2.5% sterical stabilization probably contributed to the stabilization of the emulsion.

Table 2.3 Particle size determined by photon correlation spectroscopy (PCS).

Sample	mg Poloxamer [w/w]	z-average <sup>a</sup> [nm]	PDI <sup>c</sup>	potential [mV]
PLA-NC	30	232 $\pm$ 11 <sup>b</sup>	0.130 $\pm$ 0.013 <sup>b</sup>	-25.1
PLA-NC	60	253 $\pm$ 12	0.120 $\pm$ 0.016	-23.5
PEG-PLA-10%-NC	0	168 $\pm$ 10	0.111 $\pm$ 0.054	-28.3
PEG-PLA-10%-NC	30	189 $\pm$ 19 <sup>b</sup>	0.110 $\pm$ 0.004 <sup>b</sup>	-16.7
PEG-PLA-10%-NC	60	207 $\pm$ 10	0.116 $\pm$ 0.016	-14.8
PEG-PLA-25%-NC	0	150 $\pm$ 19	0.140 $\pm$ 0.021	-20.0
PEG-PLA-25%-NC	30	172 $\pm$ 7	0.102 $\pm$ 0.007	-14.5
Poloxamer-NE	250	197 $\pm$ 2	0.136 $\pm$ 0.013	-2.7

<sup>a</sup> n = 3

<sup>b</sup> n = 10

<sup>c</sup> PDI = polydispersity index

## 2.4.2 Spin probe distribution in nanocapsules studied by ESR and NMR

The spin probes TB (Figure 2.4 a) and HD-PMI I+II (Figure 2.4 b+c), used in this study, are both lipophilic spin probes, that belong to the group of stable nitroxyl radicals. The octanol-water partition coefficient of TB was determined by an ESR technique introduced by Kroll [135] and a log P value of 2.46 was calculated. This value indicates that TB exhibits a lipophilicity between griseofulvin (log P = 2.18 [136]) and diazepam (log P = 2.92 [137]). Therefore the spin probe can be classified as a poorly water-soluble moderately lipophilic model drug. Approaches to determine the log P of HD-PMI by the same ESR technique failed because of the insufficient sensitivity of the spectrometer. Under the given conditions the smallest measurable spin probe concentration in the water phase was 0.2  $\mu\text{M}$ . A test calculation with this concentration yielded a log P value of 3. Since no signal was detectable from HD-PMI in the water phase during the partition experiment, the log P of HD-PMI must be above 3. Due to the C17-chain in the HD-PMI molecule a realistic value for its log P is >6. This assumption can be supported by a calculation of the log P of 2-Heptadecyl-2,3,4,5,5-pentamethylimidazolidine-1-ol by a cheminformatics program (Molinspiration Cheminformatics), which yielded a value of 9.4. Though one has to keep in mind that this value is not for the nitroxyl radical but the hydroxylamine. A literature value for log P of a molecule with a comparable chain length is 7.7 for oleic acid, a single unsaturated fatty acid (C18) [138].

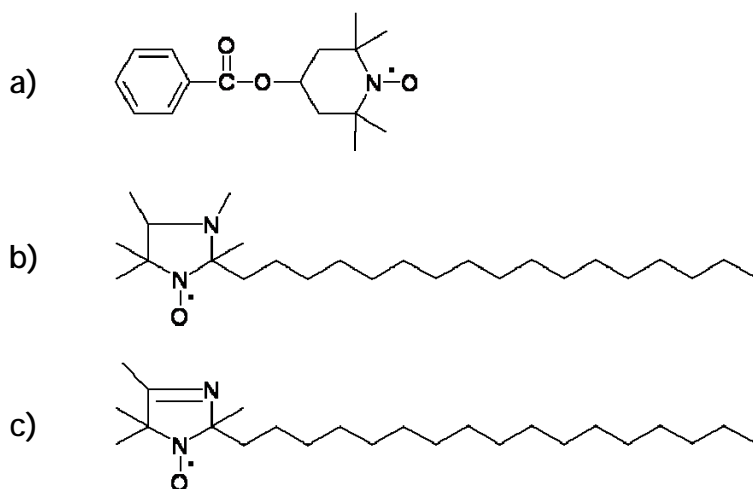
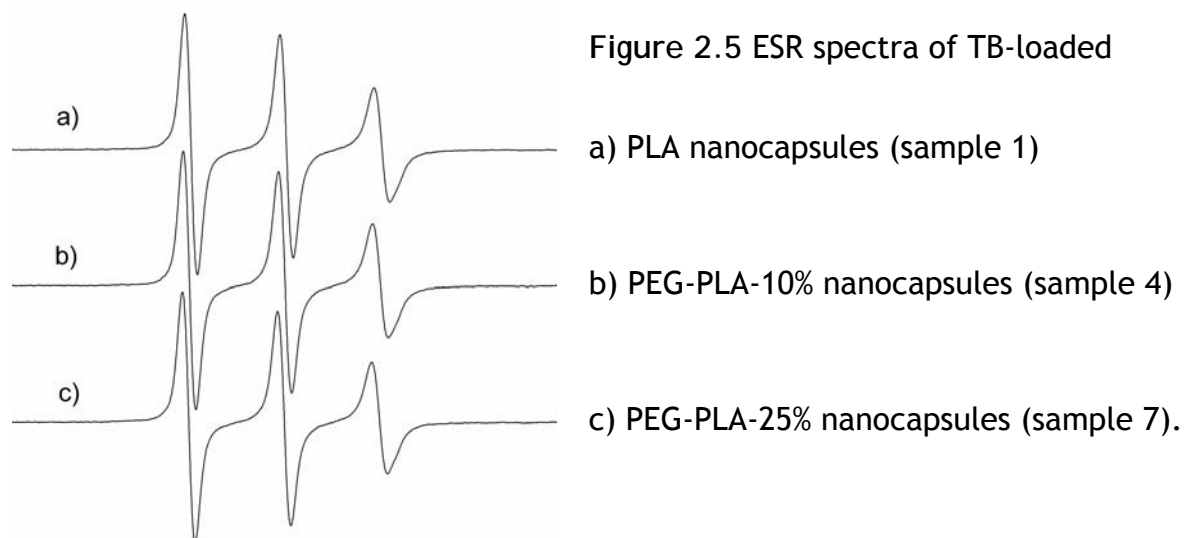


Figure 2.4 Chemical structure of  
a) Tempolbenzoate (TB) and b)+c) HD-PMI I+II

Simulation of the ESR spectra of nanocapsules containing 25 mg/ml Miglyol indicated that the majority of the TB molecules is dissolved within the oily core of the nanocapsules.

The ESR spectra of PEG-PLA nanocapsules and PLA nanocapsules (Figure 2.5) with incorporated TB can be simulated with two species (Figure 2.6). Species I ( $a_N$  between 1.508 and 1.526 mT) has a large line width and a small coupling constant, which indicates a lipophilic environment.



Since the  $a_N$  of TB in Miglyol is between 1.507 and 1.523 mT (scan range 9.800-9.893 mT) it can be attributed to TB molecules dissolved in the oily core of the nanocapsules. The ESR spectra of TB in nanocapsules (Figure 2.5) or Miglyol (Figure 2.6 a) show three lines of decreasing height.

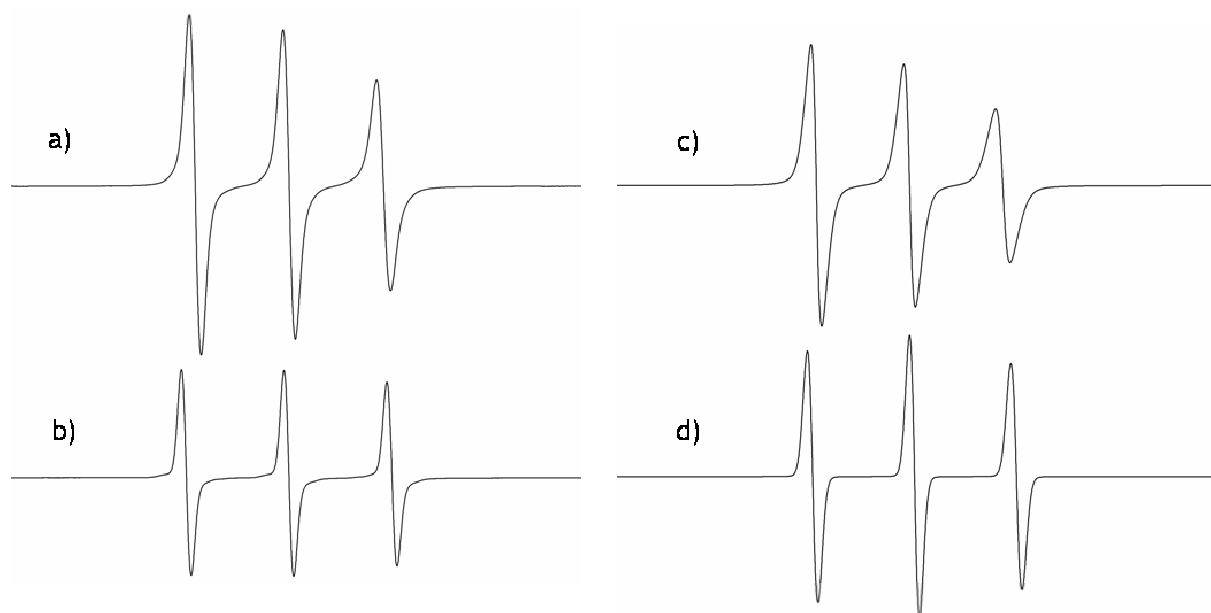


Figure 2.6 ESR spectra of (a) TB in Miglyol (experimental), (b) TB in water (experimental), (c) simulated species I (lipophilic) of Figure 2.5 b, (d) simulated species II (hydrophilic) of Figure 2.5 b.

This effect occurs when TB molecules experience a decreased mobility in all directions and can be attributed to the influence of the fatty acid chains of Miglyol. Species II has a large hyperfine splitting of 1.669-1.670 mT which indicates a polar environment. The coupling constant is similar to the one of TB solubilized in water. Therefore species II can be attributed to spin probes solubilized in the aqueous dispersion medium. This species accounts for 3-4%.

The spectra of the same nanocapsules, but with incorporated HD-PMI, can be simulated with a single species with exactly the same spectral pattern as HD-PMI dissolved in Miglyol.

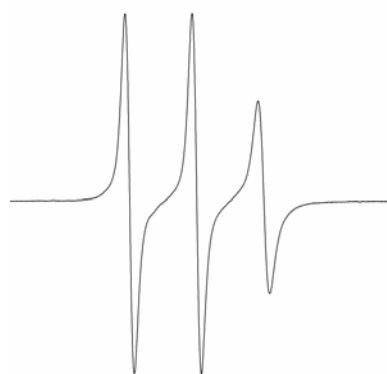


Figure 2.7 ESR spectrum of HD-PMI-loaded PEG-PLA-10% NC (sample 4).

The hyperfine coupling constant is 1.405-1.407 mT for both nanocapsules and Miglyol. Due to its high lipophilicity, the nitroxide is - in contrast to TB - completely dissolved in the oily phase of the nanocapsules whose total amount of the dispersion is only 2.5% (Figure 2.7).

Additional to ESR experiments, which provided insights into the spin probe distribution within the microenvironment of nanocapsules,  $^1\text{H}$ -NMR relaxation measurements were performed on TB-loaded nanocapsules to study the localization of the spin probe down to the molecular environment. Figure 2.8 shows  $^1\text{H}$ -NMR spectra of PLA nanocapsules (sample 1) without encapsulated TB (0 mM) and TB-loaded PLA nanocapsules containing 1, 2 and 3 mM of the spin probe.



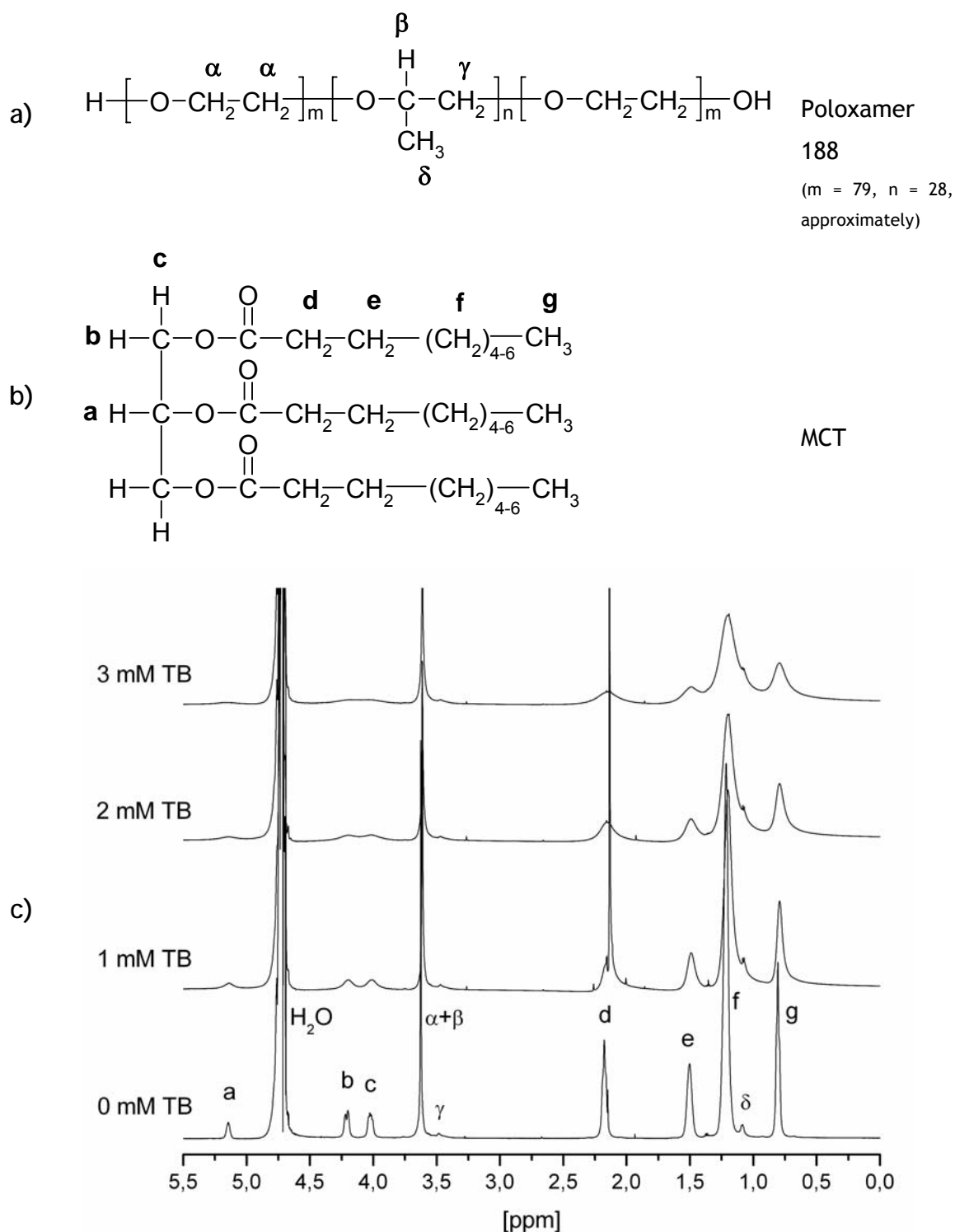


Figure 2.8

(a) Chemical structure of Poloxamer 188

(b) Chemical structure of MCT

(c)  $^1\text{H}$ -NMR spectra of PLA nanocapsules containing 0, 1, 2 or 3 mM TB.

The NMR signals of TB-free nanocapsules are derived from Miglyol and Poloxamer. Each signal is labelled corresponding to the position of the NMR-active protons in the chemical formula (Figure 2.8 a+b) above. The assignment of the NMR signals to

protons from MCT or Poloxamer is in agreement with the literature [46,115]. The ppm values of methyl and methylene protons (g+f) at the very end of alkyl chains in middle chain triglycerides typically lay around 1. Protons located near (e+d) or in the vicinity (c, b, a) of the oxygen-containing glycerol head group have higher ppm values. Poloxamer-derived signals of methyl and methylene protons can be distinguished from the corresponding MCT signals due to their higher ppm values caused by their direct vicinity to oxygen in the polymer backbone. From the nanocapsule dispersions no PLA-related signals are observed. This finding indicates the solid state of the polymer which is typically invisible to NMR due to very short relaxation times. Upon encapsulation of TB into the nanocapsules, the MCT-derived NMR lines broaden which can be attributed to a decrease of T<sub>2</sub> times. All T<sub>1</sub> times decrease by factor 10-15, the T<sub>2</sub> times by factor 10-20. Since all MCT-derived signals are equally influenced by the presence of TB, it can be concluded, that TB is homogeneously distributed within the oily phase with no preference for a special entity of the triglyceride. In contrast to MCT signals, the line width of Poloxamer-derived signals is not influenced by the presence of TB. This finding indicates that the intermolecular distance between TB molecules and Poloxamer is relatively high.

Briefly, the NMR results show a homogeneous distribution of TB in the oily phase without a preference for a special entity of the triglyceride molecules. This finding is in accordance with ESR results where the majority of the spin probe was found to be localized in the oily core of the nanocapsules. Compared to ESR results, which give information about the distribution of the spin probe in the nanoenvironment, NMR relaxation measurements facilitate the distribution profile down to the molecular scale. Since ESR experiments showed the distribution of a minority of TB molecules to the outer aqueous phase, a possible interaction of TB with Poloxamer molecules was examined by NMR. In this case no interactions were visible indicating a relatively high distance between TB and Poloxamer molecules.

### 2.4.3 Electron spin resonance study on the dynamics of polymeric nanocapsules

Nanocapsules undergo dilution both during experimental work and in-vivo application. Since no information is available on this dynamical process, dilution kinetics was studied by means of ESR spectroscopy. One part of the nanocapsule dispersion (sample 1) was diluted with one, two, three or four parts of water and changes of the spectral shape were monitored. The same dilution steps were performed with a nanoemulsion (sample 8) as a reference system.

For both systems clear changes in the spectral shape are visible (Figure 2.9). Upon dilution in the ratio 1:2 (Figure 2.9 c) a polar species with a higher coupling constant arises which leads to a splitting of the high field line. The influence of this polar species grows with further dilution (Figure 2.9 d+e).

From the simulation of the ESR spectra in equilibrium (Figure 2.9 b-d) it can be assumed that approximately 90% of the TB molecules are still solubilized in the oily core ( $a_N$  1.52 mT) and approximately 10% diffused into the polar, aqueous environment. This aqueous proportion increased to about 15% upon further dilution (Figure 2.9 e).

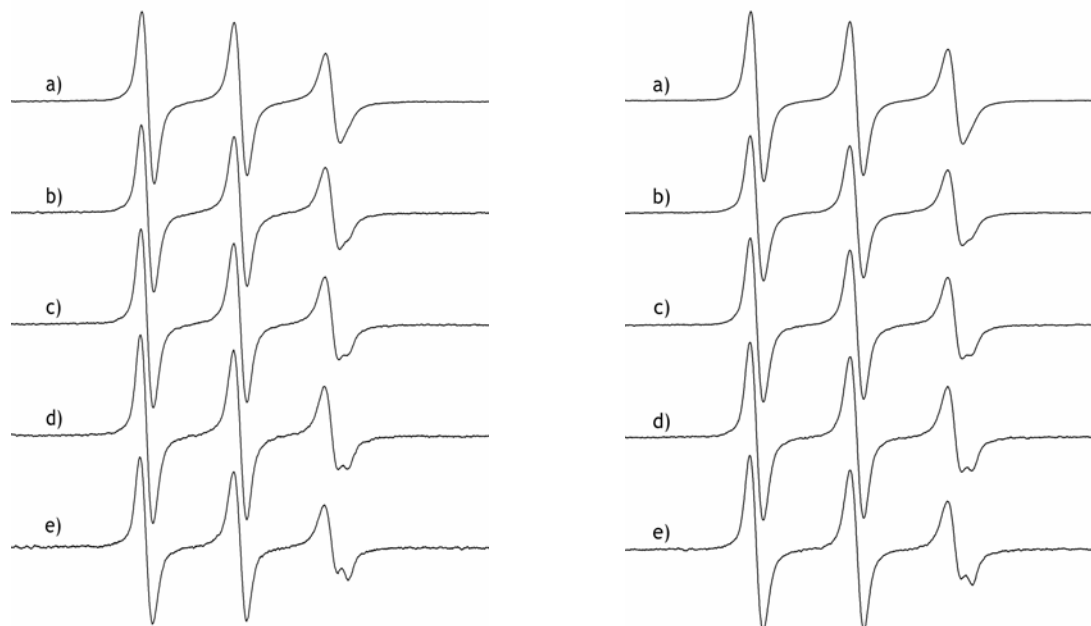


Figure 2.9 ESR spectra of TEMPOL benzoate in  
(left) (right)

- (a) PLA-NC (sample 1) undiluted
- (b) PLA-NC 1:1 diluted
- (c) PLA-NC 1:2 diluted
- (d) PLA-NC 1:3 diluted
- (e) PLA-NC 1:4 diluted

- (a) nanoemulsion undiluted
- (b) nanoemulsion 1:1 diluted
- (c) nanoemulsion 1:2 diluted
- (d) nanoemulsion 1:3 diluted
- (e) nanoemulsion 1:4 diluted.

The equilibrium of TB between the drug carrier and its new environment is reached within a minute for both the nanoemulsion and the nanocapsules. From this it can be seen that the polymer shell does not provide a barrier to encapsulated drug molecules. The same is true for the pegylated nanocapsules PEG-PLA-10%-NC and PEG-PLA-25%-NC.

The Centrisat experiment confirms the assumption that the release of TB from nanocapsules is governed by the partition rate from the oily core to the aqueous phase. Figure 2.10 a shows an undiluted PLA nanocapsule dispersion (equilibrium 97:3 oil-water). A change in the aqueous volume alters the amount of released TB immediately (Figure 2.10 b). After reconcentration of the nanocapsule dispersion to the starting volume by centrifugal ultrafiltration, the equilibrium ratio differs from the starting value (Figure 2.10 c).

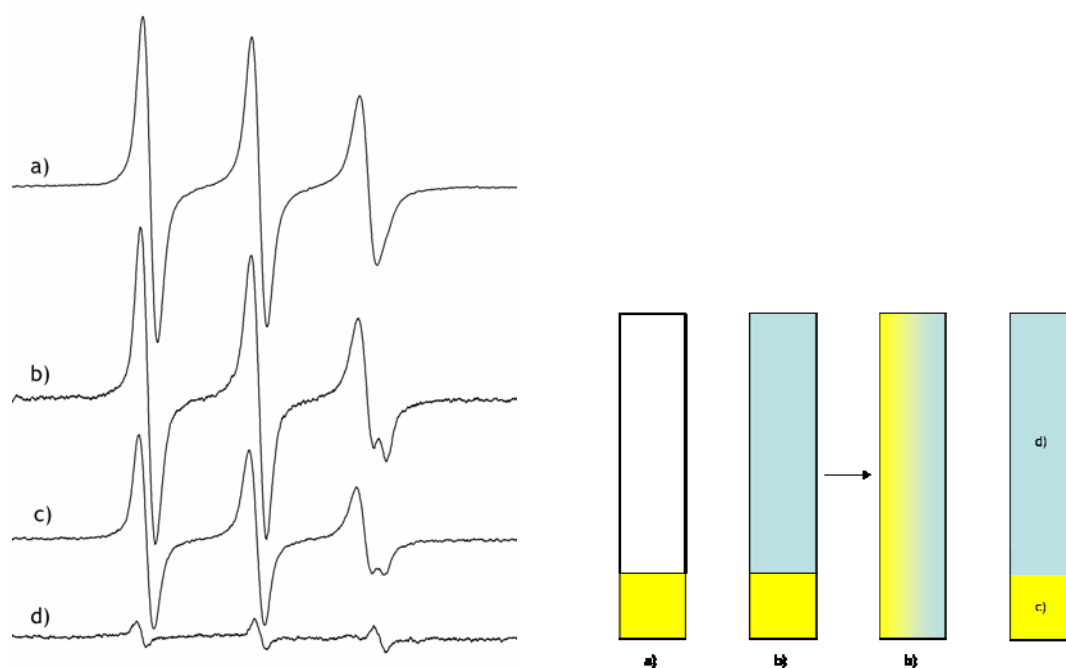


**Figure 2.10** Centrisat experiment

(left) ESR spectra of TB in

a) PLA nanocapsule dispersion undiluted (500  $\mu$ l)

b) PLA nanocapsule dispersion 1:4 diluted (500  $\mu$ l + 2000  $\mu$ l)

c) PLA nanocapsule dispersion after reconcentration to starting volume (500  $\mu$ l)

d) Filtrate

(right) Schematic sketch of Centrisat assay (note: the single sketches belong to the ESR spectra with the corresponding letters).

This can be explained as follows. TB molecules which are located in the aqueous environment of the nanocapsule dispersion (Figure 2.10 c scheme) diffuse through the membrane of the Centrisat tube into the aqueous filtrate (Figure 2.10 d ESR spectra + scheme). As a consequence a relocation of TB molecules from the nanocapsules to the aqueous environment occurs. This leads to a different equilibrium than before the addition of water although the volume of the nanocapsule dispersion is the same.

Similar findings concerning diffusion within nanocapsule dispersions have been reported in the literature for nanocapsule systems prepared by the same technique independent on the nature of the polymer [71,83]. With the ESR dilution assay the first real-time shots of this partition process could be produced and quantified.

As a consequence for practical applications this finding means that for drug molecules of moderate lipophilicity complete protection from the environment and vice versa can not be ensured in nanocapsules prepared by interfacial nanodeposition.

In contrast to colloidal carriers with TB the dilution assay of nanocapsules with incorporated HD-PMI shows no diffusion of nitroxide radicals to the polymer-water interface. No splitting of the high-field peak is visible (Figure 2.11). Only the signal intensity decreases due to the decreased spin probe concentration.

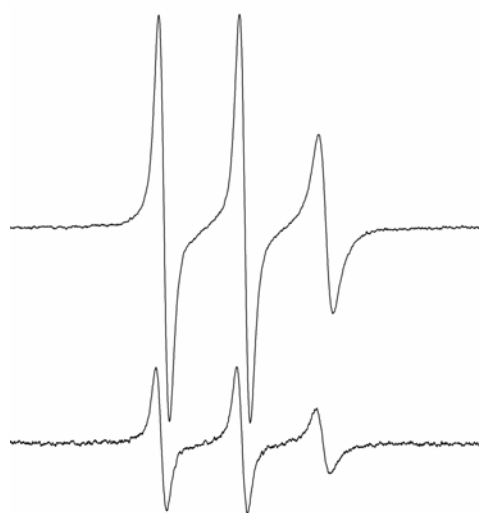


Figure 2.11 ESR spectra of HD-PMI in (top) PEG-PLA-10% nanocapsules (bottom) PEG-PLA-10% nanocapsules (1:4 diluted).

As a reversal experiment, an attempt was made to load spin-probe-free nanocapsules (Figure 2.12 b) with TB from the outside belatedly. TB (0.1 mM) was dissolved in the water phase of a TB-free nanocapsule dispersion and ESR spectra were recorded immediately.

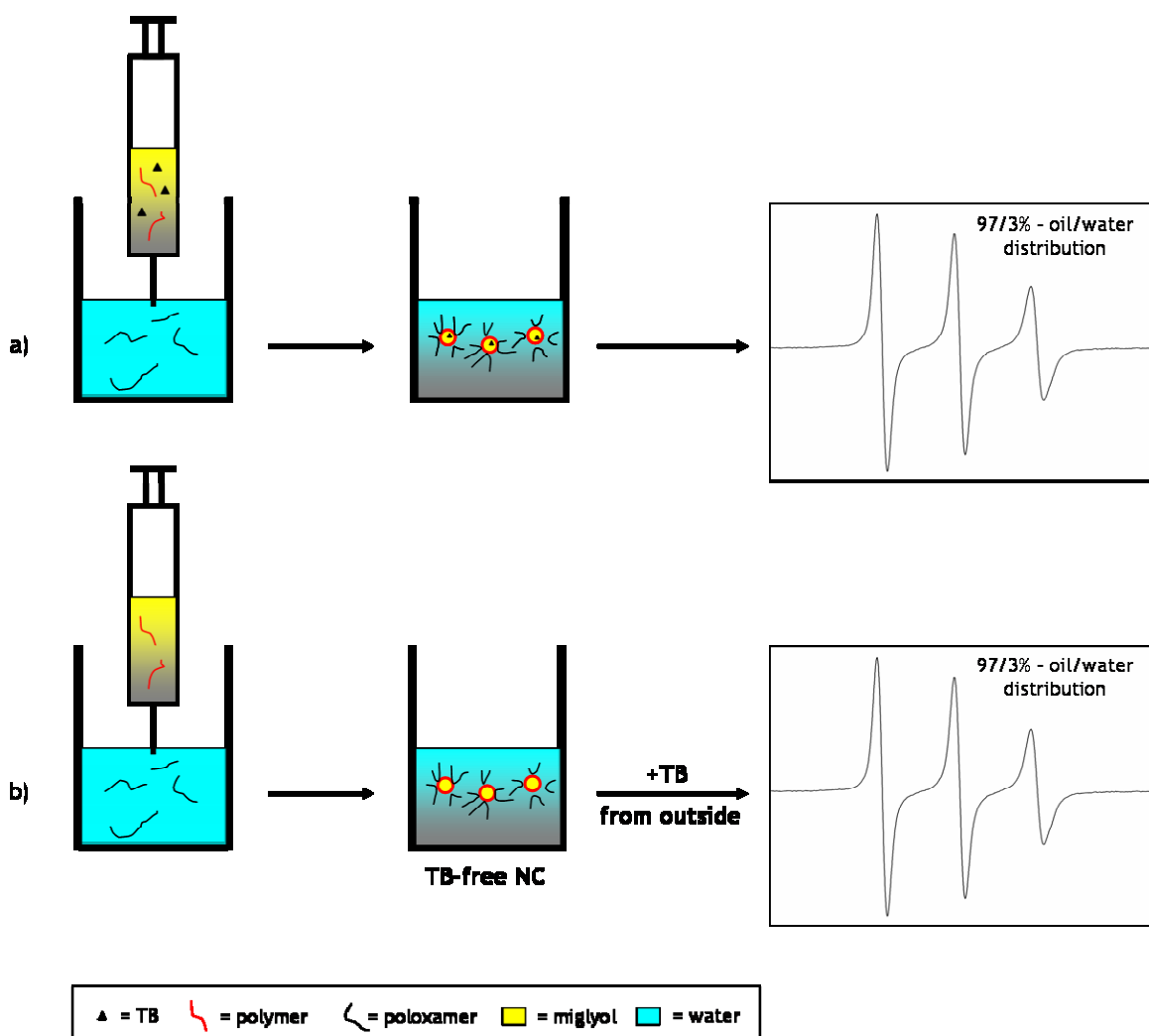


Figure 2.12 Schematic representation of  
a) standard nanocapsule preparation with TB encapsulation during production  
b) preparation of TB-free nanocapsules with belated TB incorporation from outside.  
Note that resulting ESR spectra are identical!

Surprisingly, the spectra were identical to those which contained TB in the oily core from the production process (Figure 2.12 a+b). This means that the lipophilic spin probe was able to diffuse through the shell within a minute and the system was equilibrated at once. This leads to the conclusion that diffusion of the TB molecules both from the core to the water phase and the other way around from water to oil is very fast.

This fast reallocation observed by ESR spectroscopy can be understood with the assistance of TEM results. The observed shell thickness in the photomicrographs of nanocapsules (Figure 2.3 e) provides with 10 nm only a very thin barrier between the oily and the water phase and therefore diffusion kinetics are fast.

When taking into account the Einstein-Smoluchowski equation [139]

$$D = \frac{d^2}{2t} \rightarrow t = \frac{d^2}{2D},$$

whereas D is the diffusion coefficient, d the distance (Figure 2.13) and t the time, this finding is not surprisingly.

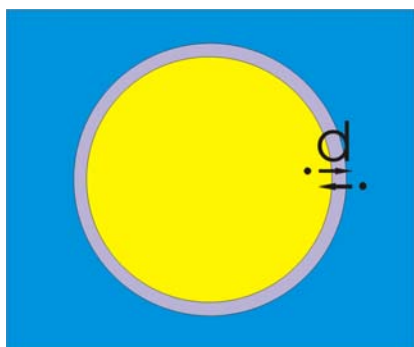


Figure 2.13 Schematic representation of diffusion paths within nanocapsules.

Assuming a diffusion coefficient of  $10^{-12} \text{ cm}^2 * \text{s}^{-1}$  [140], which is typical for polymers containing a softener, and taking into account a diffusion distance of 10 nm which is the thickness of the shell, the diffusion time for a molecule from the oil to the water and vice versa will take 0.5 sec.

Besides diffusion paths within the carrier and charge effects at the interface, the polymer shell plays a determining roll for the accessibility of incorporated drugs. The reduction assay with ascorbic acid (Figure 2.14) gives a description of the accessibility of the nitroxide to the aqueous phase.

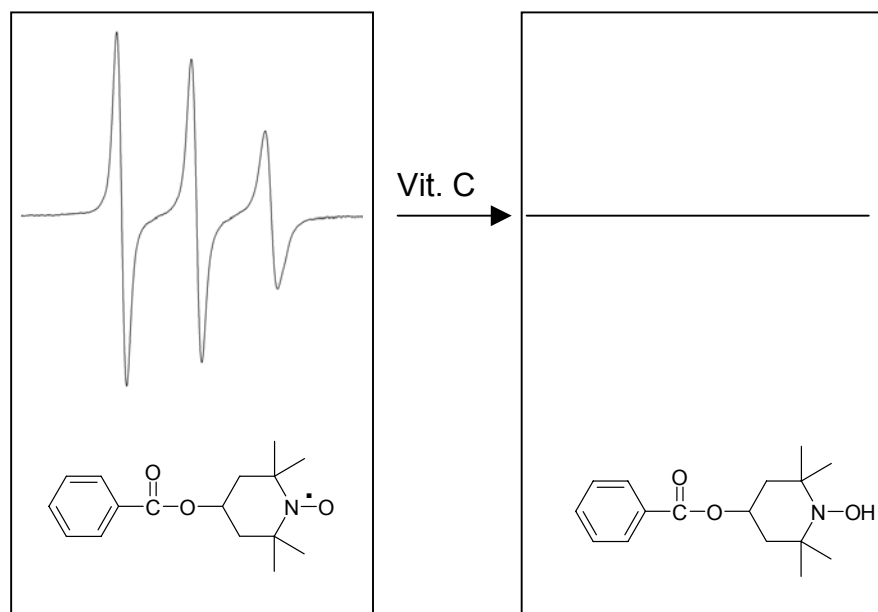


Figure 2.14 Schematic representation of vitamin C reduction assay: Reduction of the TB radical (left) to the ESR-silent hydroxylamine (right) by ascorbic acid.

For the reduction assay the physiological function of vitamin C as a radical catcher is used. The hydrophilic ascorbic acid rapidly reduces accessible TB to the ESR-silent hydroxylamine and quenches thereby the ESR signal. The reduction kinetics of the spin probe monitor the resistance of different nanocapsules to a reduction to ascorbic acid.



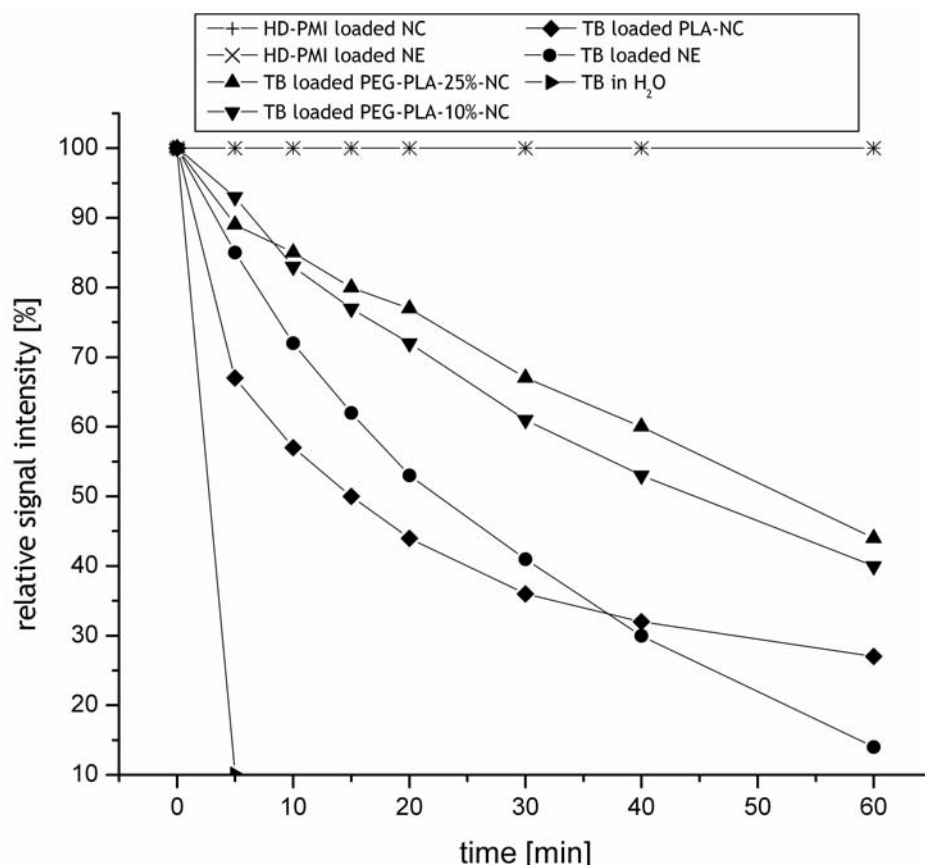


Figure 2.15 Decrease of electron spin resonance signal intensity (time against changes in the signal area) of different nanocarriers during the ascorbic acid reduction assay.

While more than 90% of the TB molecules in water are reduced to the ESR silent hydroxylamine within the first minute, PEG-PLA nanocapsules (sample 4+7), PLA nanocapsules (sample 1) and the nanoemulsion (sample 8) protect the TB molecules before reduction (Figure 2.15). The magnitude of protection is greater for the PEG-PLA nanocapsules than for the PLA nanocapsules. While in PEG-PLA nanocapsules after 15 minutes still 80% of the ESR active spin probe molecules are present, in PLA nanocapsules this fraction amounts only 50% at this particular time. PLA nanocapsules are not superior to a nanoemulsion. From this it can be concluded that modification of the shell with covalently bound PEG chains is repellent to ascorbic acid molecules, higher PEG densities leading to a higher degree of repelling. This finding can be attributed to the restricted mobility of ascorbic acid molecules due to the PEG chains at the nanocapsule-water interface. The distribution equilibrium of TB molecules between PLA nanocapsules or a nanoemulsion and water is approximately the same, therefore the reduction kinetics are similar. For the first 40 minutes the nanoemulsion showed slightly

better protection than the PLA nanocapsules. This might be due to the 8-fold higher content of Poloxamer molecules in the aqueous environment which decreases the mobility of the ascorbic acid molecules. The fact that non-modified PLA nanocapsules are not superior to a nanoemulsion and that the reduction assay of nanocapsules and a nanoemulsion with the highly lipophilic HD-PMI shows no decrease of spin probe at all times indicates that here again the partition coefficient is predominant. Since ascorbic acid is a hydrophilic molecule, it can only attack spin probe molecules which have partitioned into the water phase or are located at the oil-water interface. To ensure that the different behaviour of HD-PMI and TB towards reduction was not due to the chemistry of the molecules but due to their partition coefficient, HD-PMI was solubilized in mixed micelles and a reduction assay was performed. In this more hydrophilic drug delivery system ascorbic acid was able to reach the HD-PMI molecules which lead to reduction of the spin probe. Therefore it can be concluded that from oil-containing nanocapsules and nanoemulsions the highly lipophilic HD-PMI does not partition into the water phase and is therefore not reached by the ascorbic acid molecules.

#### 2.4.4 Core-shell structure of poly(D,L-lactide) nanocapsules studied by small-angle neutron scattering

##### Small angle neutron scattering (SANS)

Dynamics of nanocapsules in aqueous environment are mainly controlled by two processes: firstly by diffusion within the colloidal carrier and secondly by interface phenomena. The first process was settled with the help of ESR. For the characterization of the interface, namely the shell of nanocapsules, small angle neutron scattering (SANS) with additional information from DLS and TEM was applied. PLA nanocapsules (sample 1) were studied as a model system.

The purpose of the SANS experiments was to resolve the inner structure of the nanocapsules, especially to resolve the thickness of the PLA shell. A single SANS experiment was not capable to do the job for the PLA nanocapsules dispersion as the relatively broad size distribution of the Miglyol oil core smeared out the form factor of the capsules so that one did not get precise results for the shell thickness. An analysis of a single scattering experiment can only be carried out successfully for very narrow size distributions. However, for a contrast variation experiment, where the scattering length density (or refraction index) of the solvent is changed continuously, one gets a whole set of scattering curves which have to be analysed simultaneously with a common set of parameters. By this method it is possible to separate the influence of the size distribution from the influence of the form factor on the scattering intensity. The scattering length density of the solvent can be changed very easily in neutron scattering by using a mixture of light ( $\text{H}_2\text{O}$ ) and heavy ( $\text{D}_2\text{O}$ ) water. The method allows to highlight different parts of the scattering object. Highest sensitivity on the inner structure of the nanocapsules can be obtained when the scattering length density of the solvent is varied between the scattering length density of the Miglyol core ( $\eta_{\text{core}} = 0.1894 \times 10^{10} \text{ cm}^{-1} \triangleq 89.1:10.9 \text{ H}_2\text{O}:\text{D}_2\text{O}$ ) and the one of the PLA shell ( $\eta_{\text{PLA-shell}} = 1.5423 \times 10^{10} \text{ cm}^{-1} \triangleq 69.4:30.6 \text{ H}_2\text{O}:\text{D}_2\text{O}$ ).

A schematic sketch of a contrast variation experiment is shown in Figure 2.16.

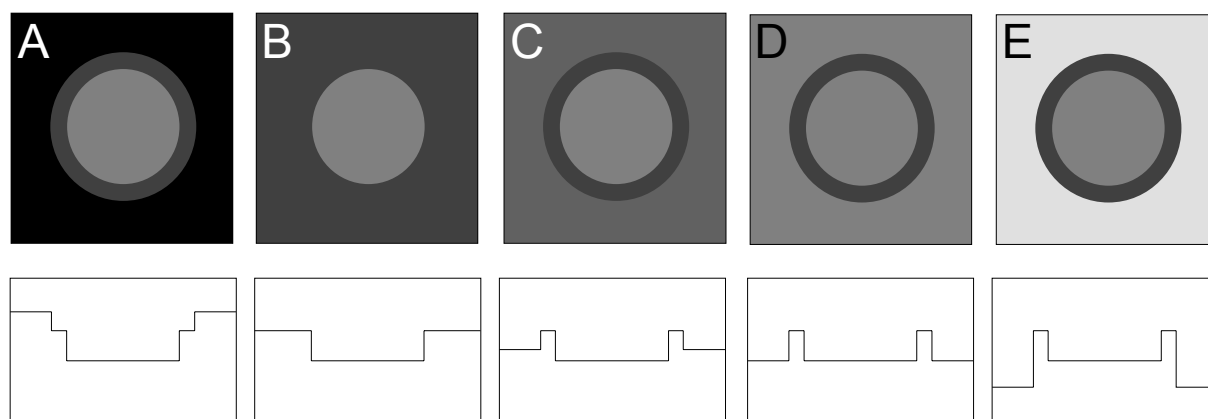


Figure 2.16 A schematic sketch of a contrast variation experiment with different  $\text{H}_2\text{O}/\text{D}_2\text{O}$  mixtures on nanocapsules. The second row shows schematically a sketch of the scattering length density profile across the shell structure.

In case A the solvent consists of 100 %  $\text{D}_2\text{O}$ . In the schematic sketch the  $\text{D}_2\text{O}$  content decreases from case A to B, C and D while in E 100 %  $\text{H}_2\text{O}$  were used.

In case B the shell is matched and only the core contributes to scattering intensity. In case D the solvent is matching the scattering length density of the oily core so that only the shell contributes to the scattering intensity. The corresponding scattering length density profiles across the capsules are drawn below the sketches. In the present experiment the scattering length density of the solvent was varied between the cases B and D. In this regime one is most sensitive to the inner structure of the capsules as the difference in the scattering length densities between Miglyol core and solvent on one hand and on the other hand between PLA shell and solvent have an opposite sign. Therefore the scattering amplitudes of the two phases are partly compensating each other. This is not the case for A and E where they have the same sign.

The results of the SANS experiment are shown in Figure 2.17 together with the theoretical fit.

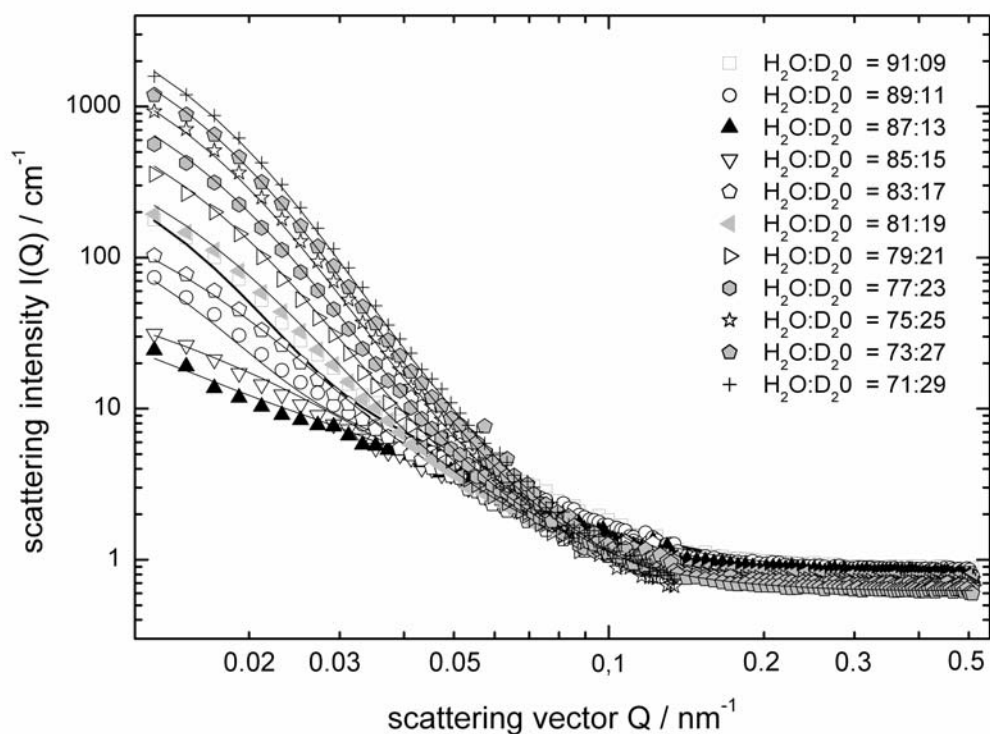


Figure 2.17 SANS scattering curves of PLA nanocapsules in different D<sub>2</sub>O/H<sub>2</sub>O mixtures.

In the contrast variation experiment the D<sub>2</sub>O/H<sub>2</sub>O was varied from 9/91 to 29/71. The scattering intensity is the lowest for a ratio of 13/87 as there the volume times the contrast of the Miglyol core is about the same as for the PLA shell, but the contrast of the core and the shell have an opposite sign.

The only free parameters of the fit were the thickness of the PLA shell and the parameters of the log normal size distribution of the Miglyol core, i.e.  $\sigma$ ,  $R_0$ , and  $\Delta R_{PLA}$ . It was assumed that the shell thickness is constant and independent on the radius of the core. The fit yielded a PLA shell thickness of  $\Delta R_{PLA} = 9.8 \text{ nm} \pm 0.7 \text{ nm}$  and for the fit parameter of the size distribution  $\sigma = 0.394 \pm 0.02$ ,  $R_0 = 84 \text{ nm} (\pm 0.5 \text{ nm})$ . Already with this model a reasonable agreement with the experiment could be obtained.

### Dynamic light scattering (PCS and 3D-DLS)

The z-average radius of the examined nanocapsules was 120.95 ( $\pm 0.32$  nm) for back scattering experiments at an angle of  $173^\circ$ . The polydispersity index was 0.132 ( $\pm 0.017$ ) which indicates a monodisperse size distribution according to real pharmaceutical colloidal dispersions. Contributions from multiple scattering can be excluded because reference measurements of diluted samples were performed. The back scattering result at  $173^\circ$  matches well with the 3D-DLS results at scattering angles taken between 20 and 140 degrees (Figure 2.18).

As can be seen in Figure 2.18 the z-averaged radii varied considerably with the scattering angle.

This is because for the cumulant analysis at small angles large particles dominate the contribution to the size distribution compared to smaller particles. At large angles this effect is partly compensated due to the slow decay of the form factor of small particles leading to smaller radius distributions. Therefore DLS measurements at small angles lead to higher values for the z-averaged radius than at large angles.

### Comparison of SANS and DLS

The z-averaged radii  $R_{DLS}$  determined from the SANS results are in good agreement with the values determined by DLS. Though the values from SANS measurements are systematically a bit smaller than the ones from light scattering (Figure 2.18), if one assumes, that the hydrodynamic radius is only the sum of the Miglyol core and the PLA shell. The hydrodynamic radius seemed to be bigger than the capsule radius. Therefore SANS and DLS results were compared and a refinement of the model was done by introducing a second shell consisting of Poloxamer and solvent.

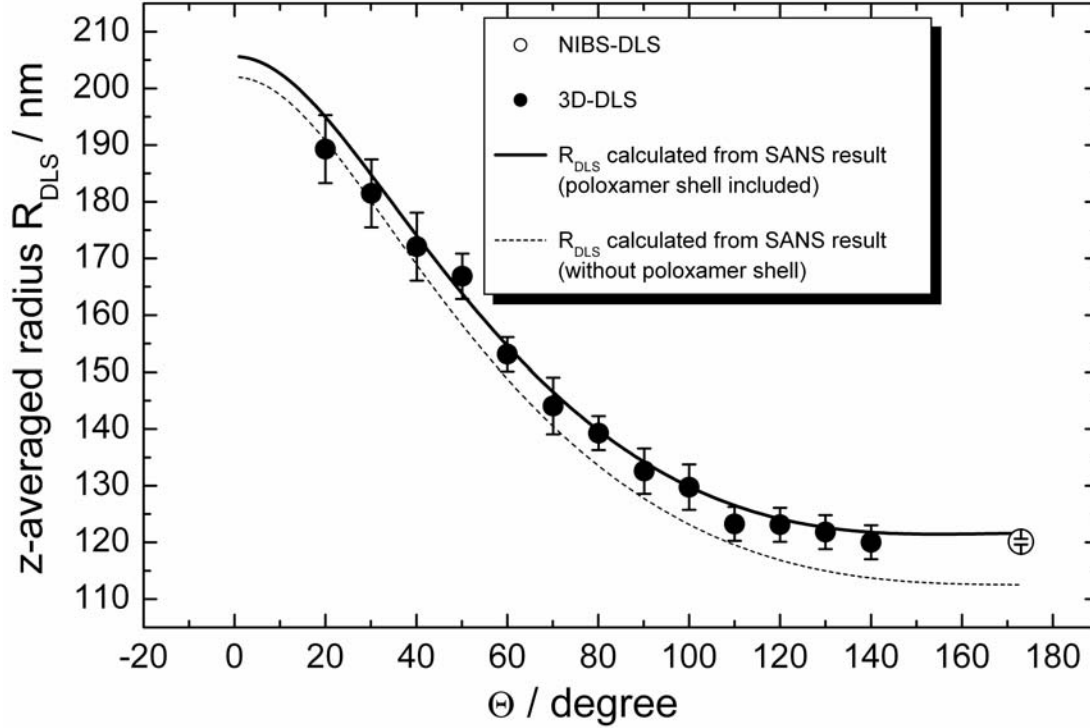


Figure 2.18 A comparison of the z-average radii obtained by DLS (3D-DLS + NIBS-DLS) and SANS measurements and the refined SANS fit model containing a second shell consisting of Poloxamer and solvent.

A comparison of SANS results with DLS results is not straight forward. One has to consider that DLS measures a z-average diffusion coefficient and therefore the resulting average radius is also a z-average. SANS results on the other hand represent a particle number size distribution. How the results from DLS have to be related to a particle number size distribution as been used for here presented SANS analysis is described in [141].

The z-average particle radius  $R_{DLS}$  and the polydispersity index  $PDI$  obtained by cumulant analysis of the DLS experiment are given by

$$R_{DLS} = \frac{\overline{R_{hyd}^6}}{\overline{R_{hyd}^5}} \quad \text{and} \quad PDI = \frac{\overline{R_{hyd}^6} \overline{R_{hyd}^4}}{\overline{R_{hyd}^5}^2} - 1 \quad (1)$$

whereby the  $n^{\text{th}}$  moment of the hydrodynamic radius  $R_{hyd}$ , which is in first approximation the sum of the Miglyol core radius  $\Delta R_{Miglyol}$ , the PLA shell thickness  $\Delta R_{PLA}$ , and possibly also of the Poloxamer shell  $R_{hyd} = R_{Miglyol} + \Delta R_{PLA} + \Delta R_{Polo-sh}$ , can be calculated together with the size distribution  $N(R_{Miglyol})$  of the Miglyol core via

$$\overline{R_{hyd}^n} = \int N(R_{Miglyol}) R_{hyd}^n dR_{Miglyol} / \int N(R_{Miglyol}) dR_{Miglyol} \quad (2)$$

For  $N(R_{Miglyol})$  from the SANS experiments a log normal size distribution was assumed,

$$N(n, R_{Miglyol}, R_0, \sigma) = \frac{n}{\sqrt{2\pi}\sigma} \frac{1}{R_{Miglyol}} \exp\left(-\frac{(\ln R_{Miglyol} - \ln R_0)^2}{2\sigma^2}\right). \quad (3)$$

As the radius  $R_{DLS}$  is calculated via high moments of the hydrodynamic radius size distribution, its value can already be influenced by only a few large particles. The reason for this observation is that the cumulant analysis to calculate the z-averaged particle  $R_{DLS}$  radius assumes a size dependent contribution of a particle to the DLS signal which is proportional to the square of its volume, i.e. proportional to  $R_{hyd}^6$ . However, this is only true in forward scattering. For larger angles one has to consider the static particle form factor for light  $F^2(\Theta, R_{sp})$ , which is responsible for the angle dependency of  $R_{DLS}$ .

However, this can easily be taken into account by weighting the size distribution  $N(R_{Miglyol})$  with  $F^2(\Theta, R_{sp})$  so that

$$\overline{R_{hyd}^n} = \int N(R_{Miglyol}) F^2(\Theta, R_{sp}) R_{hyd}^n dR_{Miglyol} / \int N(R_{Miglyol}) F^2(\Theta, R_{sp}) dR_{Miglyol}. \quad (4)$$

Combining equation 1, 3 and 4 allows now to compare the size distribution, obtained by SANS, with the z-averaged particle radius  $R_{DLS}$ , obtained by cumulant analysis of the DLS data.

The two SANS curves in Figure 2.17 are calculated by assuming a static form factor of a homogenous sphere with refraction index  $n = 1.45$  (refraction index of Miglyol and PLA are assumed to be the same, literature values of both materials vary between 1.45-1.47) in water ( $n = 1.332$ ). The radius  $R_{sp}$  of the sphere for calculating the form factor  $F^2(\Theta, R_{sp})$  in the Mie-approximation [142] was  $R_{sp} = R_{Miglyol} + \Delta R_{PLA}$ . The two curves in Figure 2.17 are calculated by taking two different shell thicknesses into account for the hydrodynamic radius, firstly only the PLA shell  $R_{hyd} = R_{Miglyol} + \Delta R_{PLA}$  and secondly also the Poloxamer/water shell  $R_{hyd} = R_{Miglyol} + \Delta R_{PLA} + \Delta R_{Polo-sh}$ .

The detailed model for the description of the nanocapsule containing a PLA and Poloxamer shell is as follows.

For describing the SANS data the form factor of concentric spherical shells has been used. The core consisted of Miglyol surrounded by either one or two concentric



shells. The first shell was build by PLA and the outer shell by Poloxamer, which acted as a hydrophilic stabiliser and contained next to the Poloxamer molecules a large amount ( $x_{solvent}$ ) of the solvent molecules (Figure 2.19).

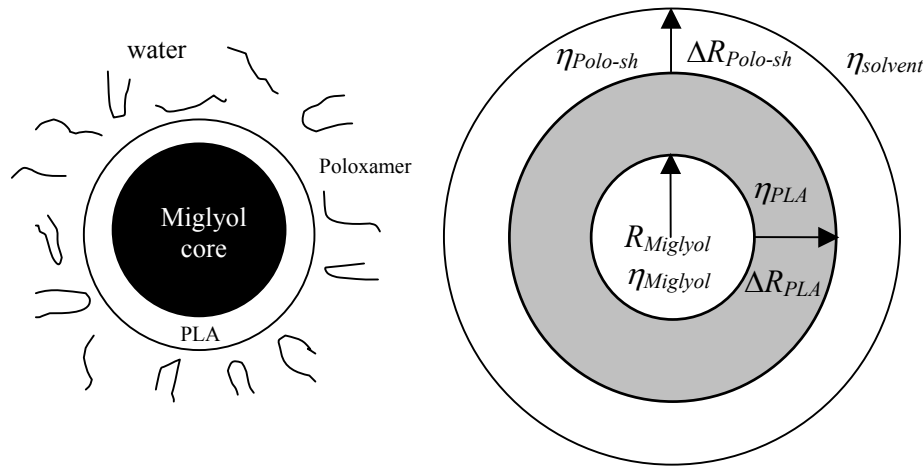


Figure 2.19 Schematic representation of PLA nanocapsules (left) and a simplified nanocapsule model (right).

The form factor of such a structure can be put down to the form factor of a homogeneous sphere  $K(Q, R, \Delta\eta)$  with radius  $R$  and scattering contrast  $\Delta$ , which is given by

$$K(Q, R, \Delta\eta) = \frac{4}{3} \pi R^3 \Delta\eta^3 \frac{\sin(QR) - QR \cos(QR)}{(QR)^3} \quad (5)$$

The scattering intensity of a spherical double shell  $I_{shell}(Q)$  with a core of radius  $R_{Miglyol}$  and the two concentric shells of thicknesses  $\Delta R_{PLA}$  (first shell) and  $\Delta R_{Polo-sh}$  (outer shell) is then given by

$$I_{shell}(Q) = \left\{ \begin{aligned} &K(Q, R_{Miglyol} + \Delta R_{PLA} + \Delta R_{Polo-sh}, \Delta\eta_{Polo-sh}) \\ &+ K(Q, R_{Miglyol} + \Delta R_{PLA}, \Delta\eta_{PLA} - \Delta\eta_{Polo-sh}) \\ &+ K(Q, R_{Miglyol}, \Delta\eta_{Miglyol} - \Delta\eta_{PLA}) \end{aligned} \right\}^2 \quad (6)$$

The material properties of the relevant materials to calculate the scattering contrasts of the different phases are tabulated in Table 2.4.

Table 2.4 Relevant material properties and scattering length densities.

		mass density	scattering length density	scattering contrast
Miglyol 812	$C_{29}H_{53}O_6$	0.945 g/cm <sup>3</sup>	$\eta_{Miglyol} = 0.189 \times 10^{10} \text{ cm}^{-2}$	$\Delta\eta_{Miglyol} = \eta_{Miglyol} - \eta_{solvent}$
PLA 50	$[C_3H_4O_2]_n$	1.13 g/cm <sup>3</sup>	$\eta_{PLA} = 1.542 \times 10^{10} \text{ cm}^{-2}$	$\Delta\eta_{PLA} = \eta_{shell} - \eta_{solvent}$
Poloxamer 188	$C_{400}H_{802}O_{187}$	1.055 g/cm <sup>3</sup>	$\eta_{Polox.} = 0.672 \times 10^{10} \text{ cm}^{-2}$	
light water	H <sub>2</sub> O	1.0 g/cm <sup>3</sup>	$\eta_{H_2O} = -0.563 \times 10^{10} \text{ cm}^{-2}$	
heavy water	D <sub>2</sub> O	1.1 g/cm <sup>3</sup>	$\eta_{D_2O} = 6.316 \times 10^{10} \text{ cm}^{-2}$	
solvent	$x_{H_2O}$ : volume fraction of H <sub>2</sub> O		$\eta_{solvent} = x_{H_2O} \eta_{H_2O} + (1 - x_{H_2O}) \eta_{D_2O}$	
Polo-xamer shell	$x_{solvent}$ : volume fraction of solvent in Poloxamer shell		$\eta_{Polo-sh} = (1 - x_{solvent}) \eta_{Poloxamer} + x_{solvent} \eta_{solvent}$	$\Delta\eta_{Polo-sh} = \eta_{Polo-sh} - \eta_{solvent}$

For calculating the SANS intensity a lognormal size distribution for the Miglyol core was assumed (eq. 3) whereby the radii of the shells are assumed to be constant and independent of the Miglyol core radius. The SANS intensity is then given by

$$I(Q, R_{Miglyol}) = \int N(R_{Miglyol}) I_{shell}(Q, R_{Miglyol}) dR_{Miglyol} + I_{inc} \quad (7)$$

All 11 scattering curves were fitted simultaneously with only five independent parameters plus a  $Q$ -independent constant incoherent background value  $I_{inc}$ , which was different for each scattering curve. The best agreement between the hydrodynamic radius calculated from the SANS results and from the cumulant analysis only could be obtained by including next to the PLA shell also a second Poloxamer shell into the model. Poloxamer was used as a sterical stabilizer. From the fit of the SANS data the parameters set for the size distribution of  $\sigma = 0.394$  ( $\pm 0.02$ ),  $R_0 = 84 \text{ nm}$  ( $\pm 0.5 \text{ nm}$ ),  $\Delta R_{PLA} = 9.8 \text{ nm}$  ( $\pm 0.7 \text{ nm}$ ) have been obtained. The fit for the Poloxamer shell provided a value of  $\Delta R_{Polo-sh} = 17 \text{ nm}$  ( $\pm 6 \text{ nm}$ ) and a Poloxamer concentration of 7% ( $\pm 5\%$ ). The error of the Poloxamer shell parameters are quite large as the thickness of the shell  $\Delta R_{Polo-sh}$  and the Poloxamer concentration are correlated, i.e. one can compensate partly the change in the scattering curve for a smaller shell radius by increasing the Poloxamer concentration of the shell and vice versa. The data also show the absence of micelles. As a result the Poloxamer concentration of 0.12% must be below the critical micelle concentration (cmc), which is in accordance with the literature [143,144].

Tadros et al. described the principal of sterical stabilisation as follows. The block copolymer adsorbs with its central, hydrophobic moiety onto the nanocapsules surface. The two hydrophilic moieties stick out into the aqueous environment and thereby create a mechanical barrier with a thickness of several nanometers. According to Tadros et al. [145] this layer should be bigger than 10 nm to allow for complete sterical stabilisation.

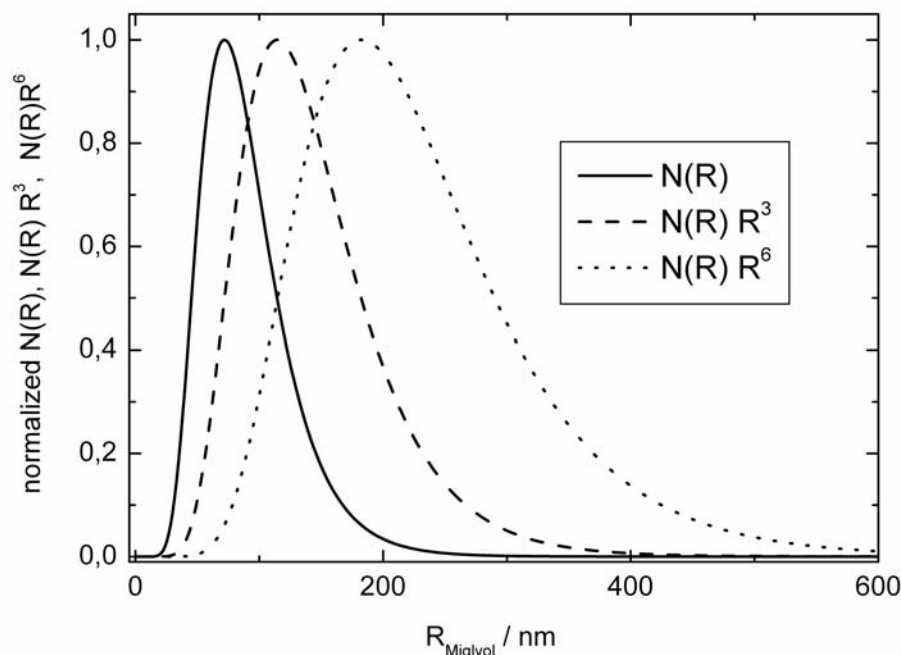


Figure 2.20 The resulting size distribution  $N(R)$  together with the volume  $N(R)R^3$  and intensity distribution  $N(R)R^6$  obtained from the fit of the SANS data.

The resulting size distribution  $N(R)$  together with the volume  $N(R)R^3$  and intensity distribution  $N(R)R^6$  are shown in Figure 2.20. From this figure it is obvious that methods which are sensitive on the particle volume or even on the square of the volume always provide larger values for the particle radius than methods which are only sensitive on the number of particles.

## 2.5 Conclusion

Electron spin resonance experiments facilitate the assessment of the nanoenvironment, including the polarity and viscosity, of the oily phase in nanocapsules. Additional NMR relaxation measurements resolved the distribution profile down to the molecular scale.

The ESR distribution assay shows that molecules with moderate lipophilicity ( $\log P \sim 2.5$ ) are rapidly relocated to a new distribution equilibrium. In contrast the distribution of very lipophilic molecules (HD-PMI) ( $\log P > 6$ ) is not influenced to a measurable extent upon dilution.

The shell of PLA and PEG-PLA nanocapsules does represent only a moderate diffusion barrier to nanoencapsulated molecules. However the resistance to reduction by ascorbic acid of spin probes incorporated into PEG-PLA nanocapsules is higher than in PLA nanocapsules.

The contrast variation technique in small angle neutron scattering (SANS) was used successfully to determine the shell thickness of poly(D,L-lactide) (PLA) nanocapsules. Highest sensitivity on the inner structure of the nanocapsules was obtained when the scattering length density of the solvent was varied between the one of the Miglyol core and the PLA shell. According to the fit data the PLA shell thickness was 9.8 nm. The z-averaged radius determined by SANS experiments correlated well with dynamic light scattering (DLS) results, although DLS values were systematically slightly higher than the ones measured by SANS. This could be explained by taking into account the influence of Poloxamer attached to the nanocapsules surface. For a refined fit model with a second shell consisting of Poloxamer, SANS values and DLS values fitted well each other.

The characterization methods presented here are significant because detailed insights into the nanoenvironment, dilution kinetics and the shell were gained for the first time. These methods could be used to develop strategies for the optimization of the shell properties concerning controlled release and to study changes in the shell structure during degradation processes.

## 3 A novel coazervation-based process for the preparation of oil-loaded polyelectrolyte nanocapsules

### 3.1 Introduction

Polyelectrolyte (PE) complexes are formed by complex coazervation which is the reaction of two dispersed hydrophilic colloids of opposite electric charges. Biopolymers, chemically modified biopolymers or synthetic polymers can function as polyions. Widely used examples for anionic biopolymers are gelatine B, sodium alginate, Arabic gum, pectin, xanthan gum, nucleic acids or proteins. Examples for chemically modified biopolyanions are carboxymethylcellulose, chitosan sulphate or dextrane sulphate. From the group of synthesized polymers poly(acrylic acid) is suitable. There are fewer examples for polycations, the most widely used are gelatine A as a biopolymer, chitosane as a modified biopolymer and poly(ethylene imin) as a synthetic polymer.

Polyelectrolytes have several applications. The polyelectrolytes themselves can be used in food industry as thickening agents for e.g. juices and chocolate. For a potential application in food industry Ogawa et al. [146-148] utilized lecithin-chitosan and lecithin-chitosan-pectin multilayered membranes to improve the stability of food emulsions.

In industrial chemistry polyelectrolytes are applied as stabilizers and emulsifiers for thixotropic paints and in textile industry as suspending agents for dyes. Polyelectrolytes are also suitable as ion exchange material for the removal of heavy metals from industrial wastewaters.

During the last 10 years research activity on polyelectrolytes and polyelectrolyte complexes has been high for pharmaceutical applications as wound healing [149] or drug-release systems. Panzner et al. [150] encapsulated liposomes with chitosan-alginate layers to prevent liposome mixtures from aggregation. Decher and Hong [151-153] introduced a layer-by-layer (LBL) self assembly technique for the production of ultra-thin polyelectrolyte films on flat substrates. The technology, using slides and beakers, is quite simple, namely a positively charged substrate on a slide adsorbs a polyanion and a polycation consecutively from solution, using washing steps for the removal of excess polyion in between. The driving force behind this method is the electrostatic attraction between the incoming polymer

and the surface. This technique has been widely used by following groups working on polyelectrolyte complexes. Möhwald and co-workers transferred the LBL principle from two-dimensional films to three-dimensional structures, namely hollow polyelectrolyte capsules and crystals in the lower micrometer range [154-157], other groups followed with hollow nanocapsules [158,159]. These capsules have a given size because the LBL assembly of polyelectrolytes is performed on preformed templates. Melamine formaldehyde (MF) or poly(styrene sulfonate) (PSS) serve as templates. Due to their acid solubility, the templates can be removed after finished LBL deposition to form hollow polyelectrolyte capsules. Loading of and release from the polyelectrolyte multilayer capsules is dependent on the number of adsorbed layers, the chosen PE pairs, their stoichiometry, pH values and salt concentrations during production and at the site of action.

The capsule wall thickness can be adjusted by the number of PE layers. Mean values for the thickness of a polyanion-polycation monolayer vary depending on the PE pair used. Values of 2-4 nm are reported [160,161] for each double layer of poly(styrene sulfonate)/poly(allylamine hydrochloride), chitosan/dextran sulphate and chitosan/polyacrylic acid PE pairs. In contrary gelatine-polyanion layers can be as thick as about 10 nm. Layer growth can be controlled by single particle light scattering and electrophoresis.

In general polyelectrolyte capsule walls are semipermeable whereas small molecules can easily penetrate the capsule wall but macromolecules are excluded from the shell. Despite the coating with several PE pair layers release from capsules can be very fast, e.g. 100% Ibuprofen release within 125 seconds from microcapsules containing five PE pair layers was reported [156].

Since encapsulation of substances into the hollow capsules has to be performed belated, approaches were made to switch the capsule walls between open and closed state. This was achieved by pH-induced permeability changes of the polyelectrolyte network. Capsules allow pH-sensitive encapsulation, namely they offer permeability at low pHs and closed walls at high pHs, when the polyelectrolyte pair contains a strong polyanion and a weak polycation. Möhwald and co-workers [80] demonstrated this principle with poly(styrene sulfonate) and poly(allylamine hydrochloride) to form multilayered microcapsules. Sauer et al. [87] created pH-sensitive nanocontainers of 45 nm using crosslinked poly(acrylic acid). The background of this approach is pH-sensitive swelling of poly(acrylic acid)

due to increasing dissociation at increasing pH. Thereby the electrostatic repulsion between the carboxylate anions within the polymer backbone is so strong that a volume increase of factor 80 was reported which can possibly be used for belated encapsulation of compounds.

Adjusting the pH to certain values is crucial during the adsorption process to induce maximal ionization. Sukhorukov [162] reported that the addition of NaCl facilitates the formation of denser PE multilayers.

Despite all features of LBL capsules, a disadvantage of this method is the time-consuming filtration or ultracentrifugation of non-adsorbed polyelectrolyte after each adsorption step. Furthermore liquid templates like emulsions are not suitable for the LBL technique because these cores cannot withstand the mechanical strength during the separation step.

In this chapter a new formulation approach for oil-loaded polyelectrolyte nanocapsules based on complex coazervation and following high pressure homogenization will be discussed. The objective of this study was to develop a technique that uses oily nanodroplets as templates for PE nanocapsule production and does not require separation steps and belated filling of hollow capsules.

First of all the optimal experimental conditions concerning choice of suitable PE pairs, their stoichiometry, pH values and temperatures for the single production steps were evaluated. Composite PE nanocapsules consisting of olive oil and polyionic biopolymers were produced. □ potential measurement have been used to confirm the reloading of the nanocapsules after each adsorption step which gives evidence for the step-wise growth of the PE shell. TEM micrographs show the morphology of the composite PE nanocapsules in comparison to the nanoemulsion template. PCS studies have been carried out to study the nanocapsule size.

### 3.2 Materials

The used polysaccharides chitosan, carrageenan and purity gum 2000 are all food grade, non-toxic and biodegradable materials.

Chitosan is a derivative of chitin, a natural biopolymer which is produced in the shell of insects and crustaceans. Since chitin provides the structure and integrity to these animals, as cellulose does to plants, it is one of the most abundant biopolymers on earth. Chitin molecules are large chains of N-acetyl glucosamine units. By slightly modifying the molecule through deacetylation, chitosan is produced, which offers exposed amino groups. Chitosan has a  $pK_s$  value between 6.3 and 7.0 [163] leading to a positive charge of the molecule upon exposure to acidic media. Due to its high binding capacity and high viscosity, the main commercial applications are the dietary supplement, where it serves as a fat binder, and cosmetic industry.

Powdered chitosan, Chito Clear FG 95 (Food grade; degree of deacetylation: 95%) from Primex, Iceland, was used.

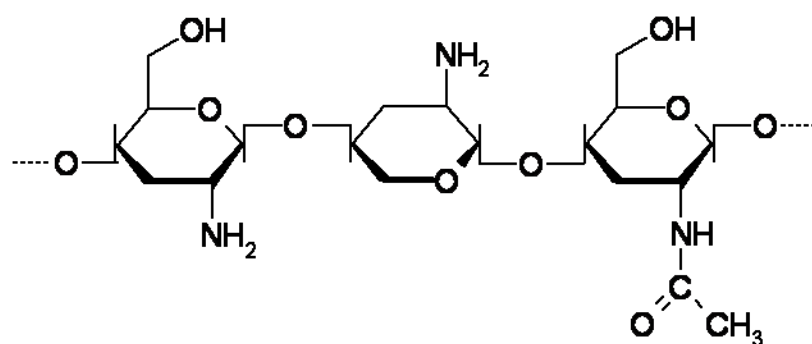


Figure 3.1 Chemical structure of chitosan (degree of deacetylation: 95%).

Carrageenan is the name given to a family of linear sulphated polysaccharides obtained from the red seaweeds, which have the ability to form all different types of gels. The carrageenan family has three main branches named kappa ( $\kappa$ ), iota ( $\iota$ ) and lambda ( $\lambda$ ) which can be differentiated by their gelling properties and protein reactivity. While  $\kappa$  carrageenans produce strong rigid gels,  $\iota$  forms only flaccid ones and  $\lambda$  carrageenans do not gel in water.  $\kappa$  carrageenan shows the strongest interactions with proteins followed by  $\iota$ . Due to their gelling properties and protein reactivity carrageenans are mainly used in the food and dentifrice industry, e.g. for chocolate milk, toothpaste and bread. It is also used in low fat products, where it



is added to replace fat and to maintain viscosity and mouth feel. In pharmaceutical technology carrageenans are used as tableting excipients which form hydrocolloid matrices. Viscarin GP 209 NF from FMC Bio Polymer, which is  $\kappa$  carrageenan, has been used. The degree of sulfatation is 35% [164].

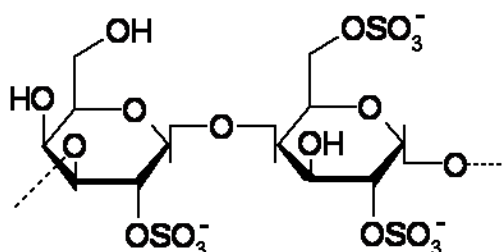


Figure 3.2 Chemical structure of  $\kappa$  carrageenan (degree of sulfatation: 35%).

Purity gum 2000 is a modified starch which is derived from waxy starch. Due to the esterification of starch with octenyl succinic acid, purity gum has good emulsion stabilising properties even at low temperatures. Applications include food emulsions such as flavoured emulsions, bakery emulsions, vitamin and health care preparations. Purity gum 2000, E1450 for food use from National Starch & Chemicals, was used. The degree of esterification is 0.2% and its aqueous solution shows an pH of approximately 4 [165].

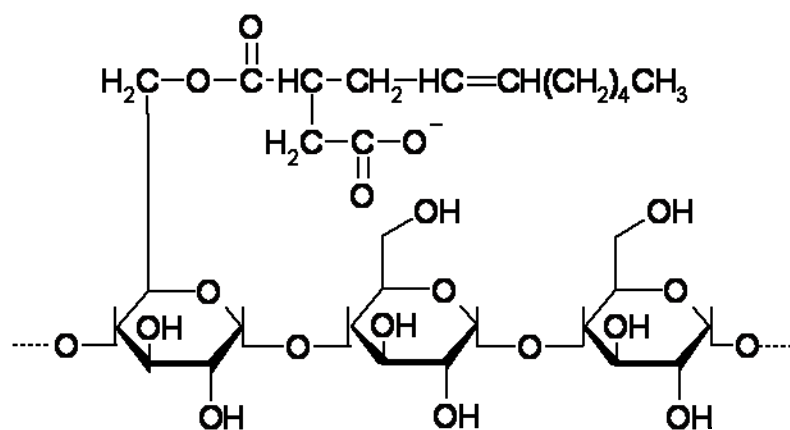


Figure 3.3 Chemical structure of purity gum (degree of esterification: 0.2%).

In pre-experiments the polyanion xanthan gum was also under investigation. Xanthan gum is a microbial biopolymer which is synthesized by *Xanthomonas campestris*. The primary structure of xanthan consists of a pentasaccharide repeating unit [(1 $\rightarrow$ 4)- $\beta$ -D-glucopyranose] to which trisaccharide side-chains are

attached which consist of two mannose and a glucuronic acid residue. Xantural™ 180 from CP Kelco was used.

For the nanoemulsion template olive oil from Sigma was used.

### 3.3 Methods

#### 3.3.1. Nanocapsule preparation

##### *Solution preparation*

For the aqueous emulsifier solution 5% (w/v) purity gum was dispersed in bidistilled water.

0.2% (w/v) of chitosan powder was dispersed in 0.1 N acetate buffer, pH 4.5 (containing 0.02 wt% sodium acide as an antimicrobial agent).

0.4% of Carrageenan were dissolved in bidistilled water by heating to 80°C to decrease the viscosity of the solution.

##### *Preparation of the nanoemulsion template*

The aqueous purity gum solution was heated to 50 °C and applied to a rotor-stator mixer (Ultra turrax®, IKA® T18 basic, IKA®-Works, NC). 5% of olive oil was added stepwise under mixing. The olive oil was injected into the aqueous solution by a pipette, which decreased the foaming compared to the addition of olive oil on top of the aqueous phase. The aqueous emulsifier solution and the oil phase were mixed for 90 seconds at 14.000 rpm before this coarse emulsion was introduced to a two-stage high-pressure valve homogenizer (nG7400.270 P, Standsted Fluid Power Ltd., UK-Stansted) to achieve droplet sizes in the nano range. Three passes were run with 900-1000 bar for stage one and 200 bar for stage two and then a fourth path with only one stage at 400 bar.

##### *Preparation of PE nanocapsules I*

10 ml of a 0.2% chitosan solution in acetate buffer were injected with a syringe into 20 ml of the primary emulsion (5% olive oil and 5% purity gum) under high-shear mixing (14.000 rpm, Ultraturrax). Addition of the chitosan solution was carried out very slowly. The solution was added tropwise with mixing breaks in between. After the complete addition of 10 ml mixing was continued for 3-4 minutes.

### *Preparation of composite PE nanocapsules II*

30 ml of the *nanocapsule I* dispersion were heated to 80°C and 10 ml of the 0.4% carrageenan solution of the same temperature were added by syringe under high shear mixing (18.000 rpm). The mixture was introduced to high pressure homogenization at once (3 runs x 900-1000 bar + 200 bar, 4<sup>th</sup> run at 400 bar).

### 3.3.2 Experimental techniques

PCS measurements were performed with a Malvern HPPS as described in chapter 2.3.2. All samples were diluted 1:3 with water.

□ potential measurements (see chapter 2.3.3) were carried out after diluting the samples in the ratio 1:4 and mixing them with KCl solution (0.002 mol/l) in the ratio 1:1. Measurements were performed with a ZetaSizer 3000HS (Malvern Instruments, UK). Each sample was measured four times with automatic measurement duration.

For TEM measurements (see chapter 2.3.4) the nanoemulsion templates were diluted with bidistilled water (1:1). The composite PE nanocapsules II were examined without further dilution.

### 3.4. Results and discussion

#### 3.4.1. Optimization of the production process

In Figure 3.4 a schematic representation of the formulation process for oil-loaded PE nanocapsules is given. Step I corresponds to the formation of nanoemulsion templates which show a negative charge due to deprotonated carboxylate groups in the backbone of purity gum. Step II leads to the formation of nanocapsules consisting of an oily core surrounded by purity gum and chitosan. These nanocapsules have a positive charge because the polycation chitosan was added in excess to neutralize all negative charges and furthermore to recharge the surfaces by surplus positive charges from protonated amino groups. Step III shows the formation of composite PE nanocapsules with an additional PE consisting of carrageenan. Here again a recharging of the nanocapsules by the sulphate groups of carrageenan is achieved leading to an overall negative charge of the final composite PE nanocapsules.

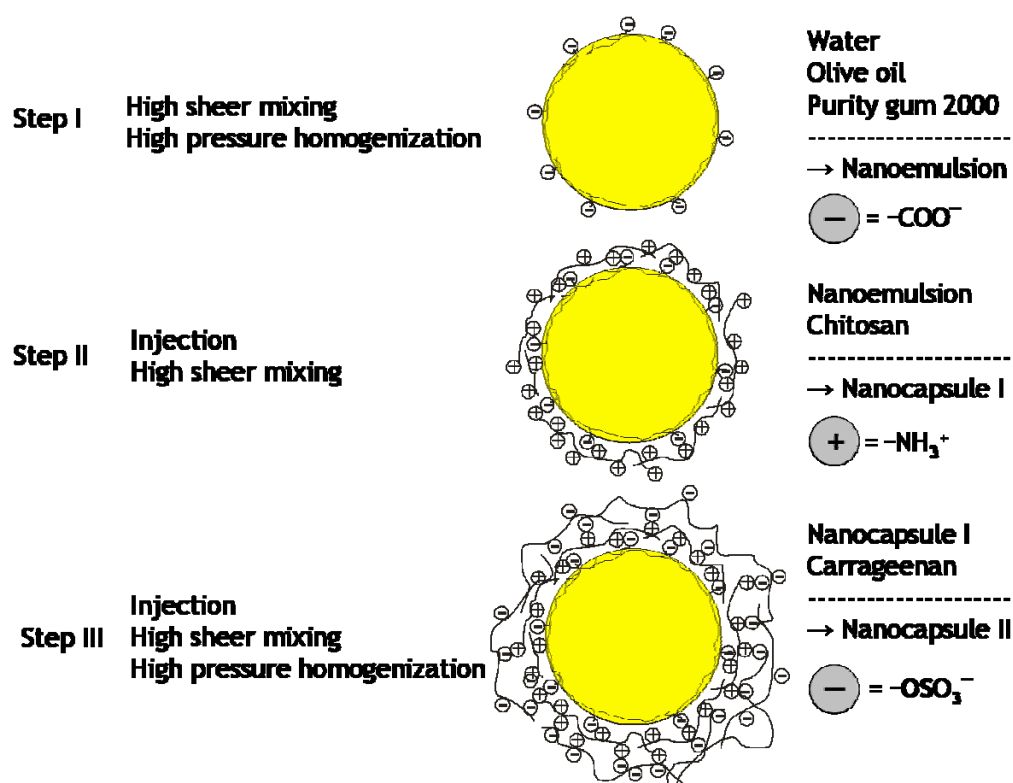


Figure 3.4 Schematic representation of the polyelectrolyte nanocapsule formation process. Step I corresponds to the formulation of the primary emulsion, step II leads to the formation of PE nanocapsules I by coazervation of a polyelectrolyte pair and step III leads to the formation of composite PE nanocapsules II.

In detail the following optimizations for the three production steps have been performed.

In step I high pressure homogenization was used to produce oily templates in the nano range with the ability to adsorb polyelectrolytes due to a surface charge. These nanotemplates will be referred to as nanoemulsion template or nanoemulsion.

The anionic and cationic biopolymers xanthan gum, purity gum and chitosan were studied for their ability to stabilize O/W nanoemulsions containing 5% (w/v) of olive oil. This primary oil concentration was chosen to achieve a final oil load of 2.5% (w/v) for composite PE nanocapsules (Table 3.1.).

Xanthan gum was disadvantageous because of its low emulsifying property combined with a high viscosity. Though it was well soluble in water forming solutions of moderate viscosity in concentrations of 0.5 to 0.7% (w/v), oil was mainly quasiemulsified by the high viscosity of the outer phase leading to large aggregates of droplets with particle sizes in the  $\mu\text{m}$  range. Chitosan in concentrations of 1% (w/v), dispersed in acetate buffer, formed nanoemulsions with a smaller size distribution though few droplets in the  $\mu\text{m}$  range were detectable by light microscopy. The weakly anionic emulsifier purity gum was found to produce nanoemulsions with the smallest droplet size and a narrow size distribution.

5% of purity gum was the optimal concentration to stabilize the nanoemulsion templates containing 5% of olive oil. Lower concentrations lead to increased polydispersity whereas higher concentrations caused increased foaming during processing. The ingredients bidistilled water and purity gum were premixed with a rotor stator mixer (Ultraturrax) and the oil phase was injected with a pipette to decrease foaming. As a following step high pressure homogenization was needed to achieve particle sizes in the nano range. Best results were achieved at increased temperature as high as 50 °C. The formation process was carried out in bidistilled water for two reasons: first to guarantee almost maximal ionization of the charged groups of purity gum and second to achieve a low influence of additional ions in the formulation.

The produced nanoemulsion templates had a z-average particle size of  $212.01 \pm 16.16$  nm and showed a very narrow polydispersity index of  $0.136 \pm 0.017$ .

In step II chitosan was used as a corresponding polycation. Having a pKs value of 6.3-7.0, chitosan is not soluble in water. Therefore the biopolymer was dissolved at pH 4.5 in acetate buffer, 0.1N. At this pH almost maximal ionization of the amino groups should be achieved leading to good solubility and offering a high quantity of charged groups for layer formation. The chitosan solution was slowly injected by syringe under high sheer mixing to prevent the formation of polymer bridges between single droplets leading to flocculation.

To decrease the viscosity of carrageenan in step III this biopolymer was processed at 80°C. After injection of the aqueous biopolymer solution to nanocapsules I, the final PE nanocapsules were introduced to high pressure homogenization to mechanically force polyelectrolytes to become detached from all but one of the droplets. The particle size of the final composite PE nanocapsules was 236.10 ( $\pm$  12.67 nm) with a PDI of 0.341 ( $\pm$  0.026).

Table 3.1 gives an overview of the sample compositions. The rational background for the stoichiometry of the three polyions will be discussed in the following chapter with regard to electrical charge of the samples.

Table 3.1 Sample composition

<i>Sample Nr.</i>	<i>Sample</i>	<i>olive oil % [v/v]</i>	<i>purify gum % [w/v]</i>	<i>chitosan % [w/v]</i>	<i>carrageenan % [w/v]</i>
1	Nanoemulsion template	5	5		
2	PE nanocapsules I	2.5	2.5	0.05	
3	PE nanocapsules II	2.5	2.5	0.05	0.1

## 3.4.2. Layer formation followed by zeta potential measurements

The primary emulsion droplets in aqueous environment had a zeta potential of -12.7 mV due to the negative charge of purity gum molecules at the oil-water interface. The relatively low zeta potential can be explained by the low substitution degree of the starch backbone with octenyl succinic acid of 0.2%. Free oleic acid or other ionic impurities might also contribute to the electrical charge of the emulsion droplets. Upon addition of the polycation chitosan the electrical charge on the droplets changed from negative to positive. The mixing ratio of the polyelectrolyte layer pair was 50 parts of the polyanion purity gum with a carboxylation degree of 0.2% with 1 part of the polycation chitosan with a substitution degree of free amino groups of 95% (Table 3.1.). There was obviously sufficient charge from the protonated amino groups of chitosan to cause surface re-charging as evident by the reversal of the zeta potential values from -12.7 mV to +8.6 mV. Following exposure to the polyanion carrageenan caused adsorption of this PE, the resulting nanocapsules having a zeta potential of -28.5 mV. The mixing ratio of chitosan to carrageenan was 1:2 (Table 3.1.), whereas the ratio of cationic to anionic groups was 95% to 35%. As the zeta potential values demonstrate there was enough negative charge provided by the sulphate groups of carrageenan to neutralize the free protonated amino groups of the chitosan layer and to re-charge the electrical charge of the nanocapsules by surplus negative sulphate groups.

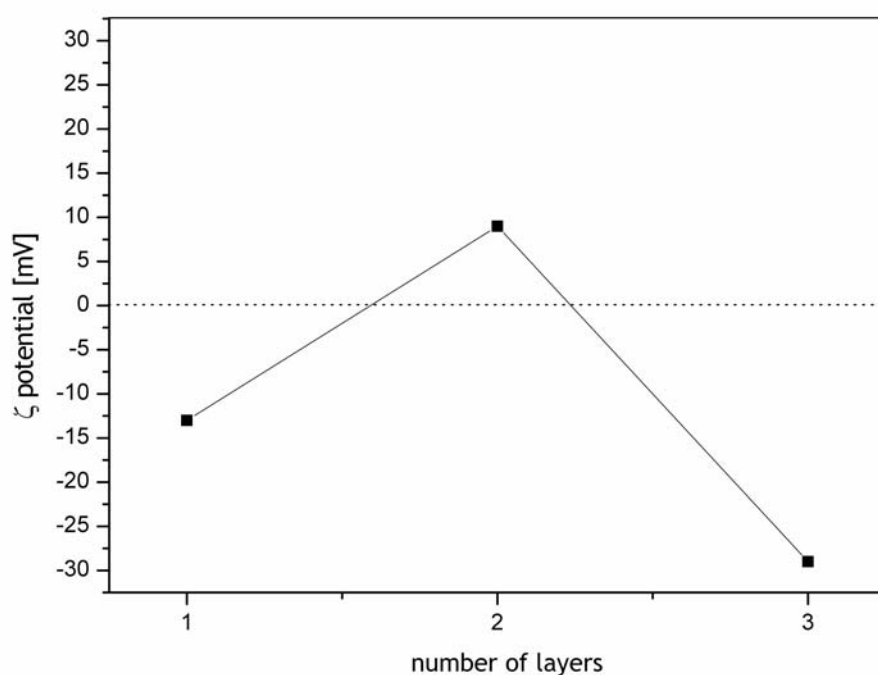


Figure 3.5 □ potential reversals for three PE adsorption steps.

The charge reversals obtained (Figure 3.5.) represent credible evidence for the step-wise growth of a composite polyelectrolyte layer on the nanoemulsion templates.

### 3.4.3 Morphology of polyelectrolyte nanocapsules

Transmission electron microscopy studies confirm the existence of shell formation on the oily template which was observed by  $\square$  potential measurements.

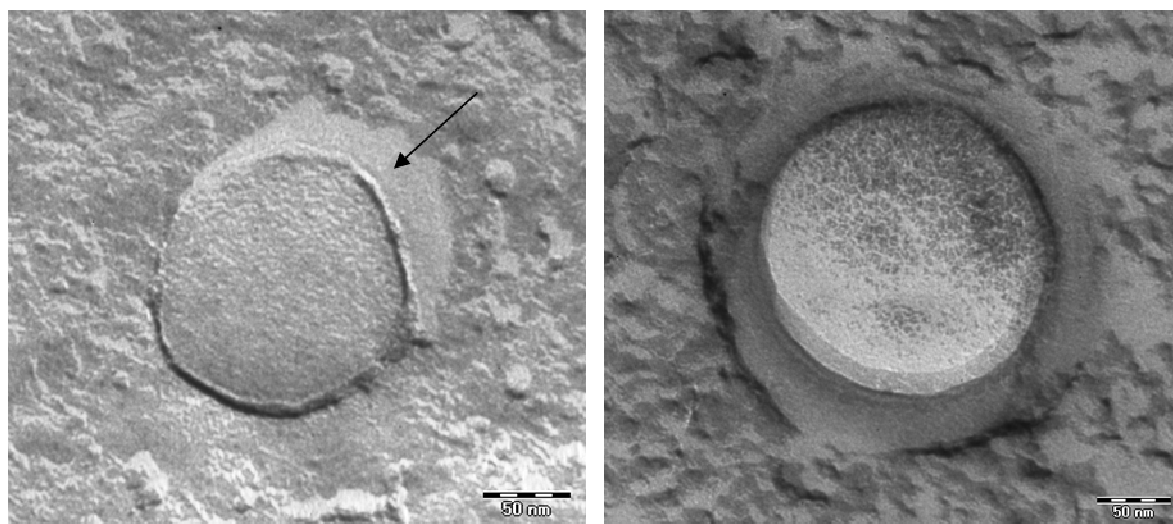


Figure 3.6 TEM photomicrographs of a nanoemulsion template (left) and a composite PE nanocapsule treated by freeze fracture and etching. The arrow (left) marks a “shadow” which emerges from sample processing for TEM.

The TEM photomicrograph on the left shows a nanoemulsion template composed of olive oil and purity gum (Table 3.1, sample 1). The arrow marks a “shadow”, which emerges from the sample processing for TEM as follows. Surfaces, which result from the freeze-fracture, are shadowed with platinum to produce good topographic contrast. Due to the shadowing angle of  $45^\circ$  a microscopic object on the surface provides a “shadow”, as it can be seen on the left photomicrograph, which remains uncoated with metal. On the right a composite PE nanocapsule composed of a nanoemulsion template which is coated with purity gum, chitosan and carrageenan (sample 3) is visible.

The difference between the two photomicrographs clearly shows that coating of the nanoemulsion template with polyelectrolytes was successful. The nanoemulsion droplet exhibits a thin coating from the emulsifying starch purity gum which arranges at the oil-water interface to stabilise the system. On the other hand the final PE nanocapsule shows an oily core which is surrounded by a composite PE



coating. A highly swollen shell is visible. The observed PE shell is much thicker than the shell of PLA and PEG-PLA nanocapsules (Figure 2.3). The diameter of the encapsulated oily core can be estimated with 200 nm, the shell has an extent of 30 nm, leading to a total nanocapsule diameter of 260 nm.

In Figure 3.7 an unbroken composite PE nanocapsule is visible having also a particle size in this range.

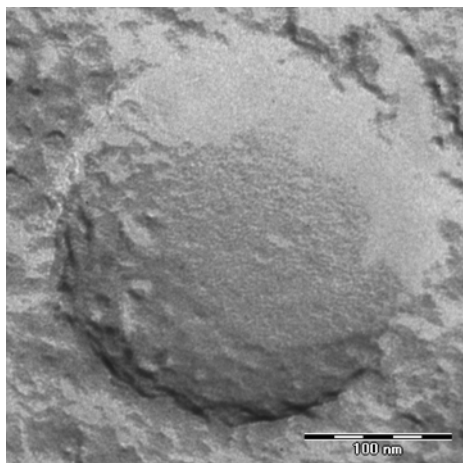


Figure 3.7 TEM photomicrograph of an unbroken composite PE nanocapsule.

These results are in accordance with PCS results. The increased layer thickness of the shell might be explained by loop formation of uncharged parts of the polymer backbone.

### 3.5 Conclusion

Complex coazervation combined with high pressure homogenization has been carried out successfully to design novel composite polyelectrolyte nanocapsules composed of olive oil and three different biopolymers.  $\square$  potential measurements confirmed the charge reversal after each adsorption step involved and thereby proved the step-wise growth of the polyelectrolyte shell. TEM studies on these nanocapsules revealed the formation of a composite shell on the oily core. PCS measurements of the final PE nanocapsules showed a z-average value of 230 nm.

In comparison to the existing interfacial layer-by-layer deposition process, the method developed here for nanocapsule preparation saves the time-consuming separation of non-adsorbed polyelectrolyte in between the adsorption steps. Furthermore it is the first work on polyelectrolyte nanocapsules which describes in detail the usage of a liquid colloidal template. The elsewhere used solid templates, which are necessary for the separation process by filtration or ultracentrifugation, have to be dissolved after nanocapsule production leaving hollow carriers. In the here presented approach the liquid template composed of olive oil serves as an ideal solvent for lipophilic drugs. Injection of the polyelectrolytes and subsequent high pressure homogenization caused disruption of aggregates due to polymer bridges between single droplets leading to acceptable oil loading of 2.5% (v/v).

## 4 Development of an ESR online-method for the monitoring of in vitro fat digestion

### 4.1 Introduction

When regarding the oral administration of lipid-based nanocapsules, gastrointestinal digestion will play a predominant role in the subsequent drug absorption. Therefore it is crucial to understand the complex series of events which occur on interaction of the lipid formulation and the gastrointestinal environment.

In recent years several groups worked on a better understanding of the mechanisms by which lipids improve absorption. *In vitro* tests were established that predict the complex series of events which occur on interaction of a simple lipid formulation and the GI environment [166-169]. Investigations based on titrimetric, high-performance thin-layer chromatography (HPTLC) and ultracentrifugation techniques showed that lipid digestion leads to the formation of new colloidal species, e.g. mixed micelles and vesicles formed by bile salts and phospholipids [170-174]. The distribution of the drug between the aqueous, oil phase and mixed micelles will affect the absorption rate. Porter et al. [175] and Kaukonen et al. [166,167] assessed the distribution of co-administered drugs between the different phases after *in vitro* digestion of long and medium chain triglycerides and Porter et al. compared these data with *in vivo* results.

Until now it was not possible to perform an online study on the distribution of the drug between water, oil and colloidal species formed during digestion.

Therefore it was the aim of these studies to develop a methodology to be able to non-invasively monitor *in vitro* fat digestion by ESR. For the setup of the method a model system was used and the time-dependent fate of the co-administered spin probe TEMPOL benzoate (TB) as a poorly water-soluble, moderately lipophilic model drug in a long chain triglyceride (olive oil) during digestion was monitored. The *in vitro* lipid digestion test used here was recently established in our laboratory [176]. Electron paramagnetic resonance (ESR) was applied as an online method to investigate the complex changes of the artificial GI environment during digestion by monitoring changes in the micropolarity and -viscosity of the lipophilic spin probe. The distribution of the model drug within the different lipid digestion

products was also recorded. The method was developed with the aim to study the fate of nanocapsules and other lipid-based nanocarriers in future.

## 4.2 Materials

Pancreatin (porcine) (P 7545, 8x USP specification activity) and bile extract (porcine) (B 8631) were purchased from Sigma (St. Louis, USA). Olive oil was purchased from Caelo, Germany.  $\text{CaCl}_2$  and  $\text{Na}_2\text{HPO}_4 \times 2\text{H}_2\text{O}$  of analytical grade, manufactured by Roth (Germany) were used.  $\text{KH}_2\text{PO}_4$  was purchased from Merck KGaA, Germany.

TEMPOL-benzoate (4-hydroxy-TEMPO-benzoate, 4-benzoyloxy-2,2,6,6-tetramethyl-piperidine-1-oxyl; TB) was obtained from Aldrich Chem. Co, USA.

## 4.3 Methods

### 4.3.1 *In vitro* digestion model

For the *in vitro digestion* experiments 1.5% (v/v) of olive oil and 1 mM of TB (referring to the TB concentration in the final volume) were dispersed by Ultraturrax in 15 ml of digestion buffer (53.4%  $\text{Na}_2\text{HPO}_4 \times 2\text{H}_2\text{O}$  1/15 M, 46.6%  $\text{KH}_2\text{PO}_4$  1/15 M, 10 mM  $\text{CaCl}_2 \times \text{H}_2\text{O}$ , pH 6.8) containing 10 mM bile salts (BS).

Experiments were initiated by the addition of 48.2 mg pancreatin extract containing 150 u/ml of pancreatic lipase activity. The *in vitro* digestion experiments were performed at 37°C in an end-over-end shaker. The pH was adjusted every 15 minutes. Digestion was monitored over 45 min using ESR spectroscopy. For ESR measurements a sample of the digest was filled into an ESR capillary which was measured with the X-Band spectrometer.

### 4.3.2 ESR-based digestion monitoring

An ESR spectrometer of 9.5 GHz (X-Band; Miniscope MS 200) from Magnettech (Berlin; Germany) was used. The measurements were conducted with the following typical parameters: modulation frequency: 100 kHz; microwave power: 20 mW; scan range: 10 mT, scan time: 30 s, modulation amplitude: 0.1 mT.

Simulation of the ESR spectra was performed by means of Public ESR Software Tools (P.E.S.T.) from National Institutes of Health (National Institute of Environmental Health Sciences, Research Triangle Park, NC 27709) [130]. The optimization method used was LMB1.

## 4.4 Results and Discussion

### 4.4.1 Monitoring of in vitro fat digestion by ESR

In order to understand the distribution process of the model drug TB between phosphate buffer, oil and mixed micelles, complex ESR spectra containing three different components had to be simulated. To reduce the amount of variable simulation parameters during the simulation process, ESR spectra of TB in the separate environments were recorded and the belonging simulation parameters were determined.

The ESR spectrum of TB in phosphate buffer (Figure 4.1 a) shows a hyperfine-coupling constant of 1.670 mT which is typical for polar environments. Due to the low viscosity, the amplitude and the line width of the three ESR lines are almost equal.

Under the more viscous conditions of TB in olive oil (Figure 4.1 c) the lines broaden, the hyperfine-coupling constant is smaller (1.525 mT), indicating an apolar environment, and the ESR spectrum shows three lines of decreasing height. This effect occurs when the spin probe does not have a free mobility in all directions and can be attributed to the influence of the fatty acid chains of the olive oil.

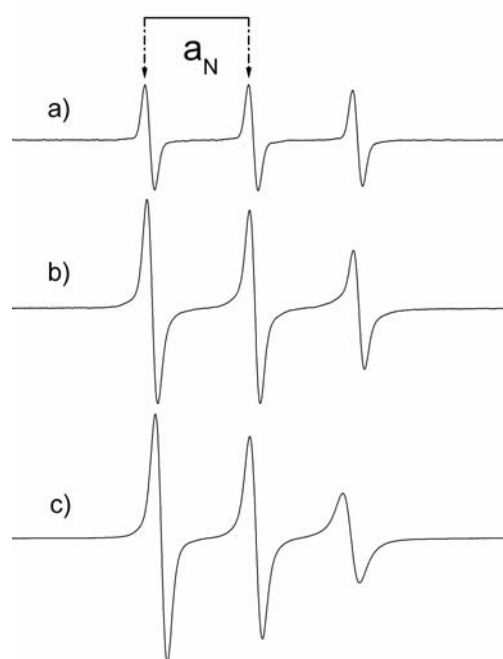


Figure 4.1 ESR spectra of TB-loaded

a) phosphate buffer

b) mixed micelles

c) olive oil

The hyperfine coupling constant of TB in mixed micelles (Figure 4.1 b) at 1.634 mT lies between the polar value of phosphate buffer and the apolar value of olive oil (Figure 4.2). It indicates an intermediate polarity. Similar to the spectrum in olive oil, the ESR spectrum of TB in mixed micelles shows three lines of decreasing height. This effect here can be attributed to TB molecules which experience a decreased mobility as they are incorporated into mixed micelles.

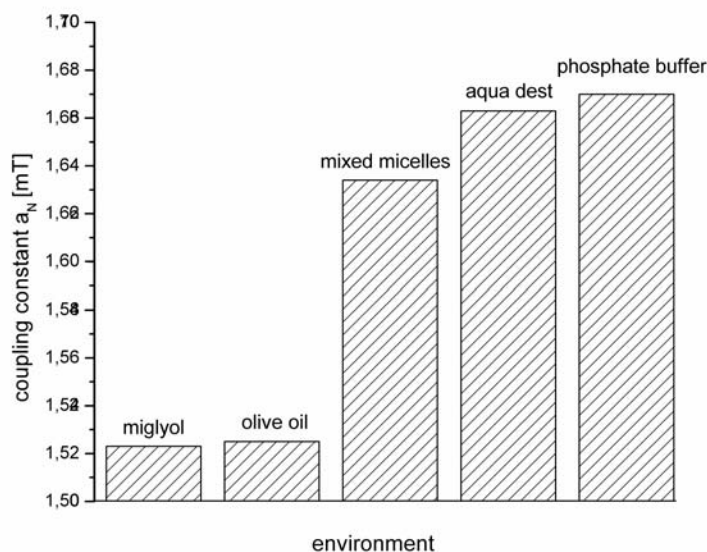


Figure 4.2 Hyperfine coupling constant ( $a_N$ ) values for TB depending on the polarity of the environment.

The magnitude of this so-called flue pipe effect is depending on the bile salt concentration in the phosphate buffer. While TB in phosphate buffer containing 5 mM bile salts exhibits still a narrow third line (Figure 4.3 a), this line and also the other two lines broaden (Figure 4.3 c) with higher bile salt concentrations. The spectra can be simulated with two species.

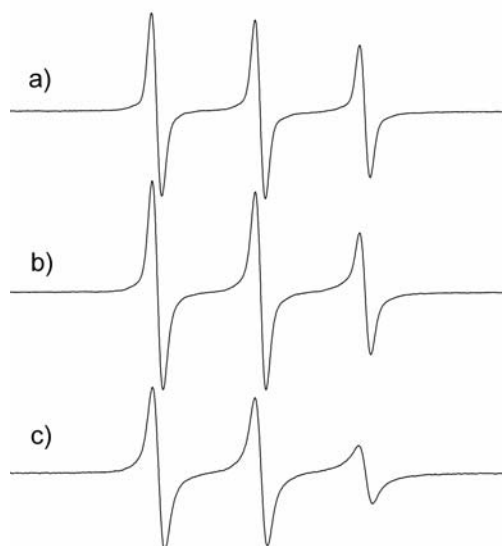


Figure 4.3 ESR spectra of TB loaded  
a) mixed micelles (5 mM) in phosphate buffer  
b) mixed micelles (10 mM) in phosphate buffer  
c) mixed micelles (40 mM) in phosphate buffer.

Species I with a coupling constant of 1.670 mT describes TB in phosphate buffer, species II ( $a_N = 1.634$  mT) TB in mixed micelles. At a concentration of 5 mM bile salts 67% of the TB molecules are located in the mixed micelles, this fraction amounts 91% when increasing the bile salt concentration up to 40 mM. For the *in vitro* model a bile salt concentration of 10 mM (Figure 4.3 b) was used. Under these circumstances 22% of the spin probe are located in the phosphate buffer and 78% are incorporated into the mixed micelles.

The ESR spectra of TB recorded at different times of the *in vitro* lipolysis were simulated with three species. The distribution of the model drug TB between phosphate buffer ( $a_N = 1.67$  mT), olive oil ( $a_N = 1.525$  mT) and mixed micelles ( $a_N = 1.634$  mT) was determined.

Lipid digestion caused significant changes in the ESR spectra (Figure 4.4).



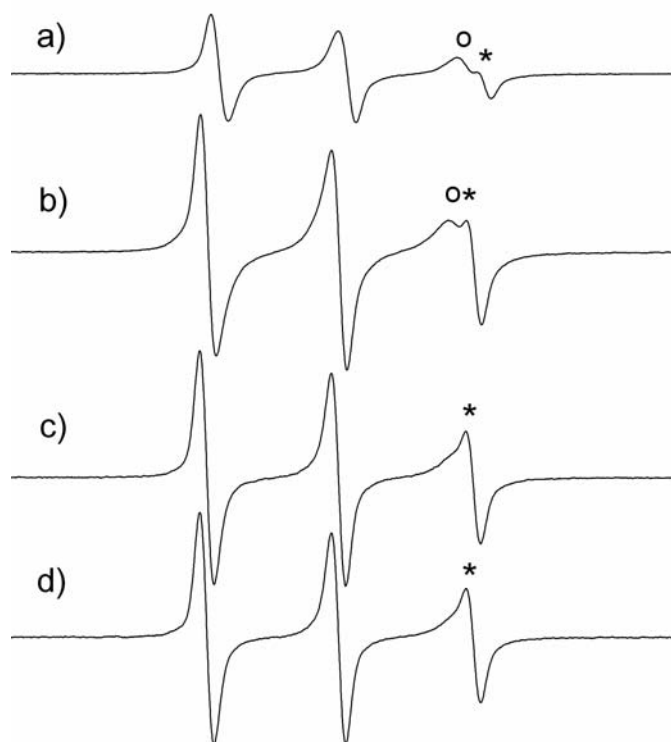


Figure 4.4 ESR spectra of TB-loaded olive oil

- a) after 0 min of digestion
- b) after 5 min of digestion
- c) after 20 min of digestion
- d) after 45 min of digestion.

In Figure 4 a) the shape of the third peak is dominated by the TB species which is located in the olive oil ( $^{\circ}$ ). Before adding the digestion enzymes 79% of the TB molecules are located in olive oil, 14% in mixed micelles and 7% in phosphate buffer. After 5 minutes of digestion the spectral shape changes significantly. While the influence of the oily species on the third peak decreases, a more polar species (\*) arises. At this state 64% of the TB molecules are still located in the oily phase, the amount of molecules in the mixed micelles increased to 27% and 8% are dissolved in phosphate buffer. After 20 minutes of digestion the outer line of the third peak becomes dominant indicating that an increasing number (50%) of TB molecules is now integrated into the mixed micelles and only 33% are still located in olive oil. At the end of the experiment, after 45 minutes, the majority of the TB molecules are located in the mixed micelles (62%), 24% are dissolved in olive oil and 14% in phosphate buffer.

In summary the redistribution of TB between oil and mixed micelles was fastest during the first five minutes and proceeded with high speed up to twenty minutes

(Figure 4.5). In the following 25 minutes the rate of redistribution decreased considerably. The amount of spin probe in the phosphate buffer was always below 17% (Table 4.1).

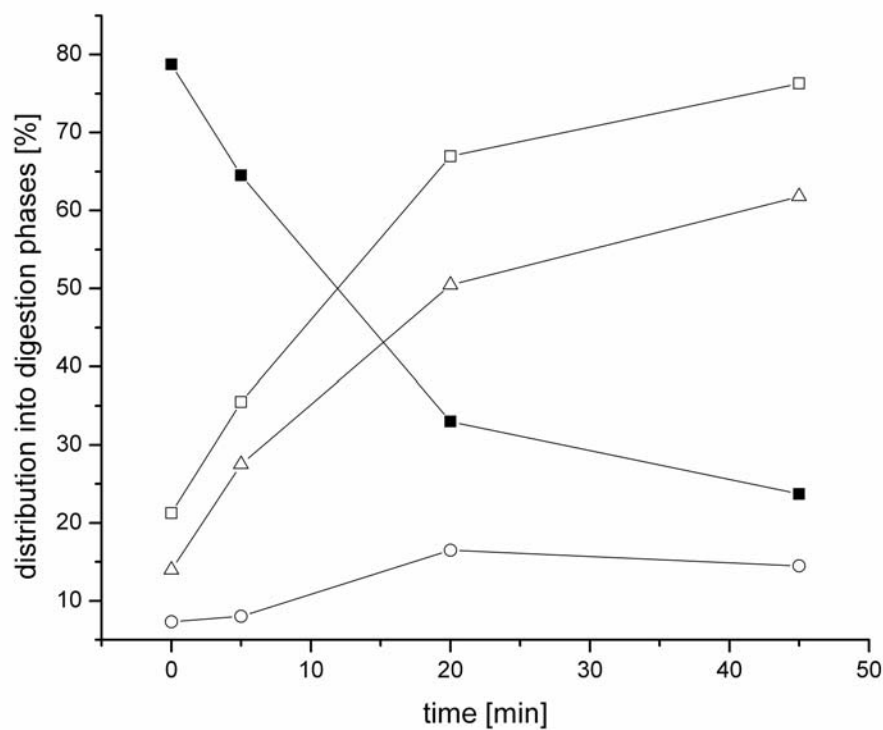


Figure 4.5 Distribution of TB into an oil phase (■), mixed micelles (Δ), phosphate buffer (○) and mixed micelles + phosphate buffer = dispersed aqueous phase (□) after 0, 5, 20 and 45 minutes digestion of 1.5 % (v/v) of a long-chain triglyceride under mediate (10 mM) bile salt conditions.

Table 4.1 Distribution of TB into an oil phase, mixed micelles and phosphate buffer.

time [min]	% TB in oil phase	% TB in mixed micelles	% TB in phosphate buffer
0	78.76	13.94	7.3
5	64.49	27.49	8.02
20	33.02	50.46	16.51
45	23.69	61.82	14.49

The major goal of this study was to develop a methodology to be able to non-invasively monitor *in vitro* fat digestion by ESR. In detail the distribution of a lipophilic paramagnetic model drug between the aqueous, oil phase and mixed micelles after the oral application of TB in a long chain triglyceride (olive oil) should be investigated. While there have been extensive prior studies investigating the formation of different phases and colloidal species during *in vitro* digestion, no prior group has reported the online monitoring of fat digestion. Spectral quantification of the ESR absorption function was performed by fitting the individual spectral components of phosphate buffer, olive oil and mixed micelles consisting of bile salts and phospholipids.

In the literature the separation of the long chain triglyceride (LCT) digests into a floating oil phase, a dispersed aqueous phase and a pellet phase after ultracentrifugation has been described [173].

Since in the here presented study simulation of the ESR spectra was at all times successful with the simulation parameters of oil, buffer and mixed micelles, the presence of TB molecules in the pellet phase can be excluded. Kaukonen et al. [167] also reported a very low drug content in the pellet phase when using LCT and drug molecules as diazepam with a log P in the range of TB.

The distribution of TB in phosphate buffer containing bile salts and phospholipids shows that with increasing bile salt concentrations the amount of TB solubilized in mixed micelles increases. This finding is important for the setup of *in vitro* digestion tests. It has been previously reported, that digestion of LCT is BS-dependent [169] and increases with higher concentrations. The results of this study show that the distribution of the drug between the different phases and therefore the rate of absorption is also dependent on the amount of bile salts used. Since several groups have reported the concentration of BS in the duodenum in the postprandial state with mean values between 5 and 15 mM with peaks up to 40 mM depending on the time after ingestion of the meal [171,177-180] and 3-7 mM during fasted state [171,177,181], varying concentrations are used for *in vitro* tests [168,172,175,182] leading to different distribution profiles of co-administered drugs during *in vitro* digestion. The drug distribution will also play a role in food-dependency of drug absorption. Depending on the different bile salt concentrations for fasted and fed state, the distribution of a drug (with a special log P) between the oil, water and micellar phases might vary leading to different rates of

absorption. When looking at TB with a log P of 2.5 the *in vitro* variations of the solubilization capacity of mixed micelles in phosphate buffer were 67% for fasted state (5 mM), 87% for fed state (20 mM) and up to 91% for BS peaks in fed state (40 mM).

Upon addition of olive oil to the phosphate buffer/mixed micelles system 79% of the spin probe were located in olive oil due to the moderate lipophilicity of TB. After addition of digestion enzymes a rapid redistribution of the spin probe within the first five minutes of digestion occurred indicating a fast degradation of olive oil. These fast changes in lipid concentrations during the first five minutes of *in vitro* lipolysis are in agreement with the literature [173]. Between 20 minutes and 45 minutes of digestion only small quantitative changes in the distribution of TB were visible. This finding is confirmed by Sek et al. [172] who reported a decrease of the rate of diglyceride and triglyceride hydrolysis after the first ten minutes. At the end of the digestion experiment after 45 minutes still 24% of the spin probe molecules were present in the oil phase indicating an incomplete digestion of the long chain triglyceride. This finding agrees with the literature [166,172], where it is reported, that the digestion of LCT compared with MCT progresses more slowly and after 30 minutes undigested lipid is present.

The distribution of TB after the digestion experiment was quantified with 76% of the spin probe in the dispersed aqueous phase and 24% in olive oil. These data are very close to HPLC results from Kaukonen et al. [166] who measured a distribution of diazepam (log P = 3) with 80% in the dispersed aqueous phase and 20% in the LCT phase.

## 4.5 Conclusion

An ESR method was developed that enabled the first online monitoring of the distribution of a paramagnetic lipophilic model drug between buffer, oil and mixed micelles after *in vitro* digestion. The redistribution of a model drug between the different phases was detectable by clear changes in the spectra which could be quantified by spectral simulation. This technique can provide important data regarding the fate of drug candidates during *in vitro* digestion and thus has great promise in the study and development of lipid-based delivery systems including lipid nanocarriers.

In future the ESR monitoring of fat digestion will be transferred to *in vivo* experiments. This online method could be a very helpful tool to study both the uptake of lipophilic drugs from a lipid formulation after oral administration and to monitor the interaction of drugs with lipid-rich meals.

## 5 Application of the ESR online-method for the monitoring of nanocapsule digestion

### 5.1 Introduction

The oral use of nanocapsules has received considerable attention in recent years because the bioavailability of poorly absorbable drugs could be increased and side effects minimized.

The group of Vauthier [183,184] suggested that after oral administration uptake of intact nanocapsules occurs because they were able to visualize insulin-loaded poly(isocynoacrylate) nanocapsules in underlying intestinal epithelium tissue. However the amount of nanocapsules that was able to pass the gastrointestinal barrier was relatively small. Therefore drug release from nanocapsules in the gastrointestinal tract is expected to play a predominant role in the subsequent drug absorption. For this reason it is essential to understand the complex mechanisms involved in the gastrointestinal degradation of biodegradable nanocapsules. A few in vitro studies are present which evaluate the drug release in media mimicking the pH and enzymes of the gut. Nanocapsules prepared by precipitation of polyesters (PLA, poly(D,L-lactide-co-glycolide) and poly( $\epsilon$ -caprolacton) (PCL)) show a very low release at pH 7.4 whereas in gastric media high release due to hydrolysis was reported [73,185]. In contrast to this poly(isobutylcyanoacrylate) PIBCA nanocapsules are more stable in acidic media but show fast release in intestinal fluids [183,184]. The release profile of polyester nanocapsules at neutral pH was studied under different conditions. The release of nanocapsules in enzyme-free phosphate buffer is controlled by the partitioning coefficient of the drug between the oily core and the buffer. The addition of albumin lead to slightly increased release profiles due to protein binding which caused an increase in the concentration gradient [73,186]. In pancreatin-rich buffer solutions more drug was released to the medium and a decrease of the molecular weight due to polymer degradation was reported at the example of PCL nanocapsules [73]. For PLA nanospheres controversy degradation profiles were reported. The group of Kreuter [187] reported fast degradation of PLA nanospheres in pancreatin-rich intestinal fluids and no degradation in pepsin-rich gastric fluids. Tobio et al. [188] studied PLA and PEG-PLA nanospheres, especially aggregation

due to interaction with enzymes, PLA degradation and drug release in enzyme-rich gastric and intestinal media. They also reported no degradation of PLA in gastric fluids and 9% of PLA degradation in intestinal fluids. The PEG coating improved the stability of nanospheres in the GI tract. On the other side Belbella et al. [189] postulated higher degradation of PLA nanospheres at acidic pH due to pH-induced hydrolysis.

The aim of this study was to apply the previously developed ESR online-method for the monitoring of PLA and PEG-PLA nanocapsule digestion in order to get a better understanding of the complex mechanisms involved in the gastrointestinal degradation of nanocapsules.

## 5.2 Materials and Methods

For the pancreatic assay the same materials were used as described in chapter 4.2. Two different nanocapsule dispersions were studied in comparison with a nanoemulsion. Namely PLA and PEG-PLA nanocapsules (sample 1+4) and a Poloxamer-stabilized nanoemulsion (sample 8) were digested.

### *In Vitro* Digestion

For the *in vitro digestion* experiments 4.5 ml of the aqueous nanocapsule dispersion or nanoemulsion, containing 2.5% (v/v) of Miglyol and 0.1 mM of TB, were added to 3 ml of digestion buffer (53.4%  $\text{Na}_2\text{HPO}_4 \times 2\text{H}_2\text{O}$  1/15 M, 46.6%  $\text{KH}_2\text{PO}_4$  1/15 M, 10 mM  $\text{CaCl}_2 \times \text{H}_2\text{O}$ , pH 6.8) containing 10 mM bile salts. The pH was adjusted to 6.8 with 1N NaOH. The final lipid concentration was 1.5%.

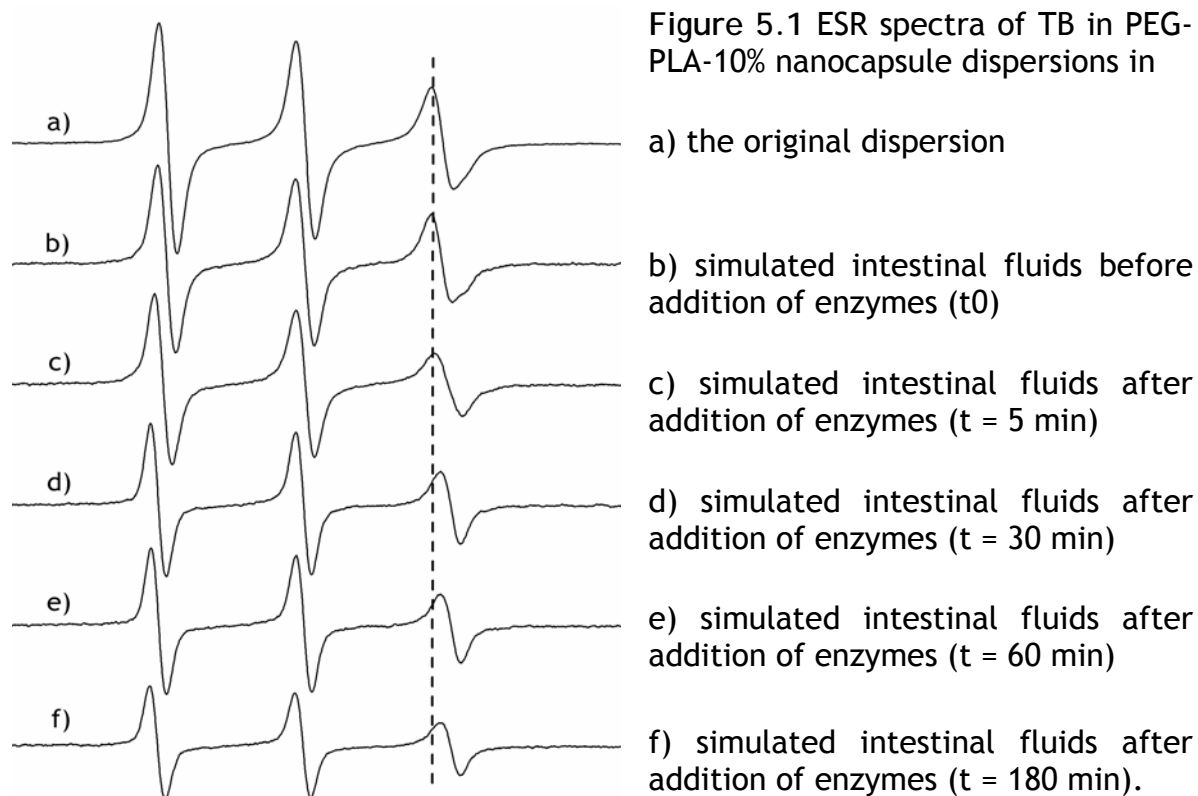
Experiments were initiated by the addition of 24.1 mg pancreatin extract containing 150 u/ml of pancreatic lipase activity. The *in vitro* digestion experiments were performed at 37°C in an end-over-end shaker. The pH was adjusted every 15 minutes with 0.1N NaOH. Digestion was monitored over 180 min using electron spin resonance (ESR). For ESR measurements a sample of the digest was filled into an ESR capillary which was measured with the X-Band spectrometer.



### 5.3 Results and Discussion

For the monitoring of nanocapsule digestion the distribution process of the incorporated model drug TB between the oily Miglyol core, phosphate buffer and mixed micelles was investigated. The underlying hyperfine-coupling constants were 1.670 mT for TB in phosphate buffer, 1.634 mT in mixed micelles and 1.523 mT in Miglyol.

Spectrum a) (Figure 5.1) of the undiluted PEG-PLA-10% nanocapsule dispersion (2.5% v/v Miglyol) can be simulated with 97% of the TB molecules in Miglyol and 3% in water. When this original nanocapsule dispersion is diluted to mimic the volume conditions of the lipase assay (4.5 ml dispersion + 3 ml phosphate buffer), only a slight increase of the hydrophilic species occurs (4%). Addition of bile salts to this dilution causes a significant redistribution of the spin probe (Figure 5.1 b and Table 5.1). At this point only 81% of the TB molecules are still located in the oily core of the nanocapsules, 16% are already solubilized in mixed micelles formed by bile salts and 3% are dissolved in the phosphate buffer. Five minutes after addition of intestinal enzymes (Figure 5.1 c) the third peak is still dominated by the TB species which is located in Miglyol, although this species decreases remarkably (Table 5.1).

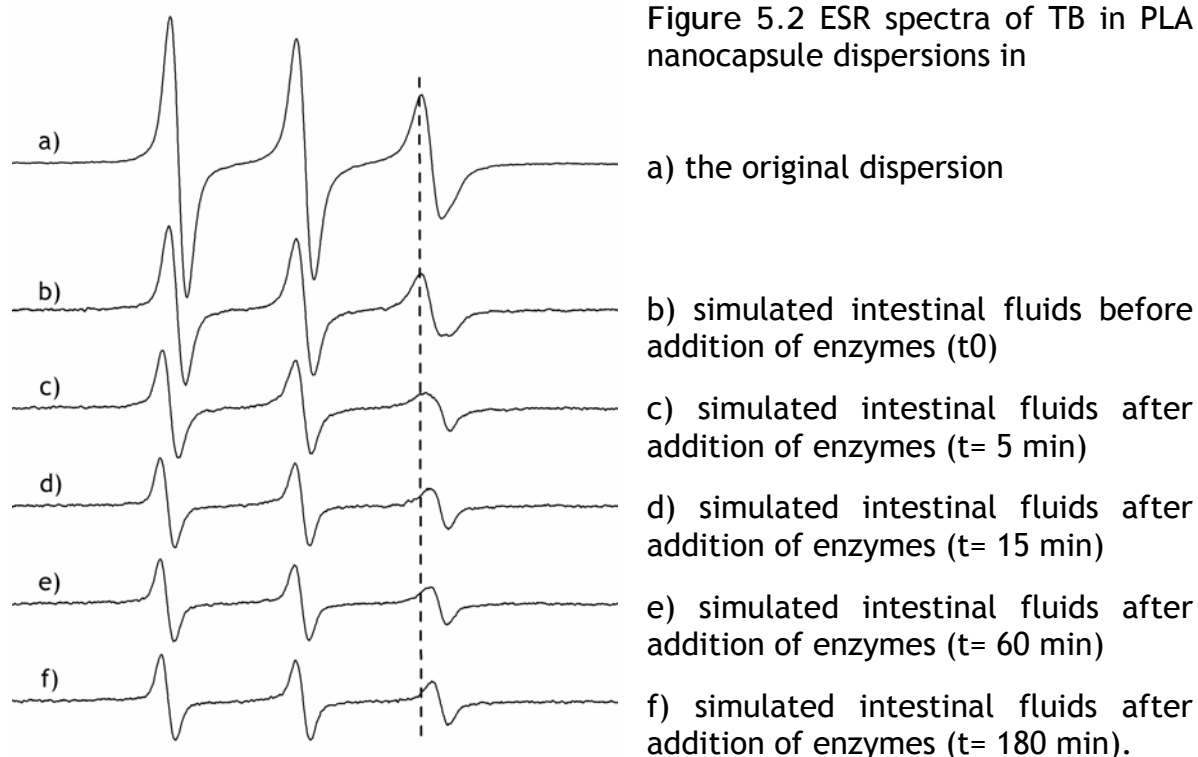


After 30 minutes of digestion the spectral shape changes significantly which is visible at a shift of the third peak to the higher field. At this time 35% of the TB molecules are left in the Miglyol phase (Table 5.1), the majority of TB is solubilized in the mixed micelles. During the following 150 minutes the distribution of the spin probe does not further change.

Table 5.1 Distribution of TB into an oil phase, mixed micelles and phosphate buffer.

time [min]	% TB in oil phase	% TB in mixed micelles	% TB in phosphate buffer
0	81.21	16.00	2.79
5	53.92	45.14	0.93
30	35.3	62.01	2.69
60	37.48	59.13	3.39
180	31.62	64.6	3.78

With PLA nanocapsules, in comparison to the pegylated carriers, significant changes of the distribution profile occur after 5 minutes already, becoming visible in the ESR spectrum after 15 minutes with a clear shift of the third peak.



Already after 5 minutes only 30% of the TB are still located in Miglyol, this species decreases down to 18% after 180 minutes.

Table 5.2 Distribution of TB into an oil phase, mixed micelles and phosphate buffer.

time [min]	% TB in oil phase	% TB in mixed micelles	% TB in phosphate buffer
0	75.42	21.71	2.87
5	32.31	56.92	10.77
15	31.9	48.44	19.66
60	31.11	46.8	22.09
120	19.51	70.84	9.66
180	18.39	67.41	14.20

When comparing the distribution profiles of PEG-PLA and PLA nanocapsules (Figure 5.3) it is noticeable that from PLA nanocapsules a higher amount of TB molecules is released into the phosphate buffer (▲) at all times. While for PEG-PLA nanocapsules the amount of TB molecules in the buffer is always below 5%, this species makes up 10 to 20% for PLA nanocapsules.

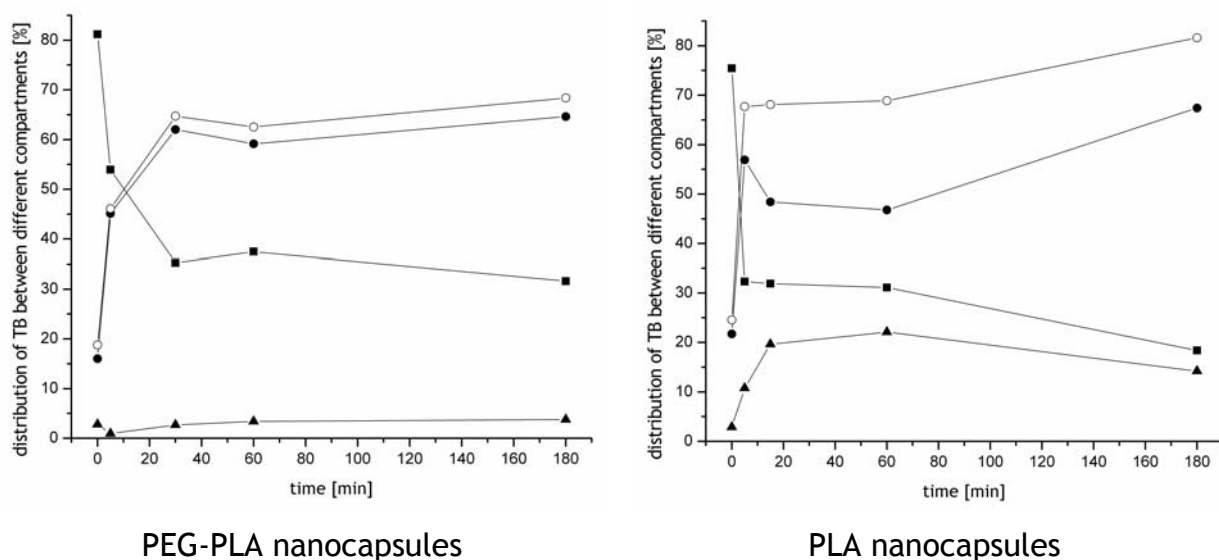
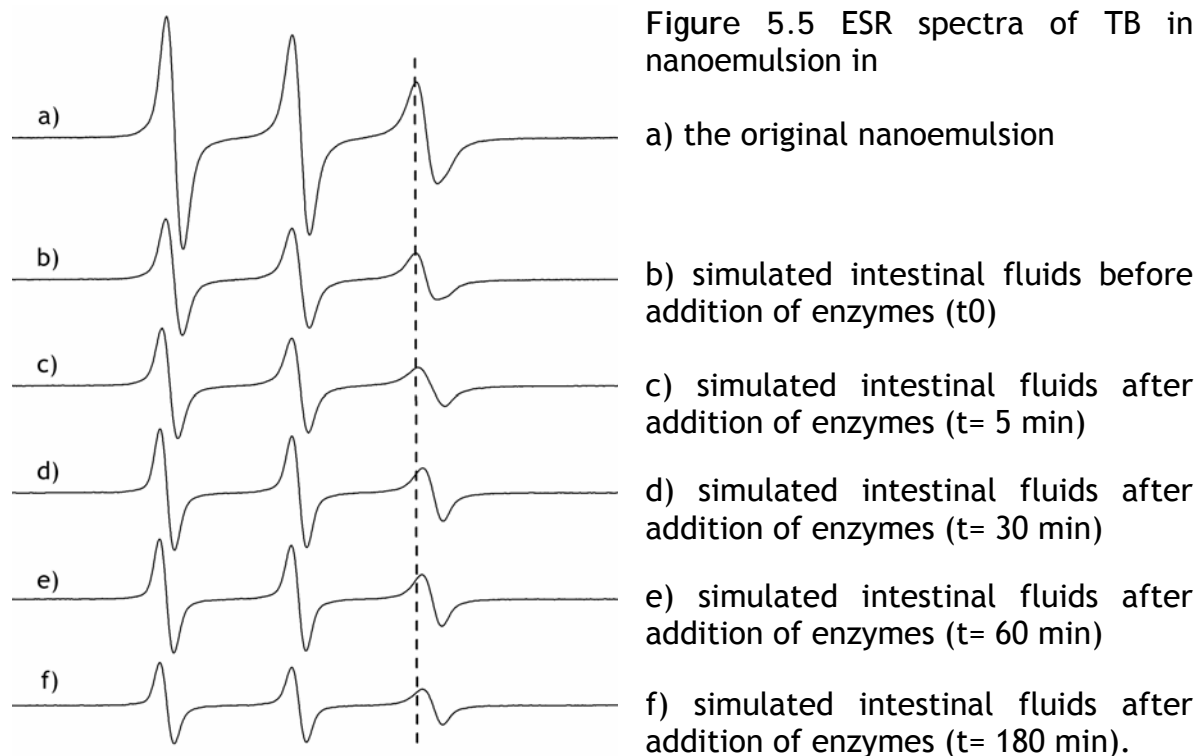


Figure 5.3 Distribution of TB between the Miglyol core of the nanocapsules (■), mixed micelles (□), phosphate buffer (▲) and the dispersed aqueous phase (○) (mixed micelles + phosphate buffer) after 0, 5, 15, 60 and 180 minutes digestion of PLA nanocapsules containing 1.5% (v/v) Miglyol under mediate (10 mM) bile salt conditions.

From the ESR spectra of the digested nanoemulsion a slight change in the spectrum can be seen after 5 minutes of digestion, a clear increase of the hyperfine coupling constant is visible at 30 minutes after addition of lipase. These times are in the same order of magnitude as for the nanocapsules.



## 5.4 Conclusion

The previously developed ESR online method was applied on lipid-based nanocapsule dispersions to study the fate of the encapsulated model drug TB.

The presence of bile salts in the simulated intestinal fluids caused a significant redistribution of the spin probe. This can be explained by the favorable acceptor properties of mixed micelles for foreign molecules like TB. The quantity of TB molecules solubilized in mixed micelles is higher for PLA nanocapsules than for PEG-PLA nanocapsules. This is not surprisingly since the PEG coating offers a diffuse interface which favors the residence of the spin probe compared to "naked" PLA nanocapsules. Upon addition of digestion enzymes the amount of spin probe localized in Miglyol decreases remarkably, this process being faster for PLA than for PEG-PLA nanocapsules. This can be attributed to the protein repellent effect [190-193] of PEG coated surfaces which leads to less interactions with the enzymes of the digestion fluids compared to PLA nanocapsules. Furthermore it is known that for its enzymatic activity the pancreatic lipase needs a co-factor, the so-called colipase, which functions as an anchor between bile salts and phospholipids at oil-water interfaces and the lipase. When the lipase is connected to interfaces via the colipase, the conformation of the enzyme changes. Thereby the active centre of the lipase, which is closed by a lid in the unbound state, opens and the enzyme is activated [194]. Covalently bind PEG chains, as in the case of PEG-PLA nanocapsules, hinder the anchoring of the colipase-lipase complex and thereby the lipase activity is reduced.

## 6 Behaviour of nanocapsules in mice after oral application - an ex vivo ESR study

### 6.1 Introduction

Already in 1987 it was shown that by oral administration of poly(cyanoacrylate) nanocapsules lipophilic drugs could be delivered to the blood [195,196]. Damgé et al. [195] reported that jejunally administered nanocapsules increased the intestinal absorption of a lipophilic drug compared to an emulsion. From this they concluded that nanocapsules accelerate, intensify and prolong the passage of a lipophilic drug through the intestinal mucosa. Other groups reported that PLA and PIBCA nanocapsules compared to simple drug solutions did not alter the pharmacological response of anti-inflammatory drugs in rats, but a dramatic reduction of mucosa side effects was seen [197,198]. Studies on PEG-PLA and PLA nanospheres showed increased intestinal absorption of the pegylated nanoparticles [188].

Though some groups give intestinal uptake of intact nanocapsules as a reason for their findings, until now it is not clear to which extent this happens. Three possible pathways for the absorption of nanocapsules have been postulated: via the M cells of Peyer's patches, via a transcellular route involving enterocytes and via "paracellular avenues" through tight junctions [199,200].

In this chapter an ex vivo ESR experiment on the behaviour of nanocapsules after oral administration to mice will be discussed. The nanocarriers were loaded with the lipophilic spin probe HD-PMI and the hydrophilic spin probe  $^{15}\text{N}$ -PCM to study the behaviour of both the oily and the aqueous phase. Ex vivo ESR spectroscopy was used to study the residence time of nanocapsules in the stomach and their distribution to other organs. Moreover the blood concentration of HD-PMI at different times was studied by ESR spectroscopy.

This ex vivo ESR study was a preparatory experiment for future in vivo ESR imaging experiments. In vivo ESR imaging offers the unique possibility to study both the location of spin probe-loaded carriers in the body and to resolve their microenvironment at certain locations in a non-invasive way. Therefore this technique might provide an answer to the open task if intact nanocapsules reach the blood stream.

Previous to animal experiments, cell toxicity studies on CaCO-2 cells have been performed to proof the non-toxicity of PLA and PEG-PLA nanocapsules.



## 6.2 Materials and Methods

### 6.2.1 Cell toxicity studies

The human coloncarcinom cell line Caco-2, which was obtained from the German Collection of Microorganisms and Cell Cultures (Braunschweig, Germany), was used for the cell toxicity studies. Caco-2-cells were routinely cultured in minimum essential amino acid solution and gentamicin (45µg/ml) [201]. Cells grown to 80% confluence were released by trypsinization and subcultured in 35-mm disposable Petri dishes (BD Biosciences, Heidelberg, Germany). The medium was replaced every two days and the day before the cell toxicity experiment. With a starting cell density of  $0.8 \cdot 10^6$  cells/dish, the cultures reached confluence within 24 h. Cell toxicity studies were performed seven days after seeding when cells on plastic dishes reached optimal differentiation.

Before the experiments, the Petri dishes were rinsed with HEPES buffer (pH 7,5, 37°C, 140 mM NaCl, 5.4 mM KCl, 1.8 mM CaCl<sub>2</sub>, 0.8 mM MgSO<sub>4</sub>, 5 mM glucose and 25 mM HEPES/Tris).

PLA-NC (sample 1) and PEG-PLA-10%-NC (sample 4) were studied for their cell toxic potential in comparison to a 0.3% Poloxamer 188 solution as a reference. All three samples were diluted with HEPES buffer, either in the ratio 1:100 or 1:10. 2 ml of each solution were added to a cell-containing Petri dish and put on a shaker. Petri dishes were shaken at a speed of 150 rpm at 37°C. After 0, 10, 20, 30, 60, 90 and 120 minutes each Petri dish was examined under the light microscope (Axiovert S100) for cell apoptosis, which is expressed by balling of cells and subsequent removal of cells from the bottom-attached cell layer.

### 6.2.2 Ex vivo ESR measurements

Female Swiss CD-1® IGS mice, weighing 22-26 g (Charles River, Germany), were used for the ex vivo ESR study. They had free access to water but were deprived of food 8 hours before the experiment. Each animal ( $n = 15$ ) received 0.5 ml of either a PEG-PLA-10% nanocapsule dispersion or a nanoemulsion by gavage. The aqueous nanocapsule dispersion contained 2.5% (v/v) Miglyol, 0.6% (w/v) PEG-PLA-10%, 0.3% (w/v) Poloxamer and 2.5% glycerol for isotonization. The nanoemulsion contained 2.5% (v/v) Miglyol, 2.5% (w/v) Poloxamer and 2.5% glycerol for isotonization. Both

formulations contained 1 mM of the highly lipophilic spin probe HD-PMI II (see chapter 2.2). In some cases 0.1 mM of the hydrophilic spin probe  $^{15}\text{N}$ -PCM (Prof. V.V. Khrantsov, Institute of Chemical Kinetics and Combustion, Novosibirsk, Russia) was also added to the formulations. The preparation of PEG-PLA nanocapsules and the nanoemulsion is described in detail in chapter 2.3.1. The z-average for nanocapsules was 185 nm (PDI = 0.144) and 203 nm (PDI = 0.148) for the nanoemulsion. Six animals were sacrificed 30 min after administration of the drug carriers, three after receiving nanocapsules and three after receiving the nanoemulsion. Six animals were sacrificed after 60 min (3 x nanocapsules and 3 x nanoemulsion), one animal after 15 min (nanocapsules) and 1 animal after 120 min (nanocapsules). From each animal a blood sample was collected from the heart and mixed with 10% of sodium citrate (Grüssing GmbH, Germany). Stomach, small intestine, lung, heart, spleen, liver and kidneys were removed from the sacrificed animals, put into a plastic vessel and stored on ice. ESR measurements were performed at once. One animal was sacrificed without administration of a drug delivery system to study the behaviour of blood and organs in the ESR spectrometer itself. The interference of signals generated by radicals derived from the animals with signals from the spin probes had to be excluded.

An ESR spectrometer of 1.1 GHz (L-Band) from Magnettech (Berlin, Germany) was used for the measurement of both blood and organs. Measurements were conducted at room temperature with the following parameters:  $B_0$  field: 49.05 mT, scan range: 10 mT, scan time: 20 s (several runs), modulation amplitude: 0.14 mT, gain: 400.

In addition blood samples were measured with an ESR spectrometer of 9.5 GHz (X-Band, Miniscope MS 200) from Magnettech (Berlin, Germany) which has a higher sensitivity. Blood samples were examined inside a glass capillary. Measurements were conducted at room temperature with the following typical parameters:  $B_0$  field: 335.4 mT, scan range: 10 mT (precisely 9.893 mT), scan time: 30 s, modulation amplitude: 0.2 mT, gain: 800.

## 6.3 Results and Discussion

### 6.3.1 Cell toxicity

On the photomicrographs healthy confluent cell structures can be identified by clearly visible junctions (Figure 6.1 left) between the cells. Upon apoptosis balling of cells can be detected (Figure 6.1 middle) and diffuse areas (Figure 6.1 right) occur, where removed cells are swimming on top of the intact cell layer.

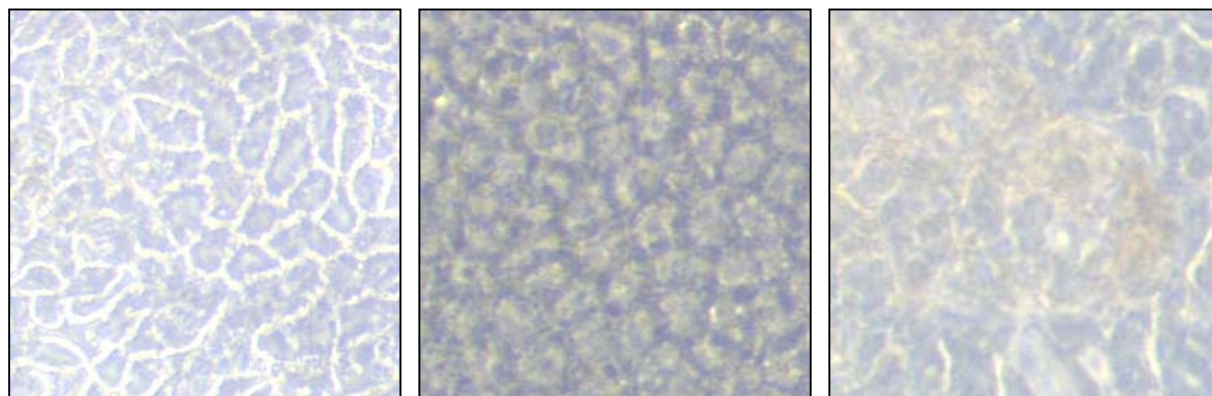


Figure 6.1 Photomicrographs of Caco-2 cells  
left) healthy cells with clearly visible junctions  
middle) balling cells upon apoptosis  
right) peeled of cells upon apoptosis.

There was no difference visible in the behaviour of Caco-2 cells after nanocapsule or Poloxamer treatment. During the first 60 minutes the cell layer stayed intact for PEG-PLA-NC, PLA-NC and Poloxamer solutions with HEPES buffer (1:100), after 90 minutes up to 120 minutes apoptosis was visible for all three samples. For the less diluted samples (1:10) cell apoptosis was already detectable after 60 minutes. Since Poloxamer 188 (Lutrol F 68) is a stabilizer and solubilizer, which is known for its non-toxicity after parenteral, dermal or peroral application [202-207], the here presented nanocapsule dispersions can be regarded as non-toxic as well. The human stomach produces 1-3 litres of gastric juice a day [208]. Therefore the dilution ratio 1:100, which was used in the cell studies, is in the range of real conditions after oral application.

### 6.3.2 Ex vivo ESR

The nanocapsule dispersion and nanoemulsion for the ex vivo ESR experiment were loaded with the highly lipophilic spin probe HD-PMI II (1 mM; Figure 6.2 left). The corresponding L-band ESR spectra can be seen in Figure 6.3 (left). In some cases the hydrophilic spin probe  $^{15}\text{N}$ -PCM (0.1 mM; Figure 6.2 right) was added to the HD-PMI-loaded (1 mM) drug delivery systems (Figure 6.3 right) to study the behaviour of the lipophilic and hydrophilic phase simultaneously.

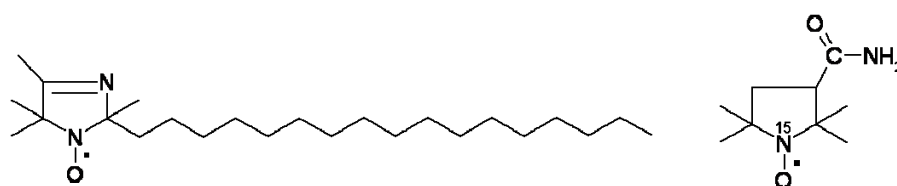


Figure 6.2 Chemical structure of HD-PMI II (left) and  $^{15}\text{N}$ -PCM (right)

The ESR signal amplitude of the spin-loaded nanocapsule dispersion and the nanoemulsion was in the same order of magnitude.



Figure 6.3 L-band ESR spectra of  
left) a HD-PMI (1 mM) loaded PEG-PLA-10% nanocapsule dispersion (grey) and nanoemulsion (black)  
right) a HD-PMI (1 mM) and  $^{15}\text{N}$ -PCM (0.1 mM) loaded PEG-PLA-10% nanocapsule dispersion (grey) and nanoemulsion (black).

L-band ESR experiments provided measurable concentrations of the spin probe HD-PMI in stomach, small intestine and in some blood samples. The hydrophilic spin probe  $^{15}\text{N}$ -PCM could only be detected in the stomach. All other organs (heart,

liver, spleen, kidneys) did not provide an ESR signal. In the lungs of three animals an ESR signal from HD-PMI was detected. Though it can not be excluded, that nanocapsules or the nanoemulsion reached the lung via the trachea during intragastric application.

In Figure 6.4 L-band ESR spectra of the stomach at 30, 60 and 120 min after intragastric PEG-PLA-10% nanocapsule administration are shown. While after 30 and 60 minutes there is a clear signal generated by HD-PMI molecules in the stomach, after 120 minutes the signal disappears. From this it can be concluded that the complete emptying of the nanocapsules from the stomach does not happen within the first 60 minutes after administration. This was also seen for the HD-PMI-loaded nanoemulsion, where after 60 minutes still an ESR signal was detectable in the stomach.

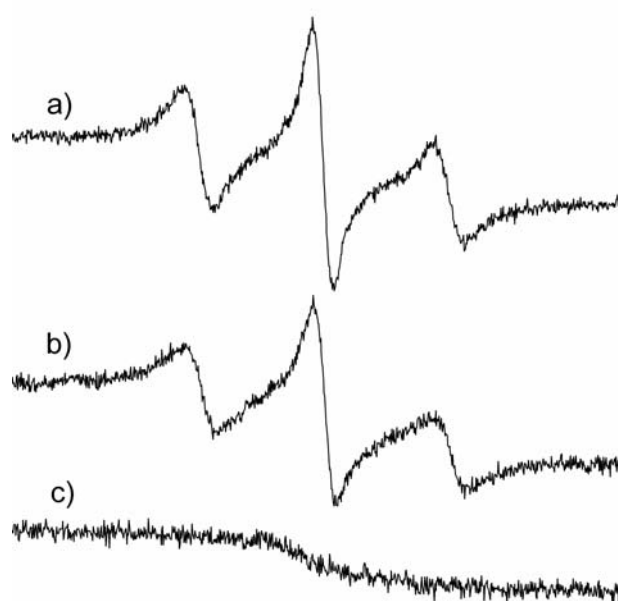


Figure 6.4 Ex vivo L-band ESR spectra of the stomach of a mouse after the intragastric administration of HD-PMI-loaded PEG-PLA-10% nanocapsules

a) 30 min  
after nanocapsule administration

b) 60 min  
after nanocapsule administration

c) 120 min  
after nanocapsule administration.

After the administration of PEG-PLA-10% nanocapsules which contained HD-PMI in the oily core and  $^{15}\text{N}$ -PCM in the aqueous phase, the ratio between the peak intensity of the HD-PMI and  $^{15}\text{N}$ -PCM peak changed (Figure 6.5) compared to the original spectrum (Figure 6.3 right). A possible explanation might be that emptying from the stomach is faster for the aqueous phase of the nanocapsule dispersion than for the nanocapsules itself. Nanocapsules might adhere to the mucosa or interact with soluble mucus and thereby stay in the stomach for a longer time than the aqueous phase. Another possibility might be aggregation of nanocapsules due

to the acidic medium. However during in vitro experiments in simulated gastric and intestinal media no aggregation was visible. Though the  $^{15}\text{N}$ -PCM signal decreases faster than the HD-PMI signal, it is visible at 15, 30 and even 60 minutes after nanocapsule administration.

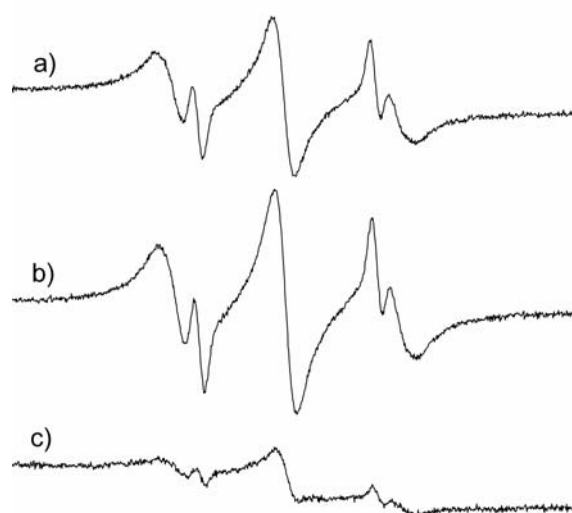


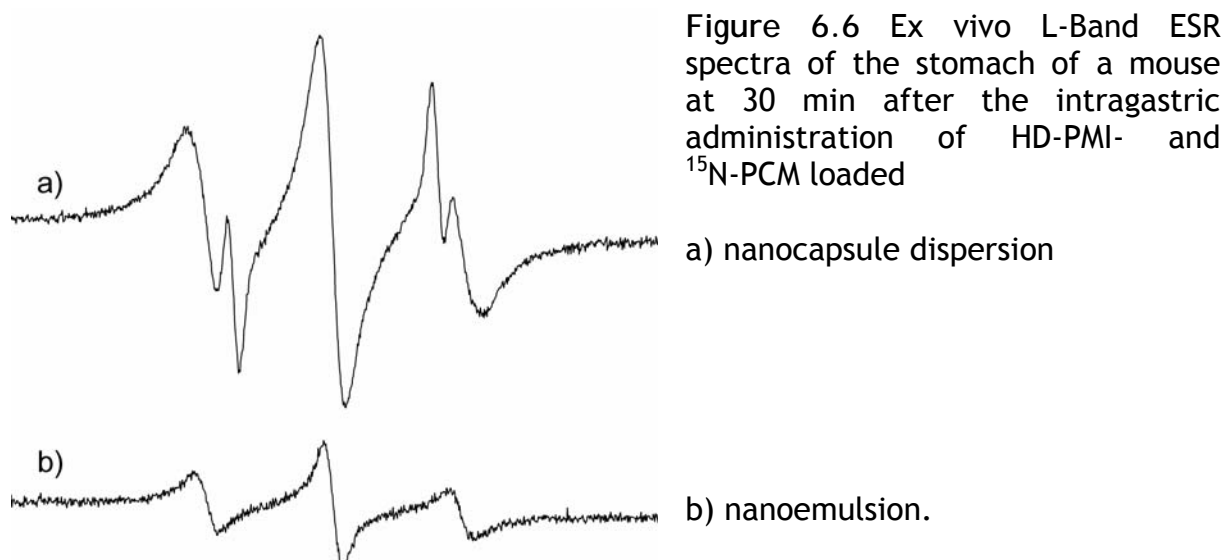
Figure 6.5 Ex vivo L-band ESR spectra of the stomach of a mouse after intragastric administration of HD-PMI- and  $^{15}\text{N}$ -PCM-loaded PEG-PLA-10% nanocapsules

a) 15 min  
after nanocapsule administration

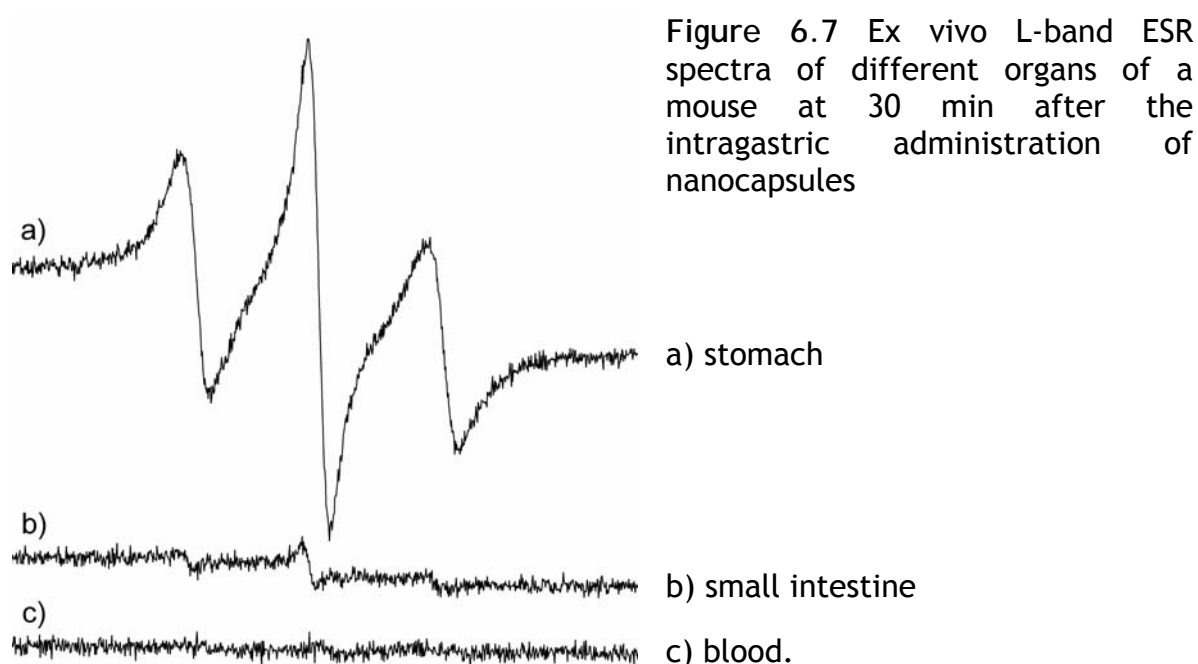
b) 30 min  
after nanocapsule administration

c) 60 min  
after nanocapsule administration.

Interestingly this finding is in contrast with the behaviour of nanoemulsions which were loaded with HD-PMI and  $^{15}\text{N}$ -PCM. While for the nanocapsule dispersion there is a peak from  $^{15}\text{N}$ -PCM clearly visible at 30 minutes after administration, this is not the case for the nanoemulsion. A possible explanation might be that concentration of PEG-PLA nanocapsules in the stomach leads to an increase of the local viscosity and thereby some of the  $^{15}\text{N}$ -PCM molecules are retarded in the stomach. The signal intensity of spectrum b) in Figure 6.6 is smaller than for spectrum a) but this was not seen for other samples.



30 minutes after intragastric administration of HD-PMI-loaded PEG-PLA-10% nanocapsules to mice, the biggest ESR signal is provided by the stomach, but a small signal can also be seen in the small intestine (Figure 6.7). The blood sample indicates that some HD-PMI molecules have reached the blood stream at this time.



Blood samples were also measured by X-band which has a higher sensitivity. At all times (15, 30, 60 and 120 minutes after administration) a signal from the lipophilic spin probe HD-PMI could be detected in the blood (Figure 6.8). The concentration

of the spin probe increased from 15 to 30 up to 60 minutes and decreased again from 60 to 120 minutes.

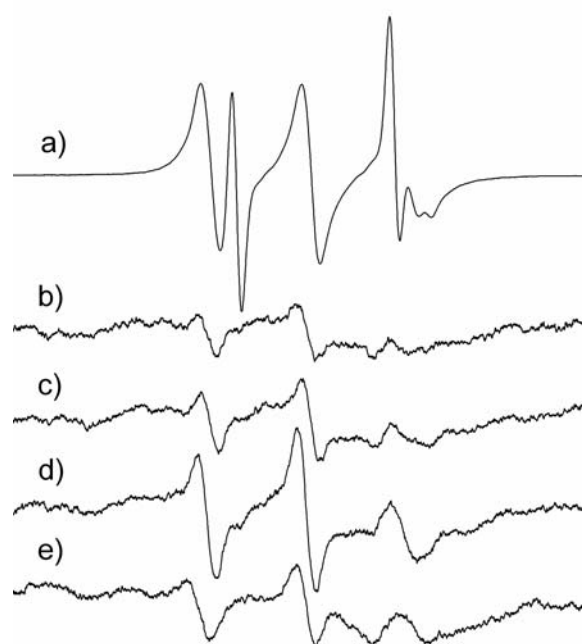


Figure 6.8 Ex vivo X-band ESR spectra of

a) anaqueous HD-PMI and  $^{15}\text{N}$ -PCM loaded PEG-PLA-10% nanocapsule dispersion

b) blood 15 min after nanocapsule administration

c) blood 30 min after nanocapsule administration

d) blood 60 min after nanocapsule administration

e) blood 120 min after nanocapsule administration.

[Note: a) modulation amplitude = 0.1 mT, gain = 7; b) modulation amplitude = 0.2 mT, gain 800].



## 6.4 Conclusion

In the cell toxicity study the behaviour of Caco-2 cells after nanocapsule treatment did not differ from the behaviour after treatment with an aqueous Poloxamer solution. Since Poloxamer 188 is known for its non-toxicity, the PLA and PEG-PLA-10% nanocapsules can be regarded as non-toxic as well.

Ex vivo ESR experiments showed that the lipophilic model drug HD-PMI reached the blood stream after intragastric administration of HD-PMI-loaded nanocapsules to mice. Both the nanocapsule dispersion and the nanoemulsion were not completely emptied from the stomach within the first 60 minutes after administration. By L-band, ESR signals were detectable in stomach, small intestine and in some blood samples. With the more sensitive X-band, ESR signals from HD-PMI were visible in blood samples at all times (15, 30, 60, 120 minutes after administration). The blood concentration of HD-PMI increased from 15 to 30 up to 60 minutes and decreased again from 60 to 120 minutes after administration.

## 7. Summary and perspectives

### 7.1 English version

Nanocapsules are a particular class of submicron colloidal carriers with special characteristics such as their unique combination of high drug solubilization (liquid core) and the possibility of high stability and controlled release (solid shell).

The aim of the present study was a physico-chemical characterization of nanocapsules in order to get a deeper understanding of these complex drug carrier systems. Furthermore the behaviour of nanocapsules in simulated intestinal fluids in the presence of enzymes should be investigated to predict their fate after peroral application. Finally the interest of this work lay on the fate of nanocapsules after peroral administration (*ex vivo*).

Nanocapsules were prepared using the method described by Fessi [66,67] based on interfacial deposition of preformed polymer after solvent displacement.

Poly(D,L-lactide) (PLA) and pegylated PLA (PEG-PLA) were used as coating polymers to produce first-generation and surface-modified second-generation [83] carriers containing an oily core of Miglyol 812. The final nanocapsule dispersions contained the hydrophilic stabilizer Poloxamer 188, but lacked the stabilizer lecithin. The average nanocapsule size was in the range of 150-250 nm.

The non-invasive electron spin resonance (ESR) spectroscopy was used to gain information on the nano-scaled carriers which can not be gained by conventional techniques. The first task was the assessment of the nanoenvironment of a lipophilic model drug, including the polarity and viscosity, of the oily phase in nanocapsules. Additional NMR relaxation measurements resolved the drug distribution profile down to the molecular scale.

Since only paramagnetic molecules are visible to ESR, as a model drug the spin probe TEMPOL benzoate (TB) was incorporated into the nanocapsules. The octanol-water partition coefficient of TB was determined by an ESR technique introduced by Kroll [135] and a log P value of 2.46 was calculated. Therefore the spin probe exhibits a lipophilicity between griseofulvin (log P = 2.18 [136]) and diazepam (log P = 2.92 [137]) and can be classified as a poorly water-soluble moderately lipophilic model drug. Besides TB the spin probe HD-PMI, containing a C17-chain in the molecule, was encapsulated as a highly lipophilic model drug. The log P of

HD-PMI could not be determined by ESR, because this technique is only suitable for molecules with a  $\log P \leq 3$ . Based on calculations with a cheminformatics program and comparison with  $\log P$  literature values for comparable molecules, a  $\log P > 6$  can be assumed for HD-PMI.

The majority of the TB molecules were located in the oily core of the nanocapsules, only a small amount of the model drug (3-4%) was dissolved in the aqueous environment.  $^1\text{H}$ -NMR results showed a homogeneous distribution of TB in the oily phase without a preference for a special entity of the triglyceride molecules. In contrast to TB, the highly lipophilic spin probe HD-PMI was completely dissolved in the oily phase of the nanocapsules whose total amount of the dispersion was 2.5%.

Nanocapsules undergo dilution both during experimental work and in-vivo application. Since no information is available on this dynamical process, dilution kinetics was studied by means of an ESR dilution assay. Dilution caused a partial relocation of the moderately lipophilic TB molecules into the aqueous environment within a minute. In contrast the distribution of very lipophilic molecules (HD-PMI) was not influenced to a measurable extend upon dilution. For both spin probes no difference was seen between a nanoemulsion and the two different types of nanocapsules. These findings confirm first assumptions that the polymer shell does not act as an effective diffusion barrier to encapsulated drug molecules. The distribution equilibrium is only dependent on the partition coefficient of the drug between the oily core and the aqueous external medium and the relative volumes of these two phases. Similar finding have been reported in the literature for nanocapsule systems prepared by the same technique independent on the nature of the polymer [71,83]. The ESR dilution assay enabled the first real-time shots of this partition process which could be quantified.

Surprisingly it was possible to load TB-free nanocapsules belatedly with TB from the outside, which leads to the conclusion that diffusion of the TB molecules both from the core to the water phase and the other way around from water to oil is very fast.

This fast relocation observed by ESR spectroscopy can be understood with the assistance of TEM results. The observed shell thickness in the photomicrographs of nanocapsules provides with 10 nm only a very short diffusion path between the oily and the water phase and therefore diffusion kinetics is fast.

As a consequence for practical applications this finding means that for drug molecules of moderate lipophilicity complete protection from the environment and vice versa can not be ensured in nanocapsules prepared by interfacial nanodeposition.

Besides diffusion paths within the carrier and charge effects at the interface, the nature of the polymer shell plays a determining roll for the accessibility of incorporated drugs. The ESR reduction assay with ascorbic acid gives a description of the accessibility of incorporated spin probes to the aqueous phase.

Resistance to reduction by ascorbic acid of TB incorporated into PEG-PLA nanocapsules is higher than in PLA nanocapsules which are for their part not superior to a nanoemulsion. PEG-PLA nanocapsules with a higher degree of PEG substitution provide higher protection indicating a repellent effect of the PEG chains to the ascorbic acid molecules. HD-PMI is not at all reduced by ascorbic acid when it is incorporated into nanocapsules or a nanoemulsion. Since HD-PMI could be reduced in more hydrophilic drug carriers as mixed micelles, it can be concluded, that here again partition plays the predominant role. HD-PMI molecules do not diffuse from the oil to the water phase and can thereby not be attacked by ascorbic acid.

After settling the diffusion process and the accessibility of model drugs with ESR, small angle neutron scattering (SANS) was applied for the quantitative characterization of the interface. Up to date only estimations regarding the shell thickness from TEM measurements existed.

SANS at a contrast-matched interface with corresponding numeric simulation procedures yielded a comprehensive model on the core-shell structure of nanocapsules that is demonstrated on poly(D,L-lactide) nanocapsules. By varying the scattering length density of the solvent continuously it was possible to separate the influence of the size distribution from the influence of the form factor on the scattering intensity. Highest sensitivity on the inner structure of the nanocapsules was obtained when the scattering length density of the solvent was varied between the one of the Miglyol core and the PLA shell. The corresponding fit yielded a PLA shell thickness of 9.8 nm and an average Miglyol core radius of 84 nm. The z-averages for the hydrodynamic diameter determined by DLS were systematically slightly higher than the values for the capsule diameter measured by SANS. When refining the fit model by introducing a second shell consisting of Poloxamer and

solvent, SANS values and DLS values fitted well. The refined model provided a thickness of 17 nm ( $\pm$  6nm) for this additional shell composed of Poloxamer and water and a Poloxamer content of 7% ( $\pm$  5%).

Complex coazervation combined with high pressure homogenization has been carried out successfully to design novel composite polyelectrolyte nanocapsules composed of biopolymers. In comparison to the existing interfacial layer-by-layer deposition technique which leads to hollow nanocapsules, the here developed method for nanocapsule preparation saves the time-consuming separation of non-adsorbed polyelectrolyte in between the adsorption steps and a belated filling of the nanocapsules. Injection of the polyelectrolytes and subsequent high pressure homogenization caused minimization of aggregates due to polymer bridges between single droplets leading to acceptable oil loading of 2.5% (v/v).  $\square$  potential measurements confirmed the charge reversal after each adsorption step involved and thereby proved the step-wise growth of the polyelectrolyte shell. TEM studies on these nanocapsules revealed the formation of a trilayered shell on the oily core. PCS measurements of the trilayered nanocapsules showed a z-average value of 230 nm.

Until now it is not entirely clarified how drugs incorporated into nanocapsules are absorbed after oral application. Though a small amount of the carriers might be taken up as intact nanocapsules, gastrointestinal digestion of nanocapsules is expected to play a predominant role in the subsequent drug absorption. Because of that it is crucial to understand the complex series of events which occur on interaction of the lipid formulation and the gastrointestinal environment. Therefore an online-method for in vitro monitoring of fat digestion based on ESR was developed and applied on nanocapsule dispersions afterwards. For the development of the monitoring method ESR spectroscopy was coupled with an in vitro lipolysis assay and degradation of the model drug TB from a long chain triglyceride (olive oil) was investigated. The first real-time study on the distribution of a model drug between buffer, oil and mixed micelles (composed of bile salts and phospholipids) after in vitro digestion was performed. The ESR online method offers the possibility to follow the redistribution of the model drug between the different phases by clear changes in the spectra which could be quantified by spectral simulation.

By application of this method on oil-loaded nanocapsule dispersions the fate of the encapsulated model drug TB was studied. The presence of bile salts in the simulated intestinal fluids caused a significant redistribution of the spin probe. This can be explained by the favorable acceptor properties of mixed micelles for foreign molecules like TB. The quantity of TB molecules solubilized in mixed micelles is higher for PLA nanocapsules than for PEG-PLA nanocapsules. This is not surprisingly since the PEG coating offers a diffuse interface which favors the residence of the spin probe compared to “naked” PLA nanocapsules. Upon addition of digestion enzymes the amount of spin probe localized in Miglyol decreased remarkably, this process being faster for PLA than for PEG-PLA nanocapsules. This is probably due to covalently bound PEG chains which hinder the lipase-colipase complex from anchoring at interfaces and thereby reduce the lipase activity.

In the cell toxicity studies nanocapsules dispersions (PLA and PEG-PLA) showed a behaviour comparable to a Poloxamer solution which was used as a reference. Since Poloxamer 188 is known for its non-toxicity after peroral, dermal and parenteral application, the examined nanocapsules can be regarded as non-toxic as well.

Ex vivo ESR experiments showed that the lipophilic model drug HD-PMI reached the blood stream after intragastric administration of HD-PMI loaded PEG-PLA nanocapsules to mice. The blood concentrations of HD-PMI increased from 15 to 30 up to 60 minutes and decreased again from 60 to 120 minutes.

Summarized in theory nanocapsules of the deposition type seem to be tailored submicron drug delivery systems because they unite a high drug load (liquid core) and the possibility of high stability and controlled release (solid shell). The high drug load is an indisputable advantage over competitive carriers as nanospheres or solid lipid nanoparticles, but unfortunately in practise it is not the solid shell but the oil-water partition coefficient that controls release. Like with other lipid-based nanocarriers a high log P is essential to prevent fast relocation of incorporated drug.

One advantage of nanocapsules over nanoemulsions can be seen in the possibility to modify their coating polymers multifunctionally for targeted delivery. Since the molecular weight of the polymer backbone is much higher compared to a ligand (e.g. antibodies, integrins), surface modification is easier compared to nanoemulsions where the molecular weight of a ligand is higher than the one of

typically used surface stabilizers (lecithin). Furthermore the higher chemical stability of nanocapsules due to the shell is advantageous over lecithin-stabilized nanoemulsions which are susceptible both to oxidation and hydrolysis.

Concerning peroral application for drug candidates with a high log P, nanocapsules might be advantageous over nanoemulsions due to a different behaviour during digestion.

### Future perspectives

Within this thesis new questions arised which could be object of future studies. Work should be focused on the following points:

1. To get a better understanding of the most unclear point concerning nanocapsules, namely their uptake after peroral application, in vivo ESR studies should be applied. By spectral information on the environment of encapsulated model drugs in real time, it might be possible to solve the question whether nanocapsules are taken up from the gut as intact carriers. In vivo studies should focus on peroral, parenteral, s.c. and i.m. application.
2. Detailed investigations on the influence of ions and pH on the developed polyelectrolyte nanocapsules should be performed.
3. To achieve slower release from polyelectrolyte nanocapsules, cross-linking of the capsule wall should be performed.
4. A method for the quantitative detection of MCT should be developed. Quantitative NMR or HPTLC in combination with a suitable detection reagent for MCT might be good approaches. In the case of PLA and PEG-PLA nanocapsules a lactate kit should also be used to follow the degradation of the shell polymer. If monitoring methods for the fate of nano-encapsulated oil and the shell polymer can be combined with the here developed ESR monitoring on the fate of incorporated model drug, a very detailed picture on the in vitro digestion of nanocapsules could be drawn.

## 7.2 German version

Nanokapseln stellen eine bestimmte Klasse von submikroskopischen kolloidalen Wirkstoffträgersystemen dar, die sich durch ihre einmalige Kombination eines hohen Wirkstoffbeladungsgrades (flüssiger Kern) und der Möglichkeit hoher Stabilität und kontrollierter Freisetzung (feste Polymerhülle) auszeichnen.

Zielsetzung der vorliegenden Arbeit war die physiko-chemische Charakterisierung von Nanokapseln, um ein besseres Verständnis für diese komplexen Wirkstoff-Carrier zu entwickeln. Darüber hinaus sollte das Verhalten von Nanokapseln in simulierter Intestinalflüssigkeit unter Einbeziehung von Enzymen untersucht werden, um Voraussagen für die perorale Applikation treffen zu können. Abschließend war das Schicksal von Nanokapseln nach oraler Administration an Mäusen (ex vivo) von Interesse.

Die Herstellung der Nanokapseln erfolgte nach dem von Fessi [67] entwickelten Verfahren, das auf Polymerpräzipitation um Öltröpfchen beruht. Poly(D,L-laktid) (PLA) und pegyliertes PLA (PEG-PLA) wurden als Hüllpolymere für die Herstellung der Nanokapseln verwendet. PLA-Nanokapseln stellen Nanokapseln der ersten Generation dar, bei oberflächenmodifizierten PEG-PLA-Nanokapseln spricht man von Nanokapseln der zweiten Generation. Als öliger Kern kam Miglyol 812 zum Einsatz. Die Nanokapseldispersionen enthielten den hydrophilen Stabilisator Poloxamer 188, aber keinen lipophilen Stabilisator wie Lecithin. Die durchschnittliche Nanokapselgröße lag bei  $200 \pm 50$  nm.

Die nicht-invasive Methode der Elektronenspinresonanz (ESR)-Spektroskopie wurde zur Charakterisierung verwendet, um Informationen über die Nanocarrier zu gewinnen, die mit konventionellen Techniken nicht zugänglich sind. Die erste Aufgabenstellung ging der Erfassung der Nanoumgebung, einschließlich deren Polarität und Viskosität, eines lipophilen Modellarzneistoffes im Ölkern von Nanokapseln nach. Zusätzliche NMR-Relaxationsstudien lösten die Arzneistoffverteilung bis zur molekularen Ebene auf. Da nur paramagnetische Moleküle mittels ESR detektierbar sind, wurde als Modellarzneistoff die Spinsonde TEMPOL-benzoat (TB) in die Nanokapseln eingebaut. Der Oktanol-Wasser-Verteilungskoeffizient von TB wurde mit einer ESR-Technik nach Kroll [135] bestimmt und ein log P-Wert von 2.46 wurde ermittelt. Dies zeigt, dass die Spinsonde in ihrer Lipophilie zwischen Griseofulvin ( $\log P = 2.18$  [136]) und



Diazepam ( $\log P = 2.92$  [137]) liegt und damit als schlecht wasserlöslicher Modellarzneistoff moderater Lipophilie eingestuft werden kann. Neben TB wurde die Spinsonde HD-PMI, die eine C17-Kette im Molekül enthält, als sehr lipophiler Modellarzneistoff in Nanokapseln eingebaut. Der  $\log P$  von HD-PMI konnte nicht mittels ESR bestimmt werden, da diese Methode nur für Moleküle mit einem  $\log P$ -Wert  $\leq 3$  geeignet ist. Für HD-PMI kann ein  $\log P > 6$  angenommen werden. Dieser Richtwert stützt sich auf Berechnungen eines Computersimulationsprogrammes und Literaturwerte Moleküle ähnlicher Struktur. Der Großteil der TB-Moleküle befand sich im Ölkern, nur ein kleiner Anteil des Modellarzneistoffes (3-4%) lag in der wässrigen Phase gelöst vor.  $^1\text{H}$ -NMR-Untersuchungen zeigten eine homogene Verteilung des TB in der öligen Phase ohne Präferenz für einen bestimmten Molekülteil des Triglycerids. Die stark lipophile Spinsonde HD-PMI war im Gegensatz zum TB komplett in der Ölphase gelöst, deren Anteil 2.5% der Nanokapselsuspension betrug. Beim experimentellen Arbeiten und der In-vivo-Applikation von Nanokapseldispersionen kommt es zur Verdünnung. Da zu diesem dynamischen Prozess keine Informationen vorliegen, wurde er mit Hilfe eines ESR-Verdünnungsassays untersucht. Für TB-Moleküle, die eine mittlere Lipophilie aufweisen, stellte sich innerhalb einer Minute ein neues Verteilungsgleichgewicht zwischen dem Arzneistoffcarrier und seiner neuen Umgebung ein. Im Gegensatz dazu wurde die Verteilung der stark lipophilen HD-PMI-Moleküle nicht sichtbar verändert. Für beide Spinsonden wurde kein Unterschied zwischen einer Nanoemulsion und den beiden Nanokapselsystemen gefunden. Daraus kann geschlossen werden, dass die Polymerhülle keine Barriere für verkapselte Arzneistoffe darstellt. Das Verteilungsgleichgewicht hängt allein vom Verteilungskoeffizienten des Arzneistoffs zwischen dem Ölkern und der wässrigen Umgebung und dem Volumenverhältnis dieser beiden Phasen ab. In der Literatur sind ähnliche Beobachtungen für Nanokapselsysteme, die durch Nanopräzipitation verschiedenster Polymere hergestellt wurden, bei Freisetzungsuntersuchungen zu finden [71,83]. Mit dem ESR-Verdünnungsassay konnten zum ersten Mal Momentaufnahmen dieses Verteilungsprozesses angefertigt werden, die quantifizierbare Ergebnisse lieferten. Erstaunlicherweise ist es gelungen, TB-freie Nanokapseln nachträglich von außen mit TB zu befüllen. Dies zeigt, dass die Diffusion von TB-Molekülen sowohl vom Ölkern in die umgebende Wasserphase als auch andersherum sehr schnell stattfindet. Diese rasche

Umverteilung kann mit Hilfe von TEM-Aufnahmen verstanden werden. Die Schichtdicke der Nanokapselwand auf den TEM-Bildern beträgt ca. 10 nm. Dies stellt in der Tat einen sehr kurzen Diffusionsweg zwischen dem Ölkern und der Wasserphase dar und erklärt die schnelle Diffusionskinetik. Als Konsequenz für die praktische Anwendung von Nanokapseln des Präzipitationstyps bedeutet dies, dass Arzneistoffe moderater Lipophilie weder komplett vor der Umgebung geschützt werden, noch dass die Umgebung vollständig vor diesen Substanzen geschützt wird. Neben Diffusionswegen innerhalb der Carrier und Ladungseffekten an der Grenzfläche spielt die Beschaffenheit des Kapselpolymers eine entscheidende Rolle für die Zugänglichkeit verkapselter Arzneistoffe. Der ESR-Reduktionsassay mit Ascorbinsäure bietet die Möglichkeit, die Angreifbarkeit verkapselter Spinsonden von der wässrigen Phase aus zu untersuchen. PEG-PLA-Nanokapseln gewährleisteten verkapselten TB-Molekülen einen höheren Schutz vor Reduktion durch Ascorbinsäure als PLA-Nanokapseln. PLA-Nanokapseln für ihren Teil zeigten keinen höheren Schutz als eine Nanoemulsion. Der Schutz in PEG-PLA-Nanokapseln stieg mit wachsendem PEG-Substitutionsgrad, was auf den abweisenden Effekt der PEG-Ketten gegenüber den Ascorbinsäuremolekülen zurückzuführen ist. HD-PMI wurde weder in Nanokapseln noch in der Nanoemulsion durch Ascorbinsäure reduziert. Da eine Reduktion desselben in einem hydrophileren Trägersystem wie Mischmizellen gezeigt werden konnte, kann man daraus schließen, dass der Verteilungskoeffizient auch hier das Geschehen bestimmt. HD-PMI-Moleküle diffundieren nicht vom Ölkern in die Wasserphase und können deshalb nicht durch Ascorbinsäure angegriffen werden. Nachdem der Diffusionsprozess und die Zugänglichkeit verkapselter Modellarzneistoffe mittels ESR geklärt werden konnte, wurde Kleinwinkelneutronenstreuung (SANS) herangezogen, um die Kern-Hüll-Struktur von Nanokapseln quantitativ zu charakterisieren. Bis zu diesem Zeitpunkt existierten nur Schätzungen bezüglich Kapselhülldicke, die von TEM-Untersuchungen stammten. Am Beispiel von PLA-Nanokapseln konnte mittels SANS mit Kontrastvariation und entsprechenden Simulationen ein detailliertes Modell des Nanokapselaufbaus aufgestellt werden. Durch Variation der Streulängendichte des Lösungsmittels konnte der Einfluss der Partikelgrößenverteilung vom Einfluss des Formfaktors auf die Streuintensität getrennt werden. Die höchste Empfindlichkeit für die innere Struktur von Nanokapseln wurde erreicht, wenn die Streulängendichte des Lösungsmittels

zwischen der des Miglyols und der PLA-Hülle variiert wurde. Der entsprechende Fit lieferte eine PLA-Hülldicke von 9.8 nm und einen durchschnittlichen Miglyolkernradius von 84 nm. Dynamische Lichtstreuung (DLS) lieferte im Gegensatz zu SANS systematisch leicht höhere Werte für den z-average-Wert des hydrodynamischen Durchmessers. Durch eine Verfeinerung des Fitmodells unter Einführung einer zweiten Hülle, die aus Poloxamer und Wasser bestand, passten SANS- und DLS-Ergebnisse gut zusammen. Das verfeinerte Modell lieferte eine Schichtdicke von 17 nm ( $\pm 6$  nm) für die zusätzliche Schale und einen Poloxameranteil von 7% ( $\pm 5\%$ ).

Komplexe Koazervation in Verbindung mit Hochdruckhomogenisation wurde erfolgreich verwendet, um neuartige dreischichtige Polyelektrolytkomplex-Nanokapseln aus Biopolymeren zu designen. Im Vergleich zu der bereits existierenden Layer-by-layer-Technik, die zu hohlen Nanokapseln führt, spart die hier entwickelte Methode den zeitaufwendigen Abtrennungsschritt von nicht adsorbiertem Polyelektrolyt nach jedem Adsorptionsschritt. Ferner müssen die Nanokapseln nicht nachträglich mit Öl befüllt werden und die Methode kommt ohne organische Lösungsmittel aus. Durch Polyelektrolytzugabe mittels Injektion und anschließender Hochdruckhomogenisation wurde die Aggregatbildung aufgrund von Polymerbrücken zwischen einzelnen Öltropfen minimiert und eine akzeptable Ölbeladung von 2.5% konnte erreicht werden.  $\zeta$ -Potentialmessungen zeigten die Umladung der Kapseloberfläche nach jedem Adsorptionsschritt und bestätigten damit das schrittweise Wachstum der Polyelektrolythülle. TEM-Bilder der Nanokapseln bewiesen die Ausbildung einer komplexen Hülle auf den Öltemplaten. Der z-average Wert für den Kapseldurchmesser wurde mit 230 nm mittels PCS bestimmt.

Bis heute konnte nicht eindeutig geklärt werden, wie in Nanokapseln inkorporierte Arzneistoffe nach oraler Applikation resorbiert werden. Man nimmt an, dass ein geringfügiger Anteil der Nanokapseln als intakte Kapseln aufgenommen wird. Die dominierende Rolle wird allerdings dem gastrointestinalen Verdau der Nanokapseln mit nachfolgender Arzneistoffresorption zugeschrieben. Deshalb ist es von Bedeutung, dass die komplexen Vorgänge, die sich bei der Interaktion der Lipidformulierung mit der gastrointestinalen Umgebung abspielen, verstanden werden. Mit dieser Motivation wurde zunächst eine ESR-Online-Methode zum In-vitro-Monitoring des Fettabbaus entwickelt und diese Methode auf

Nanokapseldispersionen übertragen. Bei der Entwicklung der Monitoringmethode wurde ESR-Spektroskopie mit einem In-vitro-Lipolyseassay gekoppelt und es wurde der Abbau des Modellarzneistoffs TB aus einem langkettigen Triglycerid (Olivenöl) verfolgt. Es gelang, die erste Echtzeitstudie über die Verteilung eines Modellarzneistoffs zwischen Puffer, Öl und Mischmizellen (aus Gallensalzen und Phospholipiden) während eines In-vitro-Verdaus durchzuführen. Durch signifikante Spektrenveränderungen konnte die Umverteilung des Modellarzneistoffs während des Verdaus verfolgt und die Anteile der Spinsonde in den einzelnen Phasen zu jeder Zeit quantifiziert werden. Die Methode wurde auf die Nanokapseldispersionen übertragen und so konnte das Schicksal des inkorporierten Modellarzneistoffs TB verfolgt werden. Die Anwesenheit von Gallensalzen in der simulierten Intestinalflüssigkeit bewirkte eine signifikante Umverteilung der Spinsonde noch vor Enzymzugabe. Dies kann man durch die guten Akzeptoreigenschaften von Mischmizellen für Fremdmoleküle wie TB erklären. Der Solubilisierungsgrad der Mischmizellen für TB-Moleküle war bei PLA-NK höher als bei PEG-PLA-NK. Diese Beobachtung ist nicht verwunderlich, da das PEG-Coating eine diffuse Grenzfläche bietet, welche im Vergleich zu „nackten“ PLA-Nanokapseln die Aufenthaltswahrscheinlichkeit von TB erhöht. Nach Zugabe von Verdauungsenzymen nahm der Anteil der im Miglyol lokalisierten Spinsonde erheblich ab, diese Abnahme fiel für PLA-NK-Dispersionen stärker aus als für PEG-PLA-NK-Dispersionen. Die pegylierte Nanokapseloberfläche behindert höchstwahrscheinlich die Verankerung des Lipase-Colipase-Komplexes an Grenzflächen und senkt damit die Lipaseaktivität.

Beim Zelltoxizitätstest zeigten die Nanokapseldispersionen (PLA und PEG-PLA) ein ähnliches Verhalten wie eine Poloxamerlösung, die als Referenz diente. Da Poloxamer 188 wegen seiner Unbedenklichkeit peroral, dermal und parenteral eingesetzt wird, können die untersuchten Nanokapseln auch als unbedenklich eingestuft werden.

Im Ex-vivo-ESR-Experiment konnte gezeigt werden, dass der lipophile Modellarzneistoff HD-PMI nach intragastrischer Applikation in Mäusen die Blutbahn erreicht. Der HD-PMI-Blutstiegel stieg während der ersten Stunde (t15, t30, t60 min) stetig an bis er 60 Minuten nach der Applikation ein Maximum erreichte, anschließend fiel er wieder ab (t120 min).

Resümierend sind Nanokapseln des Präzipitationstyps in der Theorie maßgeschneiderte Nanocarrier, die einen hohen Arzneistoffbeladungsgrad (flüssiger Kern) und die Möglichkeit hoher Stabilität und kontrollierter Freisetzung (feste Polymerhülle) vereinen. Der hohe AS-Beladungsgrad ist unbestreitbar ein Vorteil gegenüber Konkurrenzcarriern wie Nanospheren oder SLNs (solid lipid nanocarriers), doch leider ist es in der Praxis nicht die feste Hülle sondern der Öl-Wasser-Verteilungskoeffizient, der die Freisetzung kontrolliert. Wie bei anderen lipidhaltigen Nanocarriern ist ein hoher log P-Wert Voraussetzung, um eine schnelle Umverteilung des inkorporierten Arzneistoffs zu verhindern. Ein Vorteil von Nanokapseln gegenüber Nanoemulsionen kann darin gesehen werden, dass die Möglichkeit zur multifunktionellen Modifizierung des Coatingpolymers für Targetingzwecke besteht. Da das Molekulargewicht des Polymers im Vergleich zum Liganden (z.B. Antikörper, Integrine) wesentlich höher ist, kann eine Kopplung einfacher vollzogen werden als bei Nanoemulsionen, wo das Molekulargewicht des Liganden höher ist als das eines typischerweise verwendeten Grenzflächenstabilisators (Lecithin). Darüber hinaus ist die höhere chemische Stabilität von Nanokapseln, bedingt durch die Polymerhülle, vorteilhaft gegenüber lecithinstabilisierten Nanoemulsionen, welche sowohl oxidations- als auch hydrolyseempfindlich sind. Wenn man den peroralen Applikationsweg für Arzneistoffkandidaten mit einem sehr hohen log P betrachtet, könnten Nanokapseln Nanoemulsionen durch ein unterschiedliches Verdauungsprofil überlegen sein.

## Literature

1. K. Westensen. Novel lipid-based colloidal dispersions as potential drug administration systems - expectations and reality. *Colloid Polym. Sci.* 278: 608-618 (2000).
2. G. L. Amidon, H. Lennernas, V. P. Shah, J. R. Crison. A theoretical basis for a biopharmaceutic drug classification: the correlation of in vitro drug product dissolution and in vivo bioavailability. *Pharm. Res.* 12: 413-420 (1995).
3. R. Löbenberg, G. L. Amidon. Modern bioavailability, bioequivalence and biopharmaceutical classification system. New scientific approaches to international regulatory standards. *Eur. J. Biopharm.* 50: 3-12 (2000).
4. J. B. Dressman, C. Reppas. In vitro - in vivo correlations for lipophilic, poorly water-soluble drugs. *Eur. J. Pharm. Sci.* 11: 73-80 (2000).
5. I. Danielsson, B. Lindman. The definition of microemulsion. *Coll. Surfaces B* 3: 391-392 (1981).
6. G. M. Eccleston, Microemulsions. In: J. Swarbrick and J. C. Boylan (eds), *Encyclopedia of pharmaceutical technology*, Vol.9, Marcel Dekker Inc., New York, Basel, Hong Kong, (1994), pp. 375-421.
7. H. Wennerström, J. Daicic, U. Olsson, G. Jerke, P. Schurtenberger. Sponge phases and balanced microemulsions: What determines their stability?. *J. Mol. Liquids.* 72: 15-30 (1997).
8. S. P. Moulik, B. K. Paul. Structure, dynamics and transport properties of microemulsion. *Adv. Coll. Interface. Sci.* 78: 99-195 (1998).
9. R. Cortesi, C. Nastruzzi. Liposomes, micelles and microemulsions as new delivery systems for catotoxic alkaloids, *Pharm. Science and Technol. Today* 2: 288-298 (1999).
10. L. M. Prince. Microemulsions: theory and practice, Academic Press Inc., New York, San Francisco, London,(1997).

11. D. Attwood. Microemulsions. In: J. Kreuter (ed), *Colloidal drug delivery systems*, Vol. 66, Drugs and the pharmaceutical sciences, Marcel Dekker, New York, Basel, Hong Kong, (1994), pp. 31-71.
12. M. Fanun, E. Wachtel, B. Antalek, A. Aserin, N. Garti. A study of the microstructure of four-component sucrose ester microemulsions by SAXS and NMR. *Coll. Surfaces A* 180: 173-186 (2001).
13. M. Kreilgaard. Influence of microemulsions on cutaneous drug delivery. *Adv. Drug Delivery Rev.* 54: 77-98 (2002).
14. L. H. Block, Emulsions and microemulsions. In: H. A. Lieberman, M. M. Rieger, G. S. Banker (eds), *Pharmaceutical dosage forms - disperse systems*, Vol. 2, Marcel Dekker Inc., New York, (1989), pp. 335-378.
15. S. Klang, S. Benita. Design and evaluation of submicron emulsions as colloidal drug carriers for intravenous administration. In: S. Benita (ed), *Submicron emulsions in drug targeting and delivery*, Vol. 9, Drug targeting and delivery, Harwood academic publishers, Amsterdam, (1998), pp. 119-152.
16. K. Westesen, T. Wehler. Physicochemical characterization of a model intravenous oil-in-water emulsion. *J. Pharm. Sci.* 81: 777-786 (1992).
17. S.E. Tabibi. Production of disperse drug delivery systems, In: P. Tyle (ed), *Spezialized drug delivery systems*, Marcel Dekker Inc., New York and Basel, (1990), pp. 317-331.
18. M. B. Schulz, R. Daniels. Hydroxypropylmethylcellulose (HPMC) as emulsifier for submicron emulsions: influence of molecular weight and substitution type on the droplet size after high-pressure homogenization. *Eur. J. Biopharm.* 49: 231-236 (2000).
19. M. Jumaa, B. W. Müller. The effect of oil components and homogenization conditions on the physicochemical properties and stability of parenteral fat emulsions. *Int. J. Pharm.* 163: 81-89 (1998).
20. J. Schmitt. Parenterale Fetteulsion als Arzneistoffträger, In: R. H. Müller, G. Hildebrand (eds), *Pharmazeutische Technologie: Moderne Arzneiformen*, Wissenschaftliche Verlagsgesellschaft mbH, Stuttgart, (1998), pp. 137-142.

21. L. C. Collins-Gold, R. T. Lyons, L. C. Bartholow. Parenteral emulsions for drug delivery. *Adv. Drug Delivery Rev.* 5: 189-208 (1990).
22. M. A. Hammad, B. W. Müller. Solubility and stability of tetrazepam in mixed micelles. *Eur. J. Biopharm.* 7: 49-55 (1998).
23. A. Supersaxo, W. R. Hein, H. Steffen. Mixed micelles as a proliposomal, lymphotropic drug carrier. *Pharm. Res.* 8: 1286-1291 (1991).
24. V. P. Torchilin. Structure and design of polymeric surfactant-based drug delivery systems. *J. Control. Release* 73: 137-172 (2001).
25. R. H. Müller. Nanosuspensionen - eine neue Formulierung für schwerlösliche Arzneistoffe. In: R.H. Müller and G. Hildebrand (eds), *Pharmazeutische Technologie: Moderne Arzneiformen*, Wissenschaftliche Verlagsgesellschaft mbH, Stuttgart, (1998), pp. 393-400
26. K. P. Krause, R. H. Müller. Production and characterization of highly concentrated nanosuspensions by high pressure homogenization. *Int. J. Pharm.* 214: 21-24 (2001).
27. C. Jacobs, O. Kayser, R. H. Müller. Production and characterization of highly concentrated nanosuspensions by high pressure homogenisation, *Int. J. Pharm.* 214: 3-7 (2001).
28. E. Merisko-Liversidge, G.G. Liversidge, E. R. Cooper. Nanosizing: a formulations approach for poorly water-soluble compounds. *Eur. J. Pharm. Sci.* 18: 113-120 (2003).
29. A. T. Serajuddin. Solid dispersion of poorly water-soluble drugs: early promises, subsequent problems, and recent breakthroughs. *J. Pharm. Sci.* 88: 1058-1066 (1999).
30. R. H. Müller, C. Jakobs, O. Kayser. Nanosuspensions for the formulation of poorly soluble drugs. In: F. Nielloud, G. Marti-Mestres (eds), *Pharmaceutical emulsions and suspensions*, Marcel Dekker Inc., New York and Basel, (2000).
31. Y. Barenholz, D. J. Crommelin. Liposomes as pharmaceutical dosage forms. In: J. Swarbrick and J. C. Boylan (eds), *Encyclopedia of pharmaceutical technology*, Vol. 9, Marcel Dekker Inc., New York, Basel and Hong Kong, (1994), pp. 1-39.



32. R. Schubert. Liposomen in Arzneimitteln. In: R. H. Müller, G. E. Hildebrand (eds), *Pharmazeutische Technologie: Moderne Arzneiformen*, Wissenschaftliche Verlagsgesellschaft mbH, Stuttgart, (1998), pp. 219-242.
33. M. Ghyczy. Arzneimittel mit Phosphatidylcholin und Liposomen: Entwicklung, Bewertung, Perspektiven. In: R.H. Müller, G.E. Hildebrand (eds), *Pharmazeutische Technologie: Moderne Arzneiformen*, Wissenschaftliche Verlagsgesellschaft mbH, Stuttgart, (1998), pp. 207-218.
34. D.D. Lasic. *Liposomes: from physics to applications*, Elsevier Science B.V., Amsterdam, (1993).
35. M.J. Otto. *Liposomes: from biophysics to therapeutics*, Marcel Dekker Inc., New York and Basel, (1987).
36. G. Gregoriadis, A. T. Florence, H. M. Patel. Liposomes in drug delivery. In: A. T. Florence and G. Gregoriadis (eds), *Drug targeting and delivery*, Harwood Academic Publishers GmbH, Chur, (1993).
37. D. J. A. Crommelin, H. Schreier. Liposomes. In: J. Kreuter (ed). *Colloidal drug delivery systems*, Vol. 66, Drugs and the pharmaceutical sciences, Marcel Dekker Inc., New York, Basel and Hong Kong, (1994), pp. 73-190.
38. A. T. Florence, C. Cable. Non-ionic surfactant vesicles (niosomes) as vehicles for doxorubicin delivery. In: G. Gregoriadis, A. T. Florence, H.M. Patel (eds), *Liposomes in drug delivery*, Harwood Academic Publishers GmbH, Chur, (1993), pp. 239-253.
39. J. A. Bouwstra, H. E. J. Hofland. In: J. Kreuter (ed), *Colloidal drug delivery systems*, Vol. 66, Drugs and the pharmaceutical sciences, Marcel Dekker Inc., New York, Basel, Hong Kong, pp. 191-217 (1994).
40. M. G. Carr, J. Corish, O. I. Corrigan. Drug delivery from a liquid crystalline base across Visking and human stratum corneum. *Int. J. Pharm.* 157: 35-42 (1997).
41. B. Siekmann, H. Bunjes, M. H. J. Koch, K. Westesen. Preparation and structural investigation of colloidal dispersions prepared from cubic monoglyceride-water phases, *Int. J. Pharm.* 244: 33-43 (2002).

42. B. J. Boyd. Characterization of drug release from cubosomes using the pressure ultrafiltration method, *J. Coll. Interface Science* 260: 404-413 (2003).
43. R. H. Müller, K. Mäder, S. Gohla. Solid lipid nanoparticles (SLN) for controlled drug delivery - a review of the state of the art. *Eur. J. Biopharm.* 50: 161-177 (2000).
44. K. Westesen, B. Siekmann. Solid lipid particles, particles of bioactive agents and methods for the manufacture and use thereof. United States Patent 5,785,976 (1998).
45. B. Siekmann and K. Westensen. Submicron-sized parenteral carrier systems based on solid lipids. *Pharm. Pharmacol. Lett.* 1: 123-126 (1992).
46. K. Jores. Lipid nanodispersions as drug carrier systems - a physicochemical characterization, Ph.D. thesis, Halle (2004).
47. K. Jores, W. Mehnert, K. Mäder. Physicochemical investigations on solid lipid nanoparticles (SLN) and on oil-loaded solid lipid nanoparticles: a nuclear magnetic resonance and electron spin resonance study. *Pharm. Res.* 20: 1274-1283 (2003).
48. J. Kreuter, Nanoparticles. In: Kreuter (ed), *Colloidal drug delivery systems*, Vol. 66, Drugs and the pharmaceutical sciences, Marcel Dekker Inc., New York, Basel and Hong Kong, (1994), pp. 219-342.
49. D. Lemoine, C. Francois, F. Kedzierewicz, V. Peat, M. Hoffman, P. Maincent. Stability study of poly(epsilon-caprolactons), poly(D,L-lactide) and poly(D,L-lactide-co-glycolide). *Biomaterials* 17: 2191-2197 (1996).
50. B. M. Discher, Y.-Y. Won, D. S. Ege, J. C.-M. Lee, F. S. Bates, D. E. Discher, D. A. Hammer. Polymersomes: Tough vesicles made from diblock copolymers. *Science* 284: 1143-1146 (1999).
51. M. Antonietti, S. Förster. Vesicles and Liposomes: A self-assembly principle beyond lipids. *Adv. Mater.* 15: 1323-1333
52. D. Quintanar-Guerrero, E. Allémann, E. Doelker, H. Fessi. Characterization of nanocapsules from preformed polymers by a new process based on emulsification-diffusion technique. *Pharm. Res.* 15: 1056-1062 (1998).

53. P. Couvreur, G. Couarraze, J. Devissaguet, F. Puisieux. In: S. Benita (ed), *Microencapsulation: Methods and Industrial Applications*, Marcel Dekker, New York, (1996), p.183.
54. A. Dingler. Feste Lipid-Nanopartikel als kolloidale Wirkstoffträgersysteme zur dermalen Applikation, Ph.D. thesis, Berlin, (1998).
55. R. H. Müller, W. Mehnert, J.-S. Lucks, A. z. Mühlen, H. Weyhers, C. Freitas, D. Rühl. Solid lipid nanoparticles (SLN) - an alternative colloidal carrier system for controlled drug delivery. *Eur. J. Biopharm.* 41: 62-69 (1995).
56. E. Ugazio, R. Cavalli, M.R. Gasco. Incorporation of cyclosporine A in solid lipid nanoparticles (SLN). *Int. J. Pharm.* 241: 341-344 (2002).
57. W. Mehnert, A. z. Mühlen, A. Dingler, H. Weyhers, R. H. Müller. Solid lipid nanoparticles - ein neuartige Wirkstoff-Carrier für Kosmetika und Pharmazeutika, 2. Mitteilung: Wirkstoff-Inkorporation, Freisetzung und Sterilisierbarkeit. *Pharm. Ind.* 59: 511-514 (1997).
58. K. Westesen, H. Bunjes, M. H. J. Koch. Physicochemical characterization of lipid nanoparticles and evaluation of their drug loading capacity and sustained release potential. *J. Control. Release* 48: 223-236 (1997).
59. K. Westesen, B. Siekmann. Investigation of the gel formation of phospholipids-stabilized solid lipid nanoparticles. *Int. J. Pharm.* 151: 35-45 (1997).
60. W. Mehnert, K. Mäder. Solid lipid nanoparticles: production, characterization and applications. *Adv. Drug Delivery Rev.* 47: 165-196 (2001).
61. C. W. Pouton. Lipid formulations for oral administration of drugs: non-emulsifying, self-emulsifying and "self-microemulsifying" drug delivery systems. *Eur. J. Pharm. Sci.* 11: 93-98 (2000).
62. C.W. Pouton. Key issues when formulating with lipids. *Bull. Tech. Gattefosse* 92: 41-50 (1999).
63. P. Couvreur, P. Tulkens, M. Roland, A. Trouet, P. Speiser. Nanocapsules: a new type of lysosomotropic carrier. *Fed. Eur. Biochem. Soc. Letters* 84: 323-326 (1977).

64. C. Damgé, C. Michel, M. Aprahamian, P. Couvreur. New approach for oral administration of insulin with polycyanoacrylate nanocapsules as drug carrier. *Diabetes* 37:246-251 (1988).
65. N. Al Khouri Fallouh, L. Roblot-Treupel, H. Fessi, J.Ph. Devissaguet, F. Puisieux. Development of a new process for the manufacture of polyisobutylcyanoacrylate nanocapsules. *Int. J. Pharm.* 28: 125-132 (1986).
66. H. Fessi, J. Ph. Devissaguet, F. Puisieux, C. Thies. Procédé de préparation de systèmes colloïdaux disoersibles d'une substance sous forme de nanoparticules. French Patent, 2,608,988 (1988).
67. H. Fessi, F. Puisieux, J. Ph. Devissaguet, N. Ammoury, S. Benita. Nanocapsule formation by interfacial polymer deposition following solvent displacement. *Int. J. Pharm.* 55: R1-R4 (1989).
68. M. J. Alonso. Nanoparticulate drug carrier technology. In: S. Cohen, H. Bernstein (eds), *Microparticulate Systems for the Delivery of Proteins and Vaccines*, Marcel Dekker, New York, (1996), pp. 203-242.
69. P. Legrand, G. Barratt, V. Mosqueira, H. Fessi, J. Ph. Devissaguet. Polymeric nanocapsules as drug delivery systems, A review. *STP Pharma. Sci.* 9: 411-418 (1999).
70. V. C. F. Mosqueira, P. Legrand, H. Pinto-Alphandry, F. Puisieux, G. Barratt. Poly (D,L-Lactide) nanocapsules prepared by a solvent displacement process: influence of the composition on physicochemical and structural properties. *J. Pharm. Sci.* 89: 614-625 (2000).
71. N. S. Santos-Magalhães, A. Pontes, V. M. W Pereira, M. N. P. Caetano. Colloidal carriers for benzathine penicillin G: nanoemulsions and nanocapsules. *Int. J. Pharm.* 208: 71-80 (2000).
72. M. Teixeira, M. J. Alonso, M. M. M. Pinto, Carlos M. Barbosa. Development and characterization of PLGA nanospheres and nanocapsules containing xanthone and 3-methoxyxanthone. *Eur. J. Biopharm.* 59: 491-500 (2005).
73. F. Kedzierewicz, P. Thouvenot, I. Monot, M. Hoffman, P. Maincent. Influence of different physiological conditions on the release of indium oxine from nanocapsules. *J. Biomed. Mater. Res.* 39: 588-593 (1998).

74. E. Cauchetier, M. Deniau, H. Fessi, A. Astier, M. Paul. Atovaquone-loaded nanocapsules: influence of the nature of the polymer on their in vitro characteristics. *Int. J. Pharm.* 250: 273-281 (2003).
75. V. C. F. Mosqueira, P. Legrand, J.-L. Morgat, M. Vert, E. Mysiakine, R. Gref, J. P. Devissaguet, G. Barratt. Biodistribution of long-circulating PEG-grafted nanocapsules in mice: effects of PEG chain length and density. *Pharm. Res.* 18: 1411-1419 (2001).
76. B. Heurtault, P. Saulnier, B. Pech, J. E. Proust, J.-P. Benoit. A novel phase inversion-based process for the preparation of lipid nanocarriers. *Pharm. Res.* 19, 875-880 (2002).
77. A. Lambrecht, Y. Bouligand, J.-P. Benoit. New lipid nanocapsules exhibit sustained release properties for amiodarone. *J. Control. Release* 84: 59-68 (2002).
78. A. Lamprecht, J.-L. Saumet, J. Rouxa, J.-P. Benoit. Lipid carriers as drug delivery system for ibuprofen in pain treatment. *Int. J. Pharm.* 278: 407 (2004).
79. D. Bazile. Influence of lipid nanocapsules composition on their aptness to freeze-drying. *Pharm. Res.* 22: 285-292 (2005).
80. G. B. Sukhorukov, A. A. Antipov, A. Voigt, E. Donath, H. Möhwald. pH-controlled macromolecule encapsulation in and release from polyelectrolyte multilayer nanocapsules. *Macromol. Rapid Commun.* 22: 44 (2001).
81. H. Ai, J. Gao. Size-controlled polyelectrolyte nanocapsules via layer-by-layer self-assembly. *J. Mat. Sci.* 39: 1429 (2004).
82. G. Sukhorukov, A. Fery, H. Möhwald. Intelligent micro- and nanocapsules. *Prog. Polym. Sci.* 30: 885-897 (2005)
83. P. Couvreur, G. Barratt, E. Fattal, P. Legrand, C. Vauthier. Nanocapsule Technology : A Review, Critical Reviews™ in Therapeutic Drug Carrier Systems 19: 99-134 (2002).
84. A. Antipov, G.B. Sukhorukov. Polyelectrolyte multilayer capsules as vehicles with tunable permeability. *Adv. Coll. Interface Sci.* 111: 49-61 (2004).

85. F. Xing, G. Cheng, K. Yi, L. Ma. Nanoencapsulation of capsaicin by complex coacervation of gelatin, acacia and tannins. *J. Appl. Polym. Sci.* 96: 2225-2229 (2005).
86. H. Gao, W. Yang, K. Min, L. Zha, C. Wang, S. Fu. Thermosensitive poly(N-isopropylacrylamide) nanocapsules with controlled permeability. *Polymer* 46: 1087-1093 (2005).
87. M. Sauer, D. Streich, W. Meier. pH-sensitive nanocontainers. *Adv. Mater.* 13: 1649-1651 (2001).
88. L. Grislain, P. Couvreur, V. Lenaerts, M. Roland, D. Desrez-Decampeneere, P. Speiser. Pharmacokinetics and distribution of a biodegradable drug-carrier. *Int. J. Pharm.* 15: 335-345 (1983).
89. C. Verdun, F. Brassuer, H. Vranckx, P. Couvreur, M. Roland. Tissue distribution of doxorubicin associated with polyhexylcyanoacrylated nanoparticles. *Cancer Chemother. Pharmacol.* 26: 13-18 (1990).
90. S. M. Moghimi, A. C. Hunter, J. C. Murray. Long-circulating and target-specific nanoparticles: theory to practice. *Pharmacol. Rev.* 53: 283-318 (2001).
91. B. Stella, S. Arpicco, M. T. Peracchia, D. Desmaele, J. Hoebeker, M. Renoir, J. d'Angelo, L. Cattel, P. Couvreur. Design of folic acid-conjugated nanoparticles for drug targeting. *J. Pharm. Sci.* 89: 1452-1464 (2000).
92. B. Stella, V. Marsaud, P. Couvreur, S. Arpicco, M. T. Peraccia, G. Geraud, M. L. Immordino, L. Cattel, M. Renoir. Biological characterisation of folic acid-conjugated nanoparticles in cellular models. In: Proceedings of the Controlled Release of Bioactive Materials Congress, San Diego, No. 5200, (2001).
93. J. Weber, S. Robaina. Localized drug delivery using drug-loaded nanocapsules. International Patent WO 040/69169, (2004).
94. J. Raffi, S. Gelly, L. Barral, F. Burger, P. Piccerelle, P. Prinderre, M. Baron, A. Chamayou. Electron paramagnetic resonance of radicals induced in drugs and excipients by radiation or mechanical treatments. *Spectrochimica Acta Part A* 58: 1313-1320 (2002).

95. K. Mäder, A. Domb, H.M. Swartz. Gamma sterilization induced radicals in biodegradable drug delivery systems. *Appl. Rad. Isot.* 47: 1669-1674 (1996).
96. K. Mäder, H. M. Swartz, R. Stösser, H.-H. Borchert. The application of ESR spectroscopy in the field of pharmacy. *Pharmazie* 49: 97-101 (1994).
97. I. Katzhendler, K. Mäder, M. Friedman. Structure and hydration properties of hydroxypropyl methyl cellulose matrices containing naproxen and naproxen sodium. *Int. J. Pharm.* 200: 161-179 (2000).
98. C. Kroll, W. Herrmann, R. Stösser, H. H. Borchert, K. Mäder. Influence of drug treatment on the microacidity in rat and human skin - an in vitro electron spin resonance imaging study. *Pharm. Res.* 18: 525-530 (2001).
99. L. J. Berliner (ed), In Vivo EPR (ESR): Theory and Applications, Kluwer Academic / Plenum Publishers, New York, (2003).
100. K. Kuppusamy, M. Chzhan, J. L. Zweier. Principles of Imaging: Theory and Instrumentation in in vivo EPR (ESR): Theory and Applications. In: L. J. Berliner (ed), New York: Kluwer Academic / Plenum Publishers 6: 99-152 (2003).
101. T. Ymaguchi, S. Itai, H. Hayashi, S. Soda, A. Hamada, H. Utsumi. In vivo ESR studies on pharmacokinetics and metabolism of parenteral lipid emulsion in living mice. *Pharm. Res.* 13: 729-733 (1996).
102. M. Petelin, Z. Pavlica, S. Bizimoska, M. Sentjunc. In vivo study of different ointments for drug delivery into oral mucosa by ESR oximetry. *Int. J. Pharm.* 270: 83-91 (2004).
103. K. Mäder, B. Bittner, Y. Li, W. Wohlauf, T. Kissel. Monitoring microviscosity and microacidity of the albumin microenvironment inside degrading microparticles from polylactide-co-glycolide (PLG) or ABA -triblock polymers containing hydrophobic poly(lactide-co-glycolide) A blocks and hydrophilic poly(ethylenoxide) B blocks. *Pharm. Res.* 15: 787-793 (1998).
104. K. Jores, W. Mehnert, K. Mäder. Physicochemical investigations on solid lipid nanoparticles and on oil-loaded solid lipid nanoparticles: a nuclear magnetic resonance and electron spin resonance study. *Pharm. Res.* 20: 1274-1283 (2003).
105. I. Katzhendler, K. Mäder, M. Friedman. Correlation between drug release kinetics from protein matrix and matrix structure: ESR and NMR study. *J. Pharm. Sci.* 89: 365-381 (2000).

106. H. Halpern. Stable soluble paramagnetic compounds. In L. J. Berliner (ed), *In vivo EPR (ESR), theory and applications*, Kluwer Academic / Plenum publishers, (2003).
107. N. Ammoury, H. Fessi, J.-P.Devissagnet, F. Puisieux, S. Benita. Physicochemical characterization of polymeric nanocapsules and in vitro release evaluation of indomthacin as a model drug, *STP Pharma* 5: 647-651 (1989).
108. N.S. Santos Magalhaes, H. Fessi, F. Puisieux, S. Benita, M. Seiller. An in vitro release kinetic examination and comparative evaluation between submicron emulsion and polylactic acid nanocapsules of clofibrade. *J. Microencaps.* 12: 195-205 (1995).
109. M. Fresta, G. Cavallaro, G. Giammona, E. Wehrli, G. Puglisi. Preparation and characterization of polyethyl-2-cyanoacrylate nanocapsules containing antiepileptic drugs. *Biomaterials* 17: 751-758 (1996).
110. B. Seijo, E. Fattal, L. R. Treupel, P. Couvreur. Design of nanoparticles of less than 50 nm diameter: preparation, characterization and drug loading. *Int. J. Pharm.* 62: 1-7 (1990).
111. M.Y. Levy, S. Benita. Drug release from submicronized o/w emulsion: a new in vitro kinetic evaluation model. *Int. J. Pharm.* 66: 29-37 (1990).
112. F. Dalençon, Y. Amjaud, C. Lafforgue, F. Derouri, H. Fessi. Atovaquone and rifabutine-loaded nanocapsules: formulation studies. *Int. J. Pharm.* 153: 127-130 (1997).
113. C. Mayer, D. Hoffmann, M. Wohlgemuth. Structural analysis of nanocapsules by nuclear magnetic resonance. *Int. J. Pharm.* 242: 37-46 (2002).
114. D. Hoffmann. NMR investigation on nanocapsule dispersions, Ph.D.thesis, Duisburg (2000).
115. M. Wohlgemuth. Diffusionsexperimente an Nanokapseldispersionen: Größenverteilung, Wirkstofffreisetzung und andere dynamische Phänomene. Ph.D. thesis, Duisburg (2002).
116. Guinebretière, S. Briançon, J. Lieto, C. Mayer, H. Fessi. Study of the emulsion-diffusion of solvent: preparation and characterization of nanocapsules. *Drug Dev. Res.* 57: 18-33 (2002).



117. C. A. Miller. Spontaneous emulsification produced by diffusion. *Colloids. Surf.* 29: 89-102 (1988).
118. J. C. Lopez-Montilla, P. E. Herrera-Morales, S. Pandey, D. O. Shah. Spontaneous emulsification: mechanisms, physicochemical aspects, modeling and applications. *J. Dispersion Sci. Technol.* 23: 219-268 (2002).
119. M. Gallardo, G. Couarraze, B. Denizot, L. Treupel, P. Couvreur, F. Puisieux. Study of the mechanisms of formation of nanoparticles and nanocapsules of poly(isobutyl 2-cyanoacrylate). *Int. J. Pharm.* 100: 55-64 (1993).
120. S. A. Vitale, J. L. Kratz. Liquid droplet dispersions formed by homogeneous liquid-liquid nucleation: „the Ouzo effect“. *Langmuir* 19: 4105-4110 (2003).
121. F. Ganachaud, J. L. Katz. Nanoparticles and nanocapsules created using the Ouzo effect: spontaneous emulsification as alternative to ultrasonic high-shear devices. *Chem. Phys. Chem.* 6: 209-216 (2005).
122. M. J. Groves, M. Wineberg, A. P. R. Brian. The presence of liposomal material in phosphatide stabilized emulsions. *J. Dispersion Sci. Technol.* 237-243 (1985).
123. G. F. Lambert, J. P. Miller, D. V. Frost. Decomposition of lecithin in parenteral fat emulsions. *Am. J. Physiol.* 186: 397-402 (1956).
124. C. Hunnius, Pharmazeutisches Wörterbuch. Walter de Gruyter, Berlin, NewYork (1998).
125. B. Chu. Laser Light Scattering, Academic Press, New York (1974).
126. R. H. Müller, R. Schuhmann, Teilchengrößenmessung in der Laborpraxis, Wissenschaftliche Verlagsgesellschaft mbH, Stuttgart (1996).
127. R. J. Haskell, J. R. Shifflett, P. A. Elzinga. Particle-sizing technologies for submicron emulsions. In: S. Benita (ed), *Submicron emulsions in drug targeting and delivery*, Vol. 9, Harwood academic publishers, Amsterdam, (1998), pp. 21-98.
128. Malvern Instruments, Customer Training, Measurement of size (2004).
129. C. Urban, P. Schurtenberger. Characterization of turbid colloidal suspensions using light scattering techniques combined with cross-correlation methods, *J. Colloid Interface Sci.* 207: 150-158 (1998).
130. D. R. Duling. Simulation of multiple isotropic spin trap ESR spectra. *J. Magn. Reson. B* 104: 105-110 (1994).

131. P. Strunz, J. Saroun, U. Keiderling, A. Wiedenmann, R. Przenioslo. General formula for determination of cross-section from measured SANS intensities. *J. Appl. Cryst.* 33: 829-833 (2000).
132. P. Legrand, B. Barratt, V. Mosqueira, H. Fessi, J. P. Devissaguet. Polymeric nanocapsules as drug delivery systems. A review. *STP Pharma. Sci.* 9: 411-418 (1999).
133. P. Calvo, J. L. Vila Jato, M. J. Alonso. Comparative in vitro evaluation of several colloidal systems, nanoparticles, nanocapsules, and nanoemulsions, as ocular drug carriers. *J. Pharm. Sci.* 85: 530-536 (1996).
134. C. Losa, L. Marchal-Heussler, F. Orallo, J. L. Vila Jato, M. J. Alonso. Design of new formulations for topical ocular administration: polymeric nanocapsules containing metipranolol. *Pharm. Res.* 10: 80-87 (1993).
135. C. Kroll. Analytik, Stabilität und Biotransformation von Spinsonden sowie deren Einsatz im Rahmen pharmazeutisch-technologischer und biopharmazeutischer Untersuchungen, Ph.D. thesis, Berlin, (1999).
136. A. Leo, C. Hansch, D. Elkins. Partition co-efficients and their uses. *Chem. Rev.* 71: 526-616 (1971).
137. A. Taillardat-Bertschinger, C. A. M. Martinet, M. R. P. A. Carrupt, G. Caro, B. Testa. Effect of molecular size and charge on IAM retention in comparison to partitioning in liposomes and n-octanol, *Pharm. Res.* 19: 729-738 (2002).
138. D. A. Cooper, D. R. Webb, J. C. Peters. Evaluation of the potential for olestra to affect the availability of dietary phytochemicals. *J. Nutr.* 127: 1699-1709 (1997).
139. P. W. Atkins (ed), *Physikalische Chemie*, VHC Verlagsgesellschaft mbH, Weinheim,(1990).
140. T. E. Shearmur, D. W. Drew, A. S. Clough, M. G. D. van der Grinten. Study of dye diffusion in polymers using Rutherford backscattering. *Polymer* 37: 2695-2700 (1996).
141. J.C. Thomas. The determination of log normal particle size distributions by dynamic light scattering. *J. Coll. Interface Sci.* 117: 187-192 (1986).

142. W. J. Wiscombe. Improved Mie scattering algorithm. *Applied Optics* 19: 1505-1509 (1980).
143. BASF. Technical information for Lutrol F 68<sup>TM</sup>. (1997).
144. P. Alexandridis, T. A. Hatton. Poly(ethylene oxide)-poly(propylene oxide)-poly(ethylene oxide) block copolymer surfactants in aqueous solutions and at interfaces: thermodynamics, structure, dynamics, and modelling. *Coll. Surf. B* 96: 1-46 (1995).
145. Th. F. Tadros. The effect of polymers on dispersion properties. Academic Press (1996).
146. S. Ogawa, E. A. Decker, D. J. McClements. Production and characterization of O/W emulsions containing cationic droplets stabilized by lecithin-chitosan membranes. *J. Agric. Food Chem.* 51: 2806-2812 (2003).
147. S. Ogawa, E.A. Decker, D.J. McClements. Influence of environmental conditions on stability of O/W emulsions containing droplets stabilized by lecithin-chitosan membranes. *J. Agric. Food Chem.* 51: 5522-5527 (2003).
148. S. Ogawa, E. A. Decker, D. J. McClements. Production and characterization of O/W emulsions containing droplets stabilized by lecithin-chitosan-pectin multilayered membranes. *J. Agric. Food Chem.* 52: 3595-3600 (2003).
149. L. Wang, E. Khor, A. Wee, L. Y. Lim. Chitosan-alginate PEC membranes as wound dressing: assesment of incisional wound healing. *J. Biomed. Mat. Res.* 63: 610-618 (2002).
150. S. Panzner, E. Gerold, S. Lutz. Stabilization of liposomes mixtures and emulsions by encapsulation of liposomes. European Patent 1,304,160 (2003).
151. G. Decher, J. D. Hong. Buildup of ultrathin multilayer films by a self-assembly process. 1. Consecutive adsorption of anionic and cationic bipolar amphiphiles on charged surfaces. *Macromol. Chem. Macromol. Symp.* 46: 321-7 (1991).
152. G. Decher, J.-D. Hong, J. Schmitt. Consecutively alternating adsorption of anionic and cationic polyelectrolytes on charged surface. *Thin Solid Films* 210/211: 831-835 (1992).
153. G. Decher. Fuzzy nanoassemblies: toward layered polymeric multicomposites. *Science* 277: 1232-1237 (1997).

154. A. Antipov, E. Vieria, G. Ibarz, G. B. Sukhorukov, L. Dähne, C. Gao, E. Donath, H. Möhwald. Controlled and sustained release properties of polyelectrolyte multilayer capsules. International Patent WO 02/17888 (2002).
155. G. B. Sukhorukov, E. Donath, S. Davis, H. Lichtenfeld, F. Caruso, V. I. Popov, H. Möhwald. Stepwise polyelectrolyte assembly on particle surfaces: a novel approach to colloid design, *Polym. Adv. Technol.* 9: 759-767 (1998).
156. X. Qiu, E. Donath, H. Möhwald. Permeability of Ibuprofen in various polyelectrolyte multilayers. *Macromol. Mater. Eng.* 286: 91-97 (2001).
157. F. Caruso, D. Trau, H. Möhwald, R. Renneberg. Encapsulation of crystals via multilayer coatings. International Patent WO 00/77281 (2000).
158. H. Al, J. Gao. Size-controlled polyelectrolyte nanocapsules via layer-by-layer self assembly. *J. Mat. Sci.* 39: 1429-1432 (2004).
159. S. Ye, C. Wang, X. Liu, Z. Tong. Multilayer nanocapsules of polysaccharide chitosan and alginate through layer-by-layer assembly directly on PS nanoparticles for release. *J. Biomat. Sci. Polymer Edn.* 16: 909-923 (2005).
160. D. B. Shenoy, G. B. Sukhorukov. Engineered microcrystals for direct surface modification with layer-by-layer technique for optimized dissolution. *Eur. J. Biopharm.* 58: 521-527 (2004).
161. G. B. Sukhorukov, E. Donath, H. Lichtenfeld, E. Knippel, M. Knippel, A. Budde, H. Möhwald. Layer-by-layer self assembly of polyelectrolytes on colloidal particles. *Colloids Surfaces A* 137: 253-266 (1998)
162. G.B. Sukhorukov. Designed nano-engineered polymer films on colloidal particles and capsules. In: D. Mobius, R. Miller (eds), Elsevier, The Netherlands (2001).
163. S. S. Koide. Chitin-chitosan: properties, benefits and risks. *Nutr. Res.* 18: 1091-1101 (1998).
164. FMC Bio Polymer, Technical Service Bulletin for Viscarin GP 209 NF (2000).
165. National Starch & Chemicals, Technical Service Bulletin for Purity® Gum 2000 (2001).

166. A. M. Kaukonen, B. J. Boyd, C. J. H. Porter, W. N. Charman. Drug solubilization behaviour during *in vitro* digestion of simple triglyceride lipid solution formulations. *Pharm. Res.* 21: 245-253 (2004).
167. A. M. Kaukonen, B. J. Boyd, W. N. Charman, C. J. H. Porter. Drug solubilization behaviour during *in vitro* digestion of suspension formulations of poorly water-soluble drugs in triglyceride lipids. *Pharm. Res.* 21: 254-260 (2004).
168. K. J. MacGregor, J. K. Embleton, J. E. Lacy, A. P. Perry, L. J. Solomon, H. Seager, C. W. Pouton. Influence of lipolysis on drug absorption from the gastro-intestinal tract. *Adv. Drug Del. Rev.* 25: 33-46 (1997).
169. N. H. Zangenberg, A. Mullertz, H. Gjelstrup Kristensen, L. Hovgaard. A dynamic *in vitro* lipolysis model-II. Evaluation of the model. *Eur. J. Pharm. Sci.* 14: 237-244 (2001).
170. J. E. Staggars, O. Hernell, R. J. Stafford, M. C. Carey. Physical-chemical behaviour of dietary and biliary lipids during intestinal digestion and absorption. 1. Phase behaviour and aggregation states of model lipid systems patterned after aqueous duodenal contents of healthy adult human beings. *Biochemistry* 29: 2028-2040 (1990).
171. Hernell, J. E. Staggars, M. C. Carey. Physical-chemical behaviour of dietary and biliary lipids during intestinal digestion and absorption. 2. Phase analysis and aggregation states of luminal lipids during duodenal fat digestion in healthy adult human beings. *Biochemistry* 29: 2041-2056 (1990).
172. L. Sek, C. J. H. Porter, W. N. Charman. Characterisation and quantification of medium chain and long chain triglycerides and their *in situ* densitometric analysis. *J. Pharm. Biomed. Anal.* 25: 651-661 (2001).
173. L. Sek, C. J. H. Porter, A. M. Kaukonen, W. N. Charman. Evaluation of the in-vitro profiles of long and medium chain glycerides and the phase behaviour of their lipolytic products. *J. Pharm. Pharmacol.* 54: 29-41 (2002).
174. N. H. Zangenberg, A. Mullertz, H. Gjelstrup Kristensen, L. Hovgaard. A dynamic *in vitro* lipolysis model-I. Controlling the rate of lipolysis by continuous addition of calcium. *Eur. J. Pharm. Sci.* 14: 115-122 (2001).
175. C. J. H. Porter, A. M. Kaukonen, A. Taillardat-Bertschinger, B. J. Boyd, J. M. O'Connor, G. A. Edwards, W. N. Charman. Use of *In vitro* lipid digestion data

- to explain the *In Vivo* performance of triglyceride-based oral lipid formulations of poorly water-soluble drugs: studies with halofantrine. *J. Pharm. Sci.* 93: 1110-1121 (2003).
176. S. Klein. Optimierung eines Pankreatin-Assays als prädiktives in vitro Modell zur Bioverfügbarkeit von Wirkstoffformulierungen. Diploma Thesis, Halle (Saale), 2006.
  177. J. Sjövall. On the concentration of bile acids in the human intestine during absorption. *Acta Physiol. Scand.* 46: 339-345 (1959).
  178. O. Fausa. Duodenal bile acids after a test meal. *Scand. J. Gastroenterol.* 9: 567-570 (1974).
  179. H. Westergaard. Duodenal bile acid concentrations in fat malabsorption syndromes. *Scand. J. Gastroenterol.* 12: 115-122 (1977).
  180. M. Rautereau, A. Bisalli, J.-C. Ranbaud. Étude de la phase aqueuse intrajéjunale des sels biliaires et des lipides au cours de la digestion d'un repas standard chez le sujet normal. *Gastroenterol. Clin. Biol.* 5: 417-425 (1981).
  181. A. Lindahl, A. L. Ungell, L. Knutson, H. Lennernas. Characterization of fluids from the stomach and proximal jejunum in men and women. *Pharm. Res.* 14: 497-502 (1997).
  182. V. Lebet, E. Arrigoni, R. Amadò. Digestion procedure using mammalian enzymes to obtain substrates for in vitro fermentation studies. *Lebensm.-Wiss.u.-Technol.* 31: 509-515 (1998).
  183. M. Aboubakar, P. Couvreur, H. Pinto-Alphandary, B. Gouritin, B. Lacour, R. Farinotti, F. Puisuex, C. Vauthier. Insulin-loaded nanocapsules for oral administration : in vitro and in vivo investigation. *Drug Dev. Res.* 49: 109-117 (2000).
  184. H. Pinto-Alphandry, M. Aboubakar, D. Jaillard, P. Couvreur, C. Vauthier. Visualization of insulin-loaded nanocapsules: in vitro and in vivo studies after oral administration to rats. *Pharm. Res.* 20: 1071-1084 (2003).
  185. H. Marchais, S. Benali, J.M. Irache, C. Tharasse-Bloch, O. Lafont, A. M. Orecchioni. Entrapment efficiency and initial release of phenylbutazone from nanocapsules prepared from different polyesters. *Drug Dev. Ind. Pharm.* 24: 883-888 (1998).

186. N. Ammoury, H. Fessi, J. P. Devissaguet, F. Puisieux, S. Benita. In vitro release kinetic pattern of indomethacin from poly(D,L-lactide) nanocapsules. *J. Pharm. Sci.* 79: 763-767 (1990).
187. F. B. Landry, D. V. Bazile, G. Spenlehauer, M. Veillard, J. Kreuter. Degradation of poly(D,L-lactic acid) nanoparticles coated with albumin in model digestive fluids (USP XXII). *Biomaterials* 17: 715-723 (1996).
188. M. Tobio, A. Sánchez, A. Vila, I. Soriano, C. Evora, J. L. Vila-Jato, M. J. Alonso. The role of PEG on the stability in digestive fluids and in vivo fate of PEG-PLA nanoparticles following oral administration. *Colloids and Surfaces B: Biointerfaces* 18: 315-323 (2000).
189. A. Belbella, C. Vauthier, H. Fessi, J.P. Devissaguet, F. Puisieux. In vitro degradation of nanospheres from poly(D,L-lactides) of different molecular weights and polydispersity. *Int. J. Pharm.* 129: 95-102 (1996).
190. J. Tan, D. Butterfield, C. Voycheck, K. Cadwell, J. Li. Surface modification of nanoparticles by PEO/PPO block copolymers to minimize the interaction with blood components and prolong blood circulation in rats. *Biomaterials* 14: 823-833 (1993).
191. S. E. Dunn, S. Stolnick, M. C. Garnett, M. C. Davies, A. G. A. Coombes, D. C. Taylor, M. P. Irving, S. C. Purkiss, T. F. Tadros, S. S. Davis, L. Illum. Biodistribution studies investigating poly(lactide-co-glycolide) nanospheres surface modified by novel biodegradable copolymers. *Proceed. Intern. Symp. Control. Rel. Bioact. Mater.* 21: 210-211 (1994).
192. R. Gref, Y. Minamitake, M. T. Peracchia, V. Trubetskoy, V. Torchilin, R. Langer. Biodegradable long-circulating nanospheres. *Science* 263: 1600-1603 (1994).
193. T. Verrechia, M. Veillard. Non-stealth (poly(lactic acid/albumin) and stealth (poly(lactic acid-polyethylene glycol)) nanoparticles as injectable drug carriers. *J. Control. Release* 36: 49-51 (1995).
194. J. K. Embleton, C. W. Pouton. Structure and function of gastro-intestinal lipases. *Adv. Drug. Deliv. Rev.* 25: 15-32 (1997).

195. C. Damgé, M. Aprahamian, G. Balboni, A. Hoeltzel, V. Andrieu, J. P. Devissaguet. Polycyanoacrylate nanocapsules increase the intestinal absorption of lipophilic drug. *Int. J. Pharm.* 36: 121-125 (1987).
196. M. Aprahamian, C. Michel, W. Humbert, J. P. Devissaguet, C. Damgé. Transmucosal passage of polycyanoacrylate nanocapsules as a new drug carrier in the small intestine. *Biol. Cell.* 61: 69-76 (1987).
197. N. Ammoury, H. Fessi, J.P. Devissaguet, M. Aliix, M. Plotkine, R.G. Boulu. Effect on cerebral blood flow of orally administered indomethacin-loaded poly(isobutylcyanoacrylate) and poly(D,L-lactide) nanocapsules. *J. Pharm. Pharmacol.* 42: 558-561 (1990).
198. N. Ammoury, H. Fessi, J. P. Devissaguet, M. Dubrasquet, S. Benita. Jejunal absorption, pharmacological activity and pharmacokinetic evaluation of indomethacin-loaded poly(D,L-lactide) and poly(isobutyl-cyanoacrylate) nanocapsules in rats. *Pharm. Res.* 8: 101-105 (1990).
199. A. T. Florence. The oral absorption of micro- and nanoparticulates: neither exceptional nor unusual. *Pharm. Res.* 14: 259-266 (1997).
200. F. Delie. Evaluation of nano- and microparticle uptake by the gastrointestinal tract. *Adv. Drug. Deliv. Rev.* 34: 221-233 (1998).
201. I. Knütter, S. Theis, B. Hartrodt, I. Born, M. Brandsch, H. Daniel, K. Neubert. A novel inhibitor of the mammalian peptide transporter PEPT1. *Biochemistry* 40: 4454-4458 (2001).
202. H. P. Fiedler. Lexikon der Hilfsstoffe für Pharmazie, Kosmetik und angrenzende Gebiete, Editio Cantor Verlag, Aulendorf, (1996).
203. A. C. Hymes, M. H. Safavian, A. Arbulu, P. Bauter, J. Thorac. A comparison of Pluronic F-68, low molecular weight dextran, mannitol, and saline as priming agents in the heart-lung apparatus. I. Pluronic F-68: first use as a plasma substitute. *Cardiovas. Surg.* 56: 16-22 (1968).
204. A. C. Hymes, K. Beck, J. Thorac. A comparison of pluronic F-68, low molecular weight dextran, mannitol, and saline as priming agents in the heart-lung apparatus. II. The in vitro influence on oxygen consumption of



- certain fluids used as priming agents in a heart-lung bypass apparatus. *Cardiov. Surg.* 56: 23-27 (1968).
205. A. V. Prancan, B. Ecanow, R. J. Bernardoni, M. S. Sadove. Poloxamer 188 as vehicle for injectable diazepam. *J. Pharm. Sci.* 69: 970-971 (1980).
206. D. Leu, B. Manthey, J. Kreuter, P. Speiser, P. P. DeLuca. Distribution and elimination of coated polymethyl [2-14C] methacrylate nanoparticles after intravenous injection in rats. *J. Pharm. Sci.* 73: 1433-1437 (1984).
207. S. Y. Lin, Y. Kawashima. Pluronic surfactants affecting diazepam solubility, compatibility, and adsorption from i.v. admixture solutions. *J. Parenter. Sci. Technol.* 41: 83-87 (1987).
208. H. Hildebrandt. Pschyrembel, Klinisches Wörterbuch, Walter de Gruyter, Berlin, New York, (1998).

## Publications

### Research articles

- A. Rübe, G. Hause, K. Mäder, J. Kohlbrecher. Core-shell structure of Miglyol/poly(D,L-lactide)/Poloxamer nanocapsules studied by small-angle neutron scattering. *Journal of Controlled Release* 107: 244-252 (2005).
- A. Rübe, K. Mäder. An electron spin resonance study on the dynamics of polymeric nanocapsules. *Journal of Biomedical Nanotechnology* 1: 208-213 (2005).
- A. Rübe, S. Klein, K. Mäder. Monitoring of in vitro fat digestion by electron paramagnetic resonance spectroscopy. *Pharmaceutical Research* (in press).

### Oral presentations

- A. Rübe, C. Augsten, K. Mäder. ESR investigations on the dynamics of colloidal drug carriers. *International Meeting on Pharmaceutics, Biopharmaceutics and Pharmaceutical Technology*, APV/APGI, Nuremberg, March 2004.
- A. Rübe, K. Mäder. ESR-Untersuchungen zu dynamischen Phänomenen an Nanokapseln. *Paul-Scherer-Institut*, Villigen, Schweiz, 2004.
- A. Rübe, K. Mäder. ESR investigations on the dynamics of colloidal drug carriers, *Hoffmann-La Roche AG*, Basel, Schweiz, 2004.
- A. Rübe, K. Mäder. ESR-Untersuchungen zu dynamischen Phänomenen an Nanokapseln. *Mitteldeutsche Doktorandentagung*, Halle (Saale), 2004.

### Poster presentations

- A. Rübe, C. Augsten, K. Mäder. An electron spin resonance study on nanocapsules and nanospheres. *The Midnight Sun Meeting on Drug Transport and Drug Delivery*, Tromsø, Norway, 2004.
- A. Rübe, S. Klein, K. Mäder. Monitoring of in vitro fat digestion by EPR. *EPR 2005 - The International Conference/Workshop on Electron Paramagnetic*

*Resonance Spectroscopy and Imaging of Biological Systems*, Columbus, Ohio, 2005.

- A. Rübe, A. Besheer, H. Metz, V. Khramtsov, K. Mäder. Microencapsulation for the protection of spin labels. *EPR 2005 - The International Conference/Workshop on Electron Paramagnetic Resonance Spectroscopy and Imaging of Biological Systems*, Columbus, Ohio, 2005.
- A. Rübe, G. Hause, K. Mäder, J. Kohlbrecher. Characterization of nanocapsule dispersions as drug carrier by SANS and DLS. *International Conference on Neutron Scattering*, Sydney, Australia, 2005.
- C. Augsten, A. Rübe, M. A. Kiselev, R. Gehrke, J. Kohlbrecher, K. Mäder. SAXS and SANS study of PLGA nanospheres containing a Poloxamer shell. *CRS German Chapter Local Meeting*, Marburg, 2005.

## Acknowledgements

### Acknowledgements

Firstly I would like to express my deep gratitude to my advisor Prof. Dr. Karsten Mäder for the very interesting topic of my PhD work, for the fruitful discussions, inspirations and for the provided freedom in research. Furthermore I would like to thank him for his understanding way and encouraging words in any situation through out my stay in Halle.

Thank-you to Dr. J. Kohlbrecher (PSI, Villigen, Switzerland) for the very fruitful cooperation (SANS) and the development of the mathematic model for the core-shell structure of nanocapsules.

I would also like to thank Dr. G. Hause, Halle (TEM measurements), Dr. J. Kohlbrecher and Dr. R. Vavrin, Fribourg, Switzerland (3D-DLS experiments), Prof. Dr. C. Mayer, Duisburg (NMR measurements) and Prof. Dr. A. Göpferich, Dr. M. Hacker, S. Drotleft, Regensburg (PEG-PLA polymer synthesis) for their support.

I would like to thank S. Klein and I. Reiche for their work on "in vitro pancreatin assay" and "polyelectrolyte nanocapsules". Furthermore I am grateful for their nice company.

Thanks to Dr. H. Metz and S. Kempe, Halle (Ex vivo ESR), S. Ullrich and PD Dr. M. Brandsch, Halle (cell toxicity studies), Prof. J. Ullrich and K. Urban, Halle ( $\zeta$  potential measurements), Prof. A. Langner and K. Schirmer, Halle (PCS measurements), C. Blümer, Halle (computer support), for their help and cooperation.

I am grateful to all colleagues for the friendly atmosphere in our group and the many common trips.

Thank-you to A. Tziridis, S. Strübing and I. Schulze for their nice company in Halle.

I also would like to thank A. Schmidt, K. Hauschild and Maximilian for many nice afternoons in Dörstewitz.

Many thanks to S. Todte for her heart-warming care and her refreshing company in our joined laboratory.

I wish to pay my gratitude to my family for their positive support.

Last but not least I wish to thank my boyfriend Phillip for appreciating my work, giving me strength and motivation to get things done.

## Curriculum vitae

### Personal details

---

Name: Andrea Rübe

Born: 15.05.1978 in Lich, Germany

Nationality: German

Marital status: Female, single

### Work experience

---

Since 02/2006 PostDoc in exploratory development/  
pharmaceutical development at Merck KGaA,  
Darmstadt, Germany

05/2005-06/2005 Lecturer at an institute for medical represent-  
tatives, FÖBIS Institute Halle, Germany

Since 10/2004 Lecturer at a private college for ergotherapists  
and medical assistants, Medizinisches Bildungs-  
zentrum Bad Kösen, Germany

02/2001-03/2001 CIMO trainee in pharmaceutical R&D at Leiras Oy,  
Turku, Finland

02/2000-03/2000 Practical training in the department of  
pharmacology and toxicology under supervision of  
Prof. Dr. K. Kuschinsky/Dr. B. Ferger, Philipps-  
University of Marburg, Germany

09/1998-10/1988 Collegiate assistant in quality control at Lilly  
Deutschland GmbH, Gießen, Germany

07/1998-08/1998 Practical training at Lilly Deutschland GmbH,  
Gießen, Germany

### Education

---

01/2003-01/2006 Ph.D. student in the group of Prof. Dr. K. Mäder,  
Pharmaceutical Technology, Martin-Luther-  
University Halle-Wittenberg, Germany

07/2003 Diploma degree in pharmacy, Halle University,  
Germany

## Curriculum vitae

---

01/2003	Approbation as a pharmacist, Philipps-University of Marburg, Germany
05/2002-10/2002	Diploma thesis in pharmaceutical technology in R&D at Hofmann-La Roche: <i>development and characterization of semisolid and solid self-emulsifying drug delivery systems</i> under supervision of Dr. K. Mäder
11/2001-04/2002	Practical training at Adler pharmacy, Cologne, Germany
07/2000-12/2000	Pharmacy studies abroad at Kuopio University, Finland
10/1997-07/2001	Pharmacy studies at Phillips-University of Marburg, Germany
08/1990-06/1997	Liebig School, Gießen (Abitur)

## Erklärung

Hiermit erkläre ich gemäß § 5 (2) der Promotionsordnung der Mathematisch-Naturwissenschaftlich-Technischen Fakultät der Martin-Luther-Universität Halle-Wittenberg, dass ich die Ergebnisse der vorliegenden Dissertationsarbeit

Development and physico-chemical characterization  
of nanocapsules

am Institut für Pharmazeutische Technologie und Biopharmazie der Martin-Luther-Universität Halle-Wittenberg unter Anleitung von Herrn Prof. Dr. Karsten Mäder selbständig erarbeitet bzw. im Rahmen der angegebenen Kooperationen erhalten habe und nur die in der Dissertation angegebenen Literaturstellen und Hilfsmittel verwendet habe.

Weiterhin habe ich diese Arbeit bisher an keiner in- oder ausländischen Fakultät als Dissertationsschrift vorgelegt.

Halle (Saale), den 30. Januar 2006

Andrea Rübe